OPTICAL STUDIES OF RADIATION INDUCED DEFECTS IN PURE AND Mn DOPED $RbMgF_3$

By

NICHOLAS KOUMVAKALIS

Diploma

Aristotelian University of Salonika

Salonika, Greece

1969

Submitted to the Faculty of the Graduate College
of the Oklahoma State University
in partial fulfillment of the requirements
for the Degree of
DOCTOR OF PHILOSOPHY
July, 1976

OPTICAL STUDIES OF RADIATION INDUCED DEFECTS IN PURE AND Mn DOPED $RbMgF_3$

Thesis Approved:

W. A. Sibley
Thesis Adviser

Richard C. Powell

E. E. Kohnke

J. Paul Devlin

Norman N. Durham
Dean of the Graduate College

ACKNOWLEDGEMENTS

I would like to take this opportunity to express my appreciation and gratitude to the many people who were responsible for the completion of this thesis. First, my many thanks to my advisor Dr. W. A. Sibley, whose constant encouragement, help and patience together with his deep understanding of the problem, made possible for me to reach some level of scientific competence. Dr. R. C. Powell's help and support throughout this research is gratefully acknowledged. Also, I am grateful to Drs. L. E. Halliburton, E. E. Kohnke and J. J. Martin for many useful discussions and to Dr. J. J. Martin for growing the crystals used.

My thanks are also extended to Dr. C. T. Butler, G. E. Venikouas, H. Hall for their assistance during this work.

Finally, I would like to thank my parents and Patricia Davis. Their kindness and generosity was one of the main reasons for my bringing this work to a completion.

TABLE OF CONTENTS

TABLE OF CONTENTS (Continued)

LIST OF TABLES

LIST OF FIGURES

LIST OF FIGURES (Continued)

CHAPTER I

INTRODUCTION

The term color center refers to a special type of point defect involving electrons or holes which gives rise to optical absorption in normally transparent crystals. Color centers in solids have been studied for nearly half a century which attests to their importance. Part of this importance is due to the fact that many important properties of solids are controlled as much by imperfection as by the nature of the host crystal.

A number of outstanding reviews on the subject have appeared. Some of them are given by Seitz (1), Schulmann and Compton (2), Compton and Rabin (3), Fowler (4) and Crawford and Slifkin (5). Much of the work done in the field of color centers has been centered on the alkali halides. Almost all of these materials crystallize in the NaCl (rock salt) structure and, most important, they show an optical transparency over a very wide range, being transparent from the far u.v. to the far I.R.

Color centers can be introduced by the method of additive coloration (6,7), electrolytic coloration (6,8) or by exposure to ionizing or particle radiation (9) (electrons, protons, x-rays and neutrons).

These processes which will be discussed later create defects in the lattice as well as changes in the state of impurities in the crystal.

Different researchers have proposed a variety of models for color

centers. Due to the importance of color centers research in materials other than alkali halides, a consistent nomenclature for color centers applicable to all polar crystals is necessary. Sonder and Sibley (9) have suggested a generalized nomenclature for color centers and a description of color centers and their properties will be given in a later section.

Perovskite materials like $KMgF_3$, $KZnF_3$ and $KMnF_3$ are of interest because of their potential usefulness in devices. Recently several investigations have been conducted on radiation induced defects in $KMgF_3$ crystals. Hall and Leggeat (10) using electron spin resonance and polarized luminescence tentatively identified F, F_2 and V_K center absorption bands. Riley, Yun and Sibley (11-14) by means of polarized bleaching and excitation spectra, identified F, F_2, F_3 and V_K center absorption bands and F_2 and F_3 emission bands in $KMgF_3$. More extensive studies on V_K centers in $KMgF_3$ have been made by Lewis et al. (15) and Alcalá et al. (16).

$RbMgF_3$ is a relatively new crystal on stage. Previous x-ray work, indicated the crystal structure was a modification of the perovskite type structure but with monoclinic symmetry (17). However, Shafer and McGuire (18) reported that $RbMgF_3$ had the hexagonal $BaTiO_3$ (19) type structure over all composition ranges of the system $RbMgF_3$-$RbCoF_3$. Our own experimental results and data indicate a hexagonal structure for the crystal. In fact, this material forms as a crystal of hexagonal symmetry with the c-axis the optic axis. The lattice constants are $a_o = 5.83\text{Å}$ and $c = 14.27\text{Å}$. Figure 1 illustrates the crystal structure. Shown are the basal plane (three layers) and the close-packed sequence of rows along the optic axis which lie in the $(\bar{1}220)$ plane. All Mg^{2+}

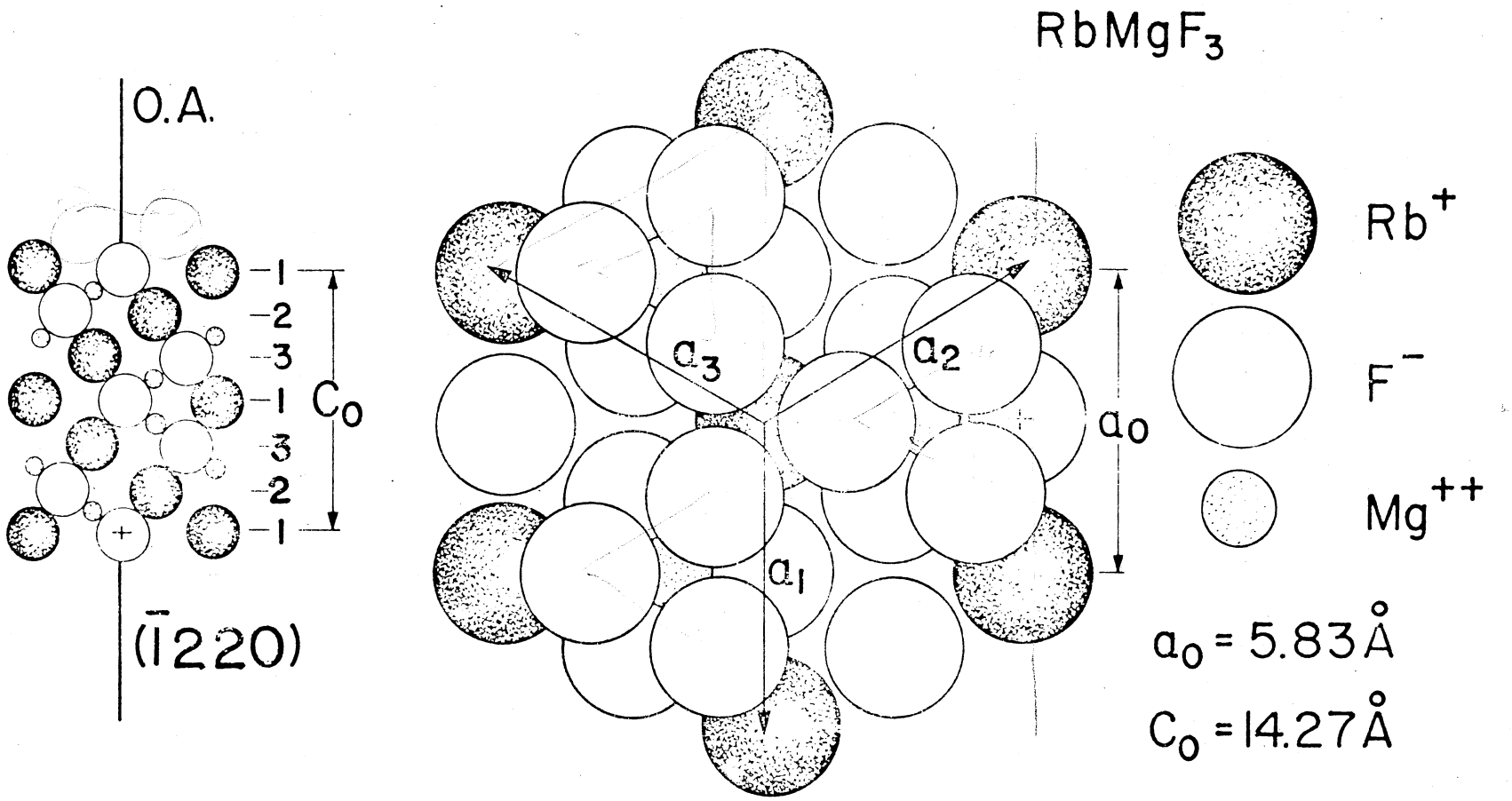

Figure 1. $RbMgF_3$ Model. Shown are the Basal Plane (Three Layers with 7 Rb^+ Ions, and 12 F^- Ions in the First Layer and 3 Mg^{2+} Ions in the Second) and the Close-Packed Sequence of Ions Along the Optic Axis Which Lie in the $(\bar{1}220)$ Plane

ions are in sites of octahedral symmetry surrounded by six fluorine ions, but this complex of MgF_6 ions can have two different orientations in the crystal (18-19). Two-thirds of the MgF_6 octahedra occur in pairs which share a face to form M_2F_9 polyhedra. The remaining one-third of the octahedra are linked to M_2F_9 groups by sharing corners.

The first objective of the present work is to identify radiation damage induced defects in this material. This includes identification of the optical absorption bands arising from F, F_2, F_3 and V_K centers as well as identification and assignment to individual centers of the emission bands. Through the use of polarized bleaching, polarized excitation and luminescence, and temperature dependence of the band we can produce a reasonably complete picture of the radiation induced defects and their behaviour.

Impurities also cause optical absorption and emission in these materials. Over the past decade or so McClure, Ferguson and others (20,21-26) with their work on the 3d impurity ion transitions have improved and extended our knowledge of crystal field theory. The crystal field concept was developed in the early 1930's by Bethe (27), Van Vleck (28-34); Schlapp and Penney (35-36). Bethe (27) first used group theoretical arguments to show how the degeneracies of the electronic terms of the free ion are removed in fields of cubic and lower symmetry.

Van Vleck (37) and Finkelstein and Van Vleck (38) were the first to apply crystal field theory to optical spectra of d-electrons in paramagnetic crystals Hartman, Schlaefer and Ilse (39-40) used crystal field theory to calculate the energy levels of 3-d transition metal ions with no more than five d-electrons. The optical properties of Ni, Mn and Co transition ions in the perovskite structure have been studied by numer-

ous researchers. Mehra and Venkatewarlu (41) were the first to study the crystal absorption spectra of $RbMnF_3$ and $KMnF_3$.

Recently a number of studies of the effect of radiation on the optical properties of 3d-impurity-ions in $KMgF_3$ and MgF_2 crystals have been made (42-44). Vehse and Sibley (45) observed a series of optical absorption bands in 80^{o}K electron irradiated $KMgF_3$ and concluded that an F center-Mn complex was responsible. Sibley, Yun and Vehse (46) and Young et al. (43) by using luminescence and excitation and EPR techniques verified the fact that the observed bands were due to perturbed Mn^{2+} ions.

One of the more interesting aspects of these investigations was the observation of large oscillator strength increases for previously forbidden transitions when radiation defects are present. These transitions are symmetry forbidden since the 3-d ions have octahedral (O_h) symmetry in a perfect crystal of $KMgF_3$ and some of them are spin forbidden. The presence of nearby defects results in a symmetry change and also possible electron exchange between the radiation damage defect and the transition metal ion both of which affect the intensity of optical transitions. Lee and Sibley (42) gave evidence that in $KMgF_3$:Mn^{2+} and some Co^{2+} transitions are enhanced by the presence of defects through exchange interaction that increases the oscillator strength.

The work of Young et al. (43) in conjunction with some earlier research indicated that in irradiated $KMgF_3$:Mn one set of perturbed Mn^{2+} transitions is due to F center -Mn^{2+} pairs. In fact the optical spectra of these perturbed transitions are very similar to the unperturbed Mn^{2+} transitions studied by McClure, Ferguson and others (58-61).

$RbMgF_3$ seemed to be an ideal material for a further investigation of the radiation damage on Mn^{2+} doped crystals. The 3-d ions have octahedral-like symmetry so we could observe the oscillator strength increases for the perturbed Mn^{2+} centers (if they could form). Furthermore and most importantly in the first part of this work it was discovered that F centers as well as negative ion vacancies are not mobile at room temperature. Because of this lack of mobility it was felt that this host crystal would indeed be excellent for determining the relative oscillator strengths of the perturbed Mn^{2+} centers as well as the mechanism of F center aggregation.

So the second objective of the present work is to report experiments on the formation and character of perturbed Mn^{2+} in $RbMgF_3$ and to give additional information on the kinetics of the defect formation in this crystal.

CHAPTER II

DEFECTS AND DEFECT NOMENCLATURE

The table below gives a summary of some of the defect centers observed in polar crystals (9).

TABLE I

DEFECT NOMENCLATURE

Description of Defect	Ionic Charge of Normal Ion at Lattice Site	Notation	Previously Used Notation
A. Single Defects			
Negative ion vacancy	-1	F^+	
	-2	F^{2+}	α
Negative ion vacancy with one electron	-1	F	F
	-2	F^+	F_1, F^+
Negative ion vacancy with two electrons	-1	F^-	F'
	-2		
Positive ion vacancy	+1	V^-	--
	+2	V^{2-}	--
Split interstitial (atom) molecular ion at halide site	0	H	H
B. Composite Defects			
Di-F center	-1	F_2, M	M, F_2
	-2	F_2	--

TABLE I (Continued)

Description of Defect	Ionic Charge of Normal Ion at Lattice Site	Notation	Previously Used Notation
Tri-F center	-1	F_3, R	R, F_3
	-2	F_3	--
Ionized Di-F center	-2	F_2^+, M^+	M^+
	-4	F_2^+	
C. Impurity-Defect Centers			
F center adjacent to cation impurity of some valence as host	-1	F_A	F_A
	-2	F_A	
H center trapped at impurity of some valence host	0	H_A	--
D. Simple Charge Defects Without Missing or Extra Ions			
Self trapped hole	-1	$[X_2^-]$	V_K
Hole trapped at halide impurity	-1	$[XY^-]$	$[XY^-]$

Figure 2 shows the models for F, F_2(M), and F_3(R) centers.

The F center model, now confirmed by electron-spin resonance techniques (5), was first postulated by de Boer. The F absorption band, a wide bell-shaped band that for alkali halides lies in the visible region

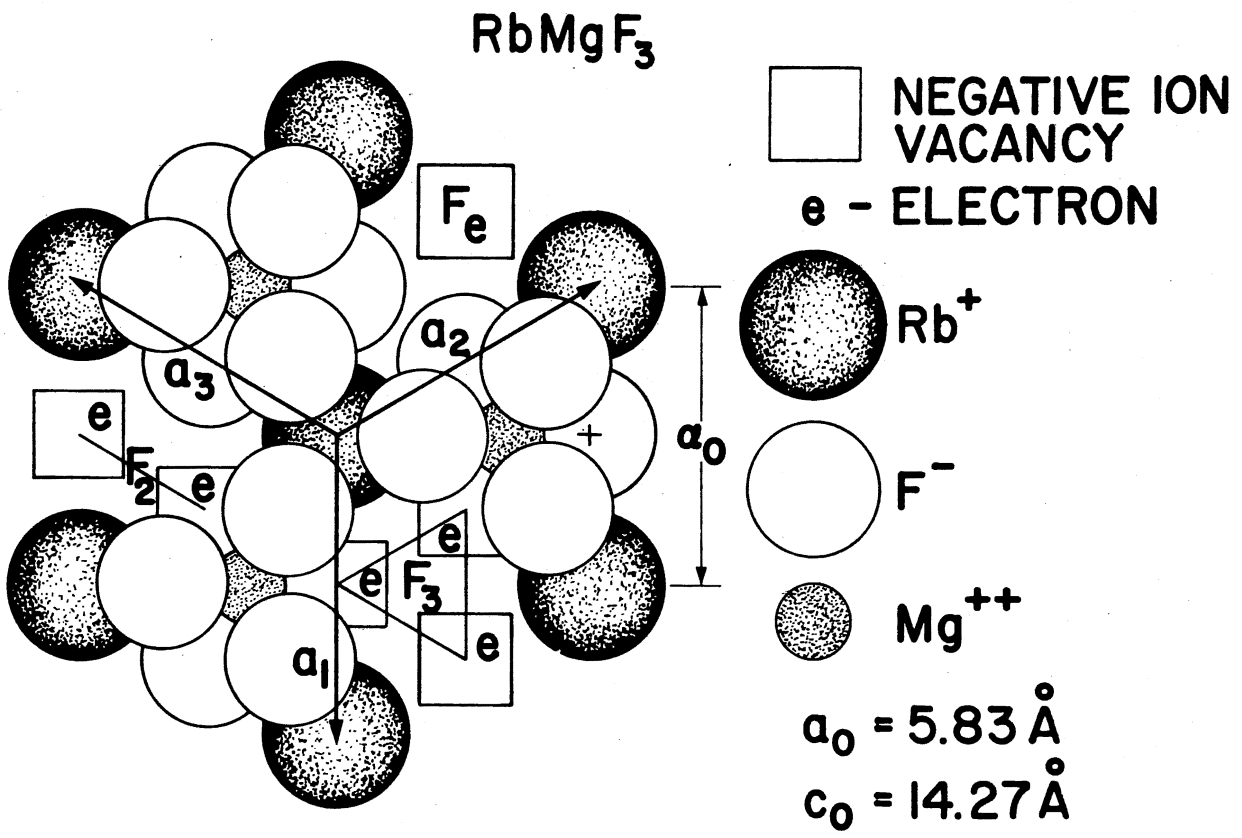

Figure 2. Models for F, F_2 and F_3 Centers in $RbMgF_3$

of the spectrum was the main reason for the name "color centers". The main feature in all the models for the F-center absorption is that in the region of the vacancy, the potential energy resembles that of a three dimensional potential well. In the simpler of these models, where the defect is treated like a particle in an infinite potential well, the energy between the ground state and the first excited state is:

$$E_{2p} - E_{1s} = \frac{3\pi^2\hbar^2}{8ma^2} \tag{1}$$

where 1s denotes the ground state, 2p the excited state and a is the distance from the origin to the potential barrier. If a is taken as the nearest neighbor separation, the F band energy E_F can be correlated with a for most alkali halides as

$$E_F = 17.7a^{-1.84} \tag{2}$$

A relation of this sort was first derived by Mollwo (1931) and later modified by Ivey and others.

The particle in the box model also qualitatively explains the large width of the band and the temperature dependence of both width and peak position.

The width arises from the vibration of neighboring ions, which leads to a variation of a and thus of E_F. The change of the peak position can arise from the thermal expansion of the lattice, which increases the equilibrium value of a.

The existence of F center aggregates was established also by means of optical and magnetic measurements.

Finally, because of the major role played by the V_K centers in the

defect production, an account of its nature and its properties will be useful in understanding better this mechanism.

The V_K center is an intrinsic defect in the sense that no defects such as vacancies or interstitials are involved. Its creation results from the localization of a hole in a covalent bond between two adjacent (halide) ions. Irradiation of ionic crystals (alkali halides and perovskites are the compounds in which V_K centers have been studied extensively) will produce V_K centers providing that the temperature is low enough that the hole cannot move and that the crystal contains extrinsic electron traps--impurities or other color centers--which can stabilize the holes against annihilation by recombination with electrons.

Because of its unpaired spin the V_K center is paramagnetic and EPR techniques proved to be very powerful for its identification (53). V_K centers are anisotropic and the crystallographic representation of their internuclear axes is shown for a cubic lattice in Fig. 3. After irradiation (x-rays, electrons) they are equally distributed among the six <110> directions.

By using polarized light, it is possible to bleach the V_K centers (54) and thus optically verify their <110> orientation.

There is a maximum of four observable absorption bands due to V_K centers in alkali halides, with the short wavelength transitions being more anisotropic than the long ones (55).

In Table II a summary of V_K absorptions observed in various crystals as well as different useful parameters is given.

The fact that a given parameter depends primarily on the identity of the halogens and less on the cations is an indication that the V_K center is slightly perturbed by the lattice.

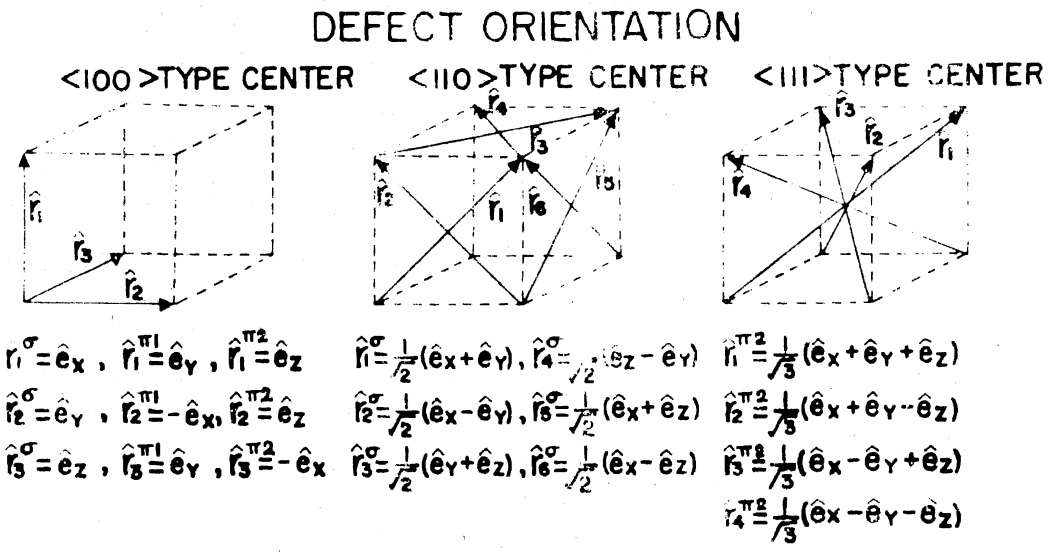

Figure 3. Vectors Specifying Orientations of <100>, <110>, and <111> Type Centers

TABLE II

$[X_2^-]$ CENTER OPTICAL ABSORPTION, PEAK ENERGIES E, WIDTHS AT HALF MAXIMUM $W_{\frac{1}{2}}$ AND DISORIENTATION TEMPERATURES Td

	E, eV	$W_{\frac{1}{2}}$, eV	Td, ^{o}K
LiF	3.65	1.20	110
	1.65	--	
NaF	3.38	0.66	155
CaF_2	3.88	1.0	130[a]
	~ 1.65	--	
SrF_2	3.80	1.0	120
	~ 1.65	--	
BaF_2	3.69	1.0	100
	~ 1.65		
LiCl	3.15	1.47	100
NaCl	3.28	1.11	130
KCl	3.40	0.81	170
	1.65	0.37	
RbCl	3.40	0.76	190
NH_4Cl	3.31	0.83 - 1.0	130[a]
	1.57	0.37	
KBr	3.22	0.73	140
	1.65	0.26	
	1.38		
NH_4Br	3.10	0.80	---
	1.55	0.27	
NaI	2.87	--	50
	1.41	--	
	~ 2		
KI	3.10	0.55	90
	1.55	0.22	
	2.12	0.36	

[a]Temperature at onset of 0^{o} jumps; Td is higher.

An atomic model of the electronic structure of the V_K center can be obtained through a set of one electron LCAO-MO made up of valence orbitals, 2p for fluorine, 3p for chlorine, etc. Electron spin and crystal field contributions will be ignored allowing orbital angular momentum parallel to the molecular axis to be conserved.

The molecular orbitals obtained are shown in Fig. 4α. The two higher orbitals are antibonding and the two lower orbitals are bonding with the $\sigma_u$np orbital being the ground state for the hole. Absence of the hole would produce a system isoelectronic with a diatomic rare gas molecule without any net molecular bonding. The presence of the hole eliminates the coulombic repulsion and gives a bound state.

The electronic states resulting from the previously constructed atomic orbitals are shown in Fig. 4β with spin-orbit coupling taken into account. Observed optical transitions are shown by solid lines. The fourth transition observed (55) is probably due to a $^2\Pi u \rightarrow {}^2\Sigma u^+$ transition, the forbiddenness being partially removed by vibrational distortions around the center.

Bleaching with polarized light in the u.v. region results in a reorientation rather than a destruction of the V_K centers (56). This arises from the fact that the transition involved is the $^2\Sigma u^+ \rightarrow {}^2\Sigma g^+$ and that the $^2\Sigma g^+$ state contains a net antibonding σ electron. This causes the state to be unstable and the hole may be freed and retrapped at the same or at a different lattice site.

Numerous experiments concerning V_K related luminescence (57-60) result in the conclusion that optical stimulation in an electron trap region releases electrons which can recombine with self trapped holes. This recombination results in excited states which decay radiatively to

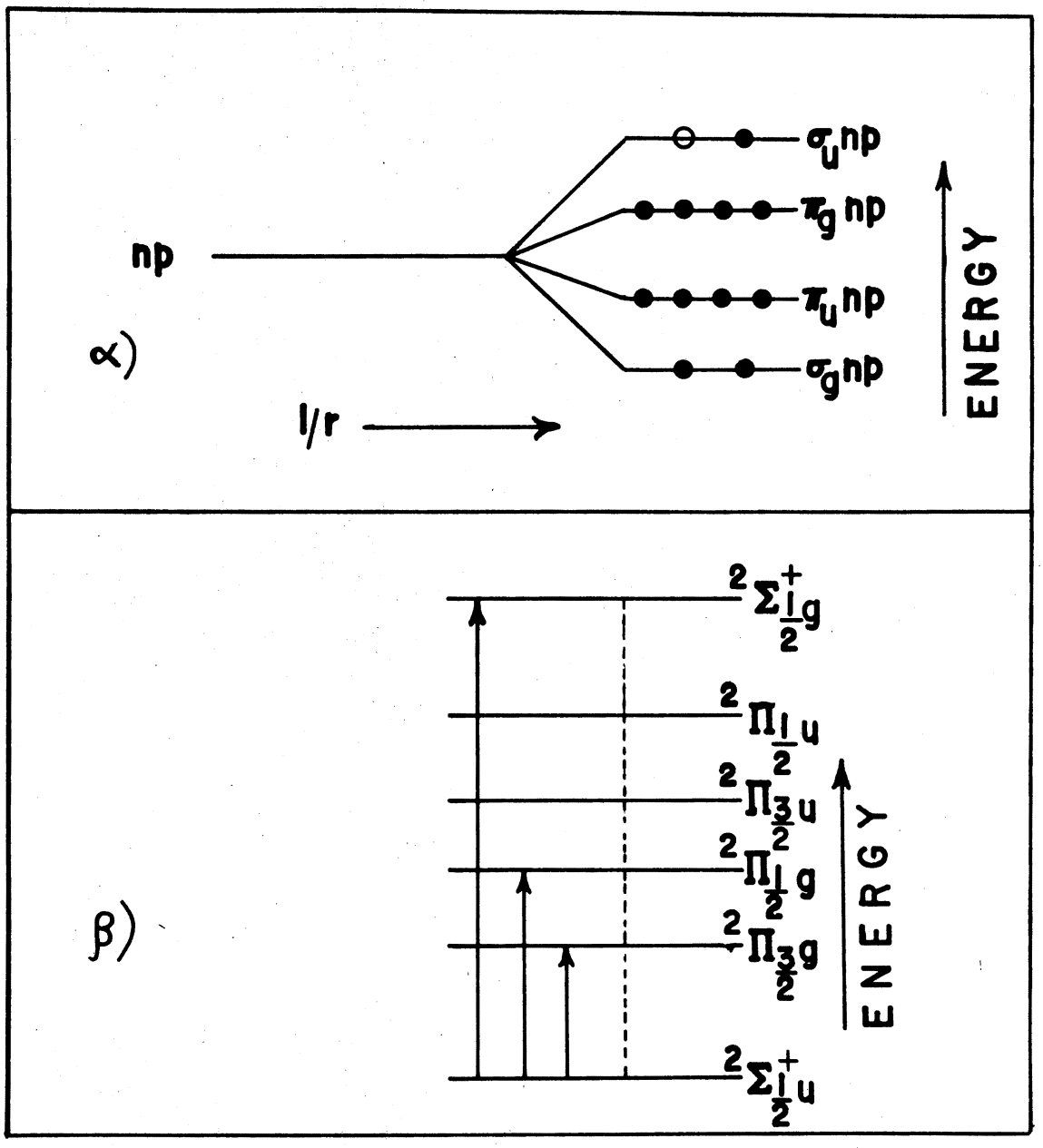

Figure 4. (a) Molecular Orbital Energy Sequence for the $[X_2^-]$ Center, (b) Electronic States of the $[X_2^-]$ Center

produce up to four observable bands. Most of these bands exhibit polarization.

An electron recombining with a V_K center to produce an excited state gives rise to a state which is a property of the pure lattice, it has the normal charge and it is non conducting with the electron and the hole being bound.

An observation of crucial importance is that these are states in which the lattice retains the axis of symmetry characteristics of the V_K center as shown by polarized luminescence experiments (57-60).

Thus the excited state must be one in which the captured electron is confined to an orbital around the V_K center while the nuclear coordinates do not relax to restore a cubic symmetry. The $(e^- + V_K)$ states correspond to a self-trapped exciton as opposed to exciton states populated by optical absorption in the fundamental band.

In most of the crystals examined the recombination luminescence consists of two bands with opposite properties. The high energy band is polarized parallel to the molecular axis, it is called a σ-transition and it has a very short lifetime, while the low energy band has opposite polarization being a π-transition with a lifetime of the order of 10^{-6} sec.

The identification of the electronic states (59) suggests that the ground state is a $^1\Sigma g^+$ state, while the two excited states are $^1\Sigma u$ and $^1\Pi u$ states.

Although the luminescence efficiency is relatively high, the radiative efficiencies and lifetimes become strongly temperature dependent at higher temperature, due to nonradiative recombination.

In general the excitation energy released as a result of nonradia-

tive recombinations can be dissipated through two principal channels.

1. Phonon creation, a process which is active to a greater or lesser extent to all crystals.

2. Production of lattice defects such as vacancy-interstitial pairs. In this case, the system is able to cross over into the ground electronic state after only a small fraction of the energy has been dissipated. The highly distorted pair of ions possesses several eV of kinetic energy which is often sufficient to thrust an ion or an atom, not necessarily one of the original ones into an interstitial position.

This is a basis of the model proposed by Pooley and Runciman (61) to explain the highly efficient defect production in alkali halides.

More definitive evidence connecting F-center production with electron-hole recombination at V_K centers appears when the temperature dependence of the $(e^- + V_K)$ recombination is compared with F center production (9). An anticorrelation has been observed to exist, the F center production efficiency increasing approximately an order of magnitude where the emission disappears.

Although the above mentioned mechanism has not been shown to hold in every case, it is a general agreement between investigators that electron-hole recombination is a source of defect production.

CHAPTER III

EXPERIMENTAL PROCEDURE

Crystal Growth

Crystals of $RbMgF_3$ pure and doped with Mn were grown in the Oklahoma State University Crystal Growth Laboratory by means of modified Bridgman and Stockbarger techniques (47,48,49).

The basic requirement for a Stockbarger growing furnace is a temperature gradient which can be moved relative to the starting material. The material is contained in a crucible and it is placed in a fixed vacuum system which is surrounded by a furnace. The temperature gradient is moved slowly thru the crucible by raising the furnace so that the temperature drops from a region slightly above the melting point to a region below the melting point of the starting material. The crystal is formed from that latter region, the growth proceeding as the temperature gradient moves.

Figure 5 is a schematic showing the main components of the Oklahoma State University Bridgman apparatus. The crucible containing the chemicals is placed in a graphite heat sink at the bottom of a Al_2O_3 vacuum tube. The crucible, made of vitreous carbon was purchased from Beck- with the heat sink from Ultra Carbon (UT-9 grade) and the Al_2O_3 vacuum tube was purchased from Coors Mullits. The Al_2O_3 vacuum tube is mounted with a "quick disconnect" connector to a vacuum with provisions made for the introduction of argon into the system.

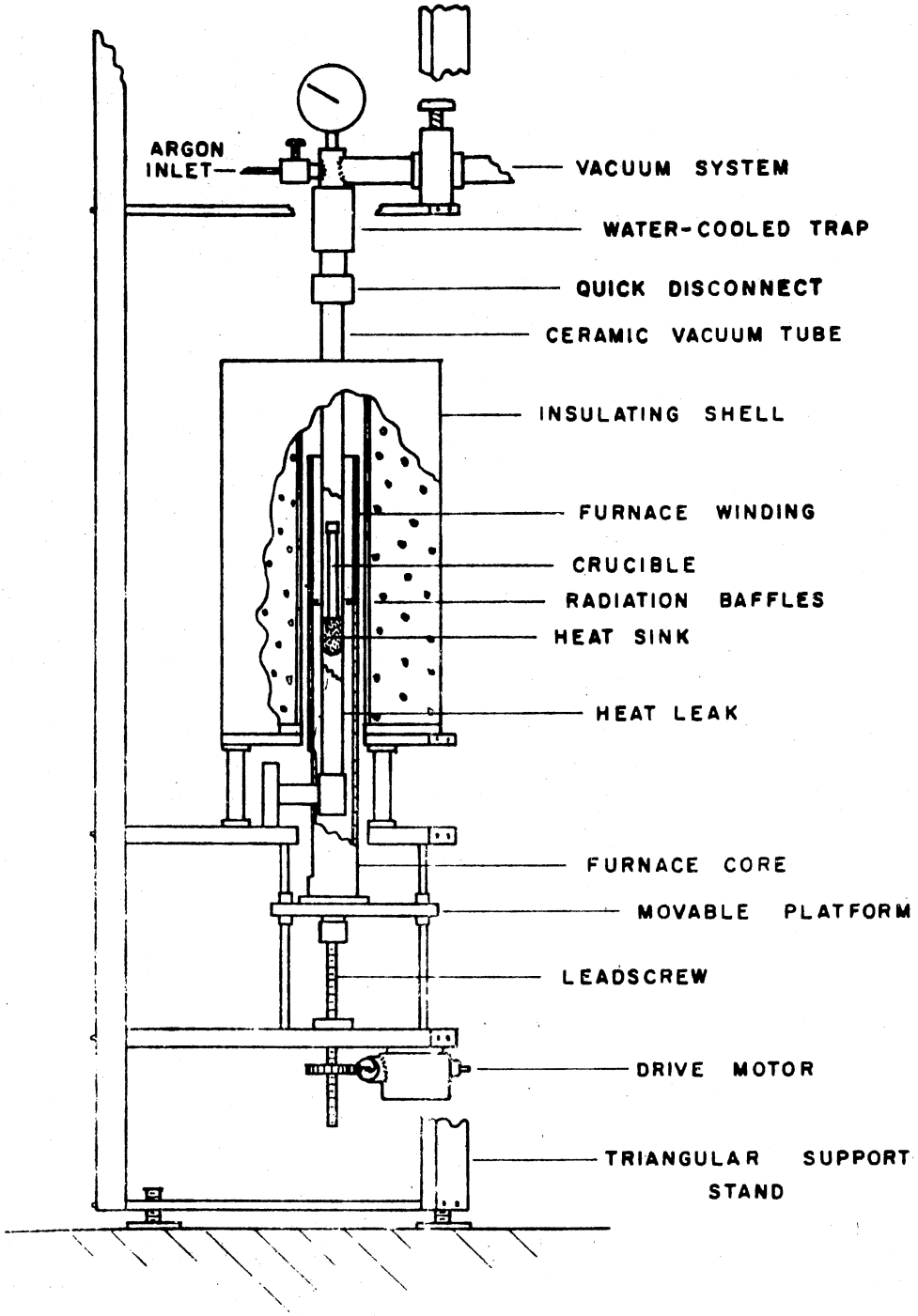

Figure 5. The Oklahoma State University Bridgeman Apparatus

The temperatures necessary for the growth of high melting point materials are provided by a platinum wire of .810 mm diameter and wound around a Norton high-purity alumina core. The winding pattern is a three section one (6 turns per inch, 3 turns per inch and 2 turns per inch) which provides a nearly uniform temperature profile.

The vacuum system for the apparatus consists of 200 ℓ/s diffusion pump and a Welch 3 ℓ/s forepump. This system can reduce the pressure to 10^{-6} Torrs in a matter of minutes. The Argon pressure--Argon is used to flush out unwanted gases and to keep a neutral "growth atmosphere"--is monitored through a bourdon gauge calibrated from -1 to +2 atmospheres. Lift speeds of 1.5, .76, .30, .15, .08, and .03 cm/hr are available. A limit switch provides the system with an automatic cutoff.

The preparation of the growth powder mixture takes place in a dry box. For the pure $RbMgF_3$, crystal chips of MgF_2 provided by Harshaw and zone refined RbF provided by Optran were used as starting material. For $RbMgF_3$:Mn crystals Optran MnF_2 was mixed with the starting material.

The Argon overpressure in the crucible together with the initial mixture of approximately 1 mm^3 of anhydrous ammonium bifluoride is necessary since the decomposition of the latter at 200°C releases hydrogen fluoride gas which flushes the absorbed water out of the system. The highest furnace temperature was ~1000°C and the furnace was raised at the rate of 1.5 mm per hour.

An impurity analysis of $RbMgF_3$ made by means of mass spectroscopy is shown in Table VI on page 72. Samples of various thickness were cut using an IMANCO Macrotome diamond saw and polished using a Syntron LP-01 vibrator polisher with a Linde Al distilled water slurry. Major irregularities were removed before polishing by hand lapping on a glass

plate with number 600 carborundum grit in mineral oil.

It was virtually impossible to find a cleavage plane for this crystal. One might assume that it should cleave along the hexagonal planes perpendicular to the optic axis, but so far we have been unsuccessful in our cleavage attempts. The orientation of crystals was first determined by using a polarizing microscope which would help us find the optic axis orientation and the crystal structure was confirmed by using Laue X-ray back reflection techniques.

Crystals with faces parallel and perpendicular to the optic axis were used.

Radiation Procedure

The samples were irradiated with either a ^{60}Co gamma source or 70 KeV x-rays or electrons using a 2.0 MeV Van de Graaff, after they had been optically polished.

The electron and γ irradiation intensity were measured by means of silver doped phosphate glass dosimeters. The way in which these are employed is the following (50). The dosimeter is placed in a spectrophotometer and its optical density is measured with 5000 Å light. A remeasurement after the exposure to the radiation source, will show an increased optical density proportional to the energy absorbed by the dosimeter. So one can use calibrated dosimeters to measure the fraction of the incident intensity absorbed by the sample. This is done by comparison of the coloration of two dosimeters exposed with and without an interposed sample. The difference in the readings then, yields the fraction of the incident intensity that is absorbed by the sample.

The electron irradiation intensity was measured to be 1.2×10^{13} $\frac{MeV}{cm^3 sec}$ (1.2×10^{12} $\frac{e}{cm^2 sec}$) and the γ-ray intensity was measured to be $\sim 10^9$ $\frac{MeV}{cm^3 sec}$.

Optical Measurements

The samples were irradiated at 300K, 196K, 80K or 20K. For room temperature irradiation the sample was placed in a copper holder.

For low temperature irradiation the samples were held in a Sulfrian liquid helium cryostat manufactured by the Sulfrian Cryogenic corporation or in a Cryodyne Cryocooler, Model 20 by CTI. Both these units were equipped with a rotatable tail section with quartz windows for optical measurements and aluminum windows for irradiation. (Actually, it was found that irradiating with 1.5 MeV electrons through the quartz window practically no damage was introduced to a $RbMgF_3$ crystal).

In the Sulfrian cryostat using a small heater immersed in the central jacket we were able to control the temperature between 80K and 300K within ±1K. A resistance heater wrapped around the cold finger of the Cryodyne Cryocooler allowed us to control temperatures from 10K to 300K within ±1K. A thermocouple consisting of number 36 gauge gold: 0.7 at % iron versus chromel P wire enabled us to read the temperature.

Optical absorption was measured by a Cary 14 spectrophotometer which records the optical density as a function of wavelength. The optical density O.D. = $\log_{10} \frac{I_o}{I}$ is related to the absorption coefficient by $a = 2.303 \left(\frac{O.D.}{t}\right)$ cm^{-1} where I and I_o are the intensities of the optical beam in the sample and reference chamber respectively and t is the sample thickness. The thickness of the samples was measured

by using a micrometer and by taking several measurements of different portions of it.

All polarized absorption measurements were made in the Cary 14 spectrophotometer using Polaroid type HNP'B unsupported ultraviolet polarizers in both the sample and reference beams. The polarizers could be oriented along any desired crystallographic direction of the crystal being studied.

Luminescence measurements were made on a Jarrel-Ash one meter monochromator with a dispersion of 8.2 $\mathring{A}$/mm, blazed at 5000 $\mathring{A}$, with excitation produced by a 75-W short arc Xenon lamp X-75 by PEK, Inc.

The exciting light passed through a Spex minimate 22 cm monochromator and was chopped at a frequency of 450 Hz with a Keithley Model 8403-450 light chopper. The sample was rotated slightly off of a 45^{o} angle to minimize reflection of the exciting light into the detection system. The detection system of a RCA C 31034 photomultiplier tube cooled to -20^{o}C via a cooler manufactured by Products for Research, Inc. and operated at 1,800 V DC. The output from this phototube was connected to the input of a Keithley Model 427 current amplifier and the output of this to a Keithley Model 840 lock-in amplifier. The reference signal of the chopper was fedback to the lock-in amplifier.

The detected luminescence intensity was plotted against wavelength on a Moseley Model 7001 A X-Y recorder. The detection system was calibrated with a standard quartz-iodine lamp, having calibration traceable to the National Bureau of Standards.

A block diagram of the luminescence apparatus is shown in Figure 6. The response factor determined from the standard lamp calibration is shown in Figure 7. The spectral irradiance of PEK X-75 Xenon short arc-

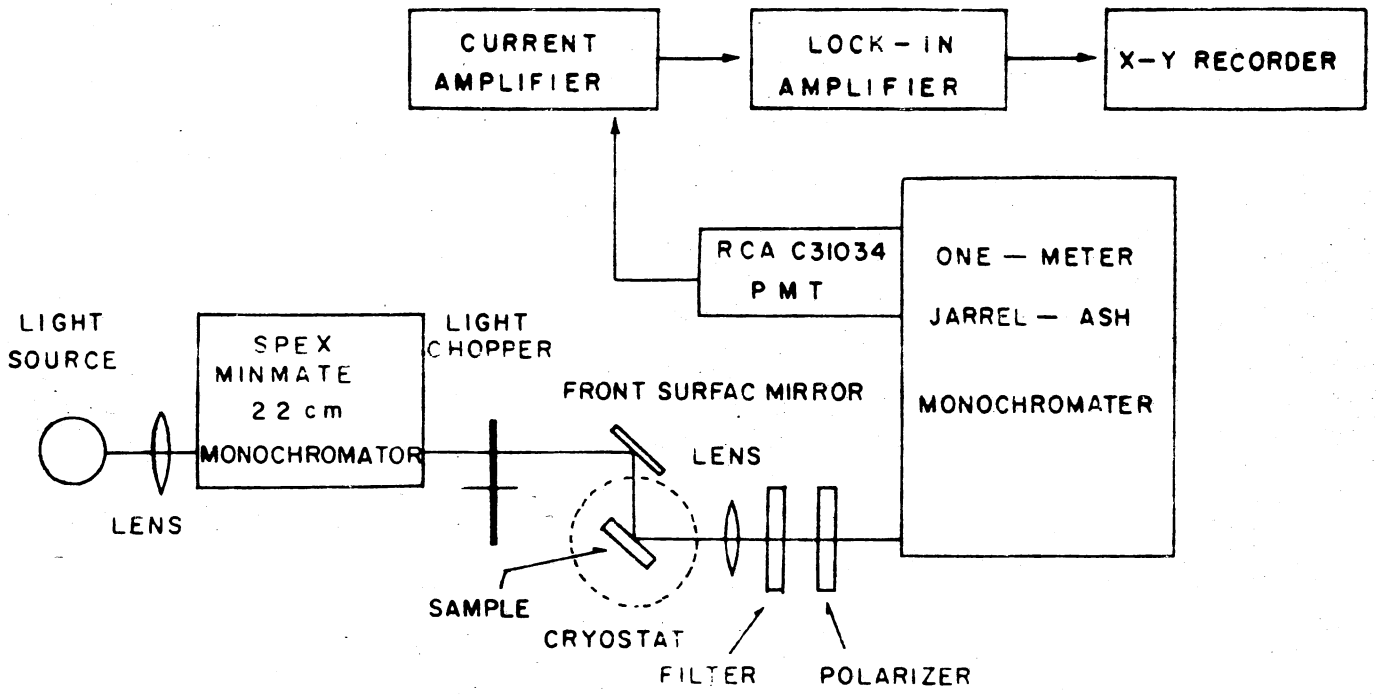

Figure 6. Block Diagram of Luminescence Apparatus

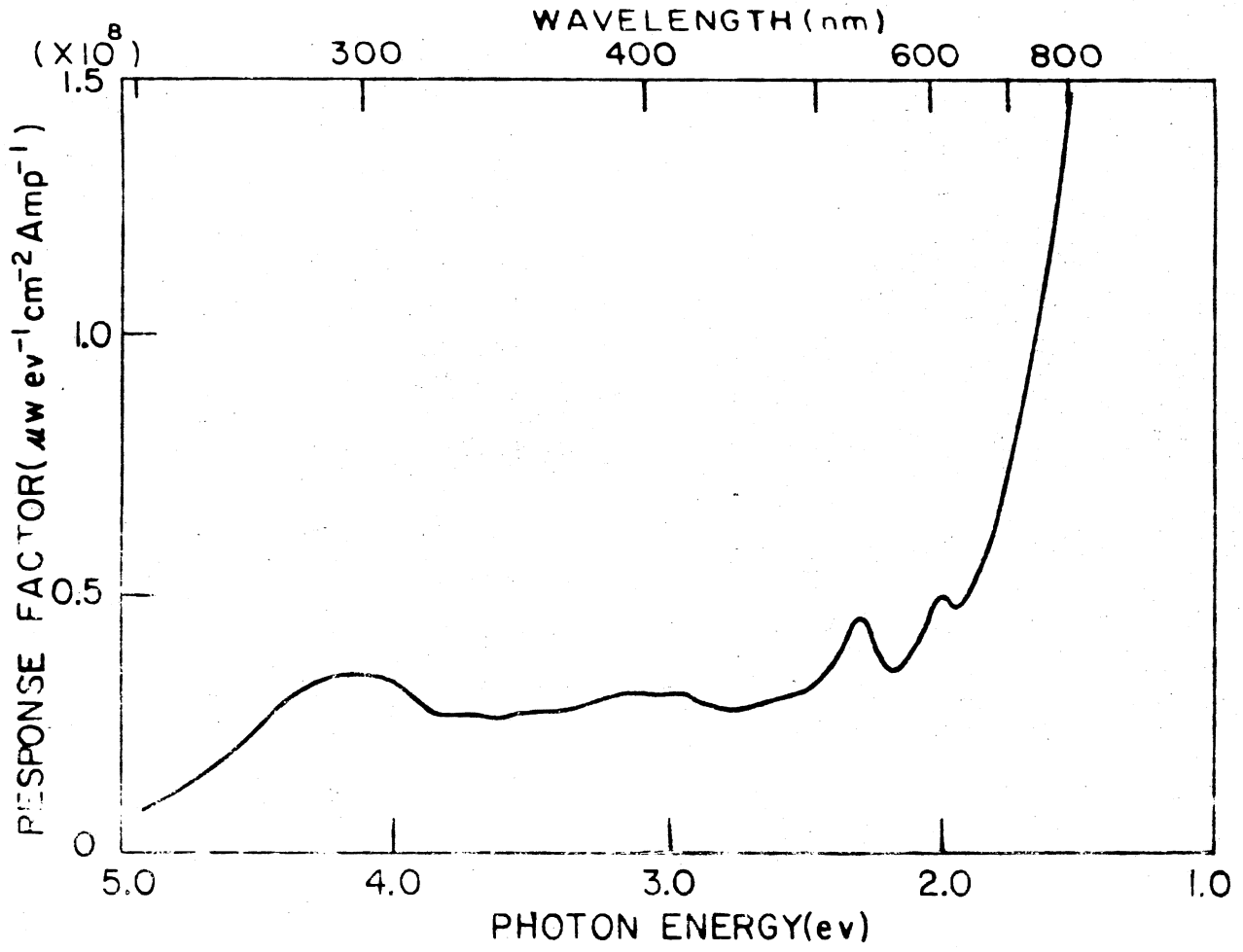

Figure 7. Response of Luminescence Detection System as a Function of Photon Energy

lamp is shown in Figure 8. For all polarization measurements a Glan polarizer or polaroid ultraviolet type HNB'B unsupported sheets were used.

The optical excitation spectrum for a luminescence band was taken with the same apparatus mentioned above with the Spex Minimate 22 cm monochromator driven by a synchronous meter drive.

In the case of X-ray excited luminescence a 1/2 meter Bausch and Lomb monochromator was used with a dispersion of 66 $\mathring{A}$/mm in the first order, blazed at 10000 $\mathring{A}$, with excitation by 70-KeV X-rays. The position of the sample was such that the X-rays would hit it perpendicularly so that a maximum luminescence could be excited and detected. The detection system consisted of an EMI 9558Q photomultiplier tube cooled to $-20^{o}C$ via a cooler manufactured by Pacific Photometric Instruments and operated at 900 V DC. The chopper, amplifier, preamplifier and X-Y recorder were identical with the ones mentioned before. There was a difference in the arrangement, the chopper being placed after the monochromator and before the photomultiplier tube. Corning glass filters with sharp optical cut off were used to eliminate higher order of the exciting light from the monochromator output.

Radiative lifetime measurements were made using single photon counting techniques (75).

Two types of annealing experiments were performed. Below room temperature, for continuous annealing an electric heater was used to warm the sample and maintain it at the desired temperature while the optical spectrum was recorded. For an isochronal annealing, the optical spectrum was recorded at 77K; then an immersion heater was used to quickly warm the sample to the desired temperature which was maintained

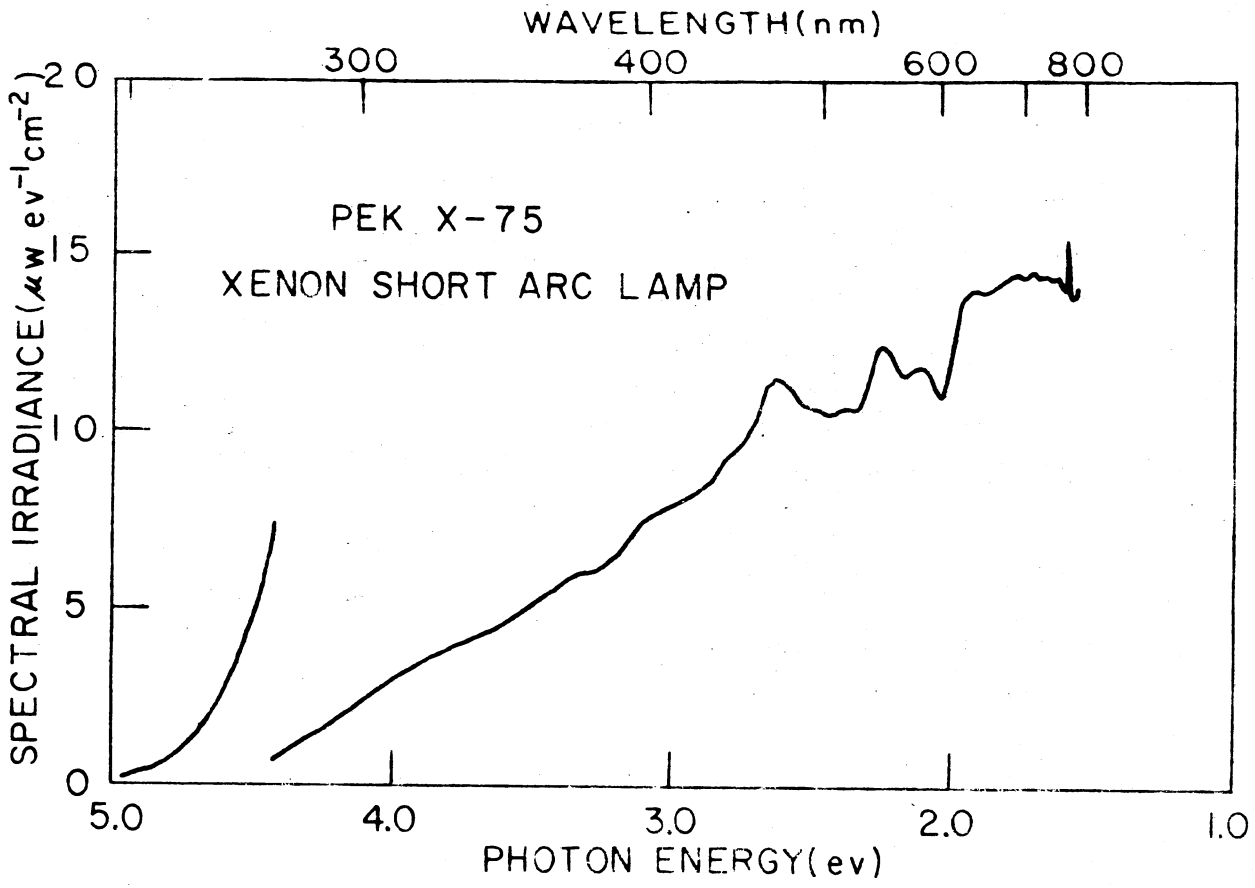

Figure 8. Spectral Output of PEK-75 Xenon Short Arc Lamp as a Function of Photon Energy

for ten minutes. Then, the sample was quenched back to 77^{o}K and again the optical spectrum recorded.

Above room temperature, a small furnace capable of holding the sample temperature constant up to 1300^{o}C was used. After the desired temperature was maintained for ten minutes, the sample was quenched back to room temperature and the optical spectrum was recorded.

Finally, optical bleaching was accomplished by either a 300W mercury lamp together with a notch filter transmitting light from 300-350 mm or without a filter.

CHAPTER IV

THEORY

A review of the theory involved in the work of this thesis is necessary before we advance to the experimental study.

Radiation Damage

When a polar crystal is subjected to radiation, numerous changes can occur in the perfect lattice and in the impurities present. The end products of these changes are classified in terms of three categories of defects.

1. Electronic defects involving changes in valence states.
2. Ionic defects consisting of displaced lattice ions.
3. Gross imperfections.

Electronic Defects

In this case the source of radiation products is twofold. Firstly, they arise because of the presence of impurities--present practically in all samples--whose valence states are changed by trapping electrons or holes created by radiation. Radiation induced valence changes have been studied in different crystals and have been reported for transition metal ions. A study of these changes can be performed with the use of optical and spin resonance techniques.

Secondly, hole charges can be trapped even in a portion of a per-

fect crystal. V_K centers $[X_2^-]$ are a typical example and a detailed account of them was given at a previous chapter.

Ionic Defects

These can be classified into vacancies, vacancy aggregates, interstitials and interstitial aggregates. In Chapter II a brief description of the nature of the vacancies and vacancy aggregates was given. An interstitial is an atom or an ion displaced from its normal site and remaining in a position which is not a normal lattice site. The only interstitial species produced in polar crystals by irradiation which has been carefully studied is an interstitial halide atom that has bonded itself to a lattice halide ion and shares that ion's lattice site. It was mostly studied in alkali halides and it is called the H center.

A definition and a distinction of the radiation damage processes is necessary before any other step is taken. There are three classes: electronic processes, elastic collision, and radiolysis.

Electronic Processes. These include all cases in which an electronic state is changed or charge is moved about by the absorption of radiant energy. No ionic or atomic defects are formed in these processes.

The initial step in the production of any electronic defect is the absorption of energy from the radiation field. A description of the mechanism is given below:

A heavy energetic particle passing through matter is stripped of some or all of its electrons and interacts as a point charge with the crystal's electrons. The energy loss per centimeter of path is obtained

from scattering experiments to be

$$\frac{dE}{dX} = (4\pi e^4 z^2 N_o Z/mv^2) \log (2 mv^2/I) \quad (3)$$

where e and m are the electron charge and mass, z and v are the irradiating particles charge and velocity, N_o is the atomic density of the crystal, Z is the number of electrons per atom and I is the average excitation potential of the crystal electrons. A relativistic correction will be needed for particles moving with velocities close to the speed of light. The energy loss of the irradiating particles equals the energy gain of the electrons of the crystal.

Electrons give up energy in a fashion similar to that of heavy particles with the only difference that in Eqn. (3) the log term should be corrected (relativistic correction).

A very important parameter in radiation damage is the penetration depth. It depends on the energy loss of the bombarding particles so it is of interest to compare the energy loss of heavy particles and electrons.

Consideration of the initial factor in Eqn. (3) suggests that the energy lost by a heavy particle is much greater than that for electrons. As a consequence of this, electrons will penetrate deep into crystals for which heavy particles are stopped near the surface.

Fast neutrons although they do not excite the crystal electronically because of their lack of charge, can, by imparting their kinetic energy to a crystal ion cause the ion to share its kinetic energy with crystal electrons and so produce electronic excitation indirectly.

Finally photons with energies in the range obtainable with x-rays or isotope sources can transfer their energy to the electronic system

of a crystal. Figure 9 gives the average distribution of energy of incident photons between scattered photons and scattering electrons (9).

The energy transferred to a thin section of a crystal by x-rays of a given wavelength is

$$\frac{dI}{dx} = \alpha I \rightarrow I_o e^{-\alpha x} \tag{4}$$

where α is the absorption coefficient and x is the distance from the surface (in the photoelectric process x-rays lose all their energy).

In case of γ-rays the high energy photons initiate a type of cascade that leads to relatively uniform energy deposition throughout fairly thick crystals.

The energy absorbed results in

(a) electrons occupying a normally empty conduction band

(b) holes in a normally occupied valence band

(c) excitons, i.e., electron hole pairs bound to each other at lattice ions, impurity ions or defects in the crystal

The electronic excitation is followed by separation of electrons and holes and subsequent trapping at impurities, defects or the perfect lattice. The electrical neutrality of the crystal requires that electrons and holes are always created in pairs.

Above certain temperatures these defects become unstable or mobile, recombining and giving different sets of electronic defects.

Elastic Collisions

The creation of defects through elastic collisions requires from the incident particle the input of sufficient energy to a lattice ion or atom so that the latter is moved to an interstitial position.

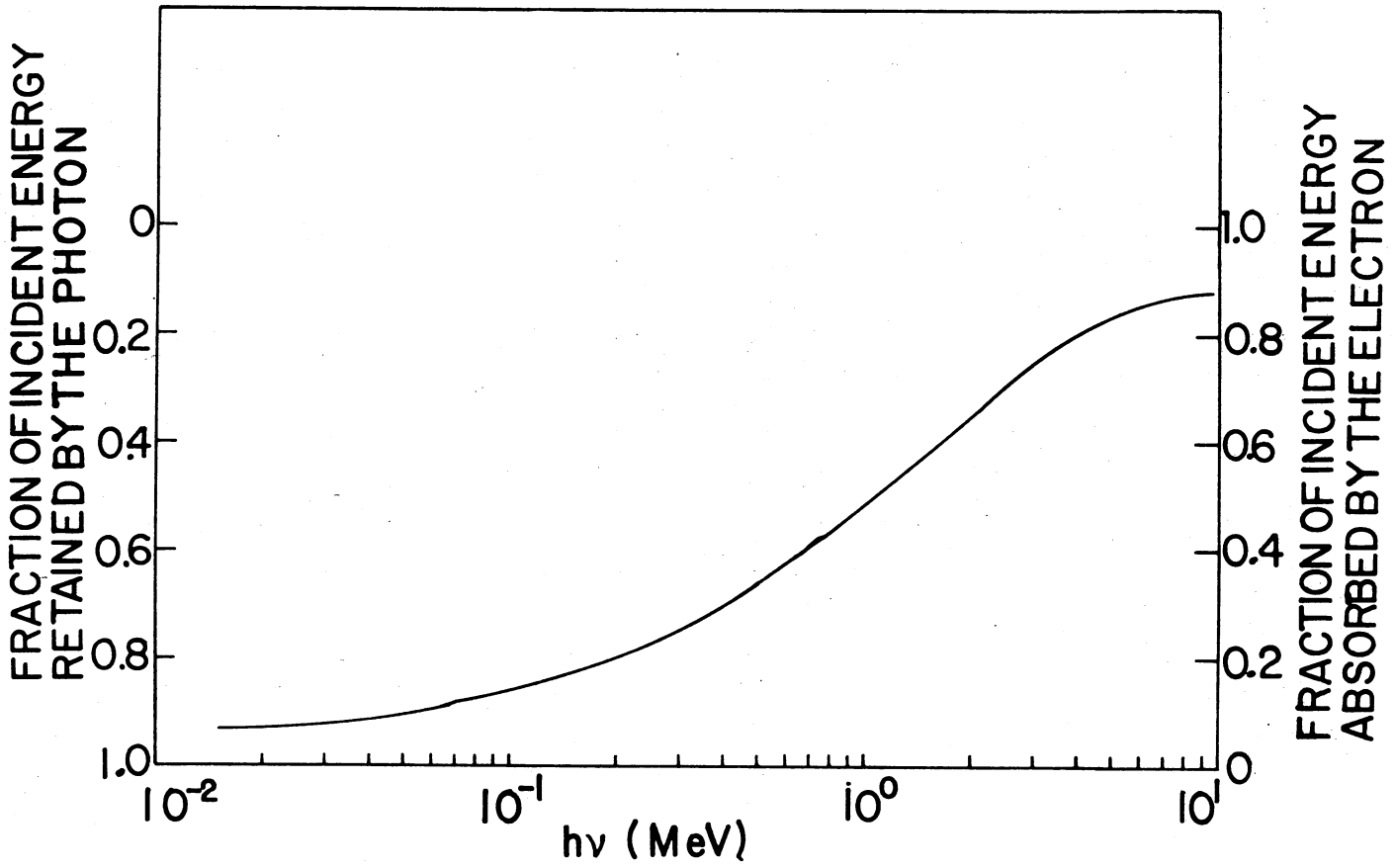

Figure 9. Average Distribution of Energy of Incident Photon Between Scattered Photon and Scattering Electron

The quantities characterizing the effectiveness of the incident particle appear in the equation

$$T_m = \frac{4 M_1 M_2 E}{(M_1+M_2)^2} \tag{5}$$

where T_m is the maximum kinetic energy that can be transferred to the lattice ion, M_1 is the mass of the incident particle, M_2 is the mass of the lattice ion and E is the energy of the incident particle.

A critical value for T_m is the displacement energy T_d which is the minimum energy required to displace a lattice atom between its nearest neighbors. For polar crystals a typical T_d value is 30 eV.

Table III shows the energy transfer between various irradiating particles and lattice ions.

Recently sufficient evidence (63) has shown that the threshold energy is strongly dependent on the crystallographic direction of the impinging electron beam and the direction of displacement of the ions. The existence of "channels" in a crystal helps a particle move to anomalous depths without much energy transfer to lattice ions or atoms.

Radiolysis

In certain ionic materials, defect creation is highly efficient and it is most likely due to the conversion of electronic excitation energy into a form capable of inducing lattice defects rather than collisions.

The three basic steps involved in a radiolysis produced defect are

(a) electron excitation resulting in a charged or polarized electronic defect in the crystal.

TABLE III

ENERGY TRANSFER BETWEEN VARIOUS IRRADIATING PARTICLES AND LATTICE IONS

Particle	Energy, MeV	T_m, eV			
		K	Cl	Mg	O
^{60}Co γ-ray	1.17	110	123	178	268
Cs γ-ray	0.667	41	46	67	101
Electron	1	110	121	179	269
	2	330	368	537	805
	14	11,500	12,000	19,000	28,000
	30	51,000	56,500	83,000	125,000
Proton	2	195,000	216,000	307,200	443,000
Neutron	2	195,000	216,000	307,200	443,000
Alpha Particle	6	2.0×10^6	2.2×10^6	2.9×10^6	3.8×10^6

(b) conversion of this energy into kinetic energy of an ion.

(c) motion and stabilization of the ion.

V_K centers play a major role in radiolysis and a detailed account of their properties was given in a previous discussion.

Optical Properties

The spectrum of an ion, in a condensed phase differs in a very important way from the free ion spectrum. The difference is in the width of the spectral region which corresponds to absorption or emission of energy as a result of transitions from one state to another. These regions are sharply defined for the free ions (~ 1 cm^{-1}) while the region corresponding to one electronic transition for the same ion embedded in a crystal range from this small up to a broad band with half intensity width of 10^3 cm^{-1}. Thus, the interpretation of the electronic spectroscopy of an anion--or a color center for that matter--involves principles concerned with electron-phonon coupling.

A brief theoretical account of the optical transitions in atoms and the basic principles of electron lattice interaction is presented below. If a monochromatic beam of N photons per unit volume, each of energy $\hbar\omega$, impinges upon an atom, the probability per unit time that the atom will make a transition from state m to state k is given by (4)

$$W_{mk} = \frac{4\Pi^2 e^2 |E_k - E_m|}{\hbar} N \left|\bar{\eta}\cdot\bar{r}_{km}\right|^2 \delta(|E_k - E_m| - \hbar\omega) \qquad (6)$$

where the electric dipole matrix r_{km} is defined as

$$r_{km} = \sum_s \int U_k^* r_s U_m \, d\tau \qquad (7)$$

The sum is over all the electrons, U_k and U_m are solutions of the time independent Schrödinger equation with energies E_m and E_k and the integral is over all the electronic coordinates. The polarization of the incident light is denoted by the vector $\bar{\eta}$.

The oscillator strength is a dimensionless tensor which in many cases reduces to a scalar quantity defined as (4)

$$f_{mk} = \frac{2m}{3\hbar} \omega_{km} |r_{mk}|^2 \tag{8}$$

where $\omega_{km} = \frac{E_k - E_m}{\hbar}$.

The absorption coefficient, defined as the energy removed per unit time per unit volume from a beam of unit intensity is given by the formula

$$\mu_{mk}(E) = \frac{W_{mk} N_A}{Nc} \tag{9}$$

where N_A is the number of ions per unit volume and c is the speed of light. The other quantities were defined before.

A very useful simple relation exists between the oscillator strength and the integrated absorption coefficient; namely,

$$N_A f_{mk} = \frac{mc}{2\pi^2 e^2 \hbar} \int \mu_{mk}(E) dE \tag{10}$$

Assume now that the atom--or the color center of interest is imbedded in a solid. The interaction of the electrons with the lattice will greatly influence the center. The most serious problem is that of accurately separating the motion of the electrons from that of the lattice. A qualitative description of a simple approximation would be

that the electron sees and responds to the instantaneous vibrations of the lattice, whereas the lattice responds only to the average positions of the electrons. In fact this description is the basis for the adiabatic (Born-Oppenheimer) approximation.

The Schrödinger equation for the solid may be written as

$$[T_e + T_N + U_{(r,R)}]\psi_{(r,R)} = E\psi_{(r,R)} \tag{11}$$

where T_e is the electronic kinetic energy, T_N is the nuclear kinetic energy and $U_{(r,R)}$ contains all of the potential energy, i.e., electron-electron, electron-nucleus and nucleus-nucleus. R refers to the nuclear and r to the electronic coordinates. Introducing a set of nuclear and electronic quantum number N,m, the wave function can be written, according to the adiabatic approximation as:

$$\psi_{mN}(\bar{r},\bar{R}) = \phi_{m,R}(\vec{r})\ \chi_{mN}(\vec{R}) \tag{12}$$

where $\phi_{m,R}(\vec{r})$ is the electronic and $\chi_{mN}(\vec{R})$ is the nuclear wave function. The dipole matrix element takes now the form

$$\bar{r}_{mN,kN'} = \int d\bar{r} \int d\bar{R}\ \chi^*_{mN}(\bar{R})\ \phi^*_{m,R}(\bar{r})\bar{r}\ \phi_{k,R}(\bar{r})\chi_{kN'}(\bar{R}) \tag{13}$$

or

$$\bar{r}_{mN,kN'} = \int d\bar{R}\ \chi^*_{mN}(\bar{R})\bar{r}_{km}(\bar{R})\ \chi_{kN'}(\bar{R}) \tag{14}$$

where

$$\bar{r}_{mk}(\bar{R}) = \int d\bar{r}\ \phi^*_{mR}(\bar{r})\bar{r}\ \phi_{kR}(\bar{r})\ .$$

A very simple and useful approximation is the Franck-Condon approxima-

tion which neglects the R dependence of r_{mk} by taking an average value of R corresponding to an equilibrium position R_o. In this case

$$\bar{r}_{mN,kN'} = \bar{r}_{mk}(\bar{R}_o) \int dR\, X^*_{mN}(\bar{R})\, X_{kN'}(\bar{R}) \tag{15}$$

The oscillator strength is written now as

$$f_{mN,kN'} = \left(\frac{2m}{3\hbar}\right) \omega_{mN,kN'} \left|\bar{r}_{mN,kN'}\right|^2 . \tag{16}$$

The broad band associated with an electronic transition must be considered to be an envelope determined by the associated vibrational states. The quantity of interest becomes the thermal average over the initial vibrational states and a sum over the final vibrational states. The average oscillator strength, taking into account Franck-Condon principle and the closure property (52) of the nuclear wavefunctions becomes

$$f_{mk} = \frac{2m}{3\hbar} W_{mk} \left|\bar{r}_{mk}(\bar{R}_o)\right|^2 \tag{17}$$

Similar arguments and comparison with the generalized absorption coefficient (52) lead to the well known Smakula's equation, which for a Gaussian shape band is

$$N_A f_{mk} = .87 \times 10^{-17}\ cm^{-3}\ \frac{n}{(n^2+2)^2}\ \alpha_{mk(max)}\ W_{mk} \tag{18}$$

where W_{mk} is the full width of the band at half maximum, n is the index of refraction of the material used and N_A corresponds now to the number of centers per unit volume.

The configuration coordinate scheme, suggested by the Born-Oppen-

heimer approximation emphasizes the qualitative features of the electron-phonon coupling.

According to this model, the electronic states of the defect are assumed to interact appreciably with only one symmetric normal mode. In the simplest version of this model, two non-degenerate electronic states, ψ_m and ψ_k of the defect are assumed to couple linearly to a single normal coordinate g of the lattice. In the assumption of the Born-Oppenheimer approximation the nuclear problem is reduced to that of solving for the vibrational states of the adiabatic potentials appropriate to the ground and excited electronic states. These potentials are

$$R_m = \frac{1}{2} M\omega^2 g^2 \quad \text{for the ground state} \tag{19}$$

$$E_k = \frac{1}{2} M\omega^2 g^2 + E_{mk} - A\hbar\omega\,(M\omega/\hbar)^{\frac{1}{2}} g \quad \text{for the excited state} \tag{20}$$

where the dimensionless constant A is a measure of the strength of the linear interaction which displaces the equilibrium position of the mode but does not change the frequency ω. M is the effective mass for this mode.

The same is true for the emission band which at low temperatures consists of a series of lines at

$$E_\mu = E_{mk} - S\hbar\omega + \mu\hbar\omega \tag{21}$$

mirrored about the zero phonon line. For S = 0, the spectrum is a single unbroadened line at the static lattice position, E_{mk}. For S > 0, the zero phonon line is displaced by an amount $S\hbar\omega$.

In those cases where the individual components of the line series are not resolved, it is convenient to describe the line shape by its moments. For a Gaussian band the second moment is related to the full width at half-maximum at T = 0 by

$$W_{\frac{1}{2}}^2(0) = 8 \ln 2 [M_2(0)]^{\frac{1}{2}} \qquad (22)$$

where $M_2(0) = S(\hbar\omega)^2$. At high temperatures

$$W_{\frac{1}{2}}^2(T) = 8 \ln 2 \, S\hbar^2\omega^2 \operatorname{csch} \frac{\hbar\omega}{2KT}$$

$$\simeq W_{\frac{1}{2}}^2(0) \coth \frac{\hbar\omega}{2KT} \qquad (23)$$

Polarized Bleaching

Polarized absorption and luminescence measurements are very powerful techniques for the identification of anisotropic defects. A detailed account of the theoretical calculations has been given in the past by Feofilov (51) and Fowler (52). A brief review for the calculations will be given below. For the sake of simplicity and clarity, a cubic lattice will be used but the principles can be applied to every lattice.

Figure 3 is a schematic of the orientation of different types of defects in a cubic lattice. The major electric dipole axis is designated σ, the dipole axis perpendicular to σ but in the same (100) plane is designated by π_1 and the dipole axis perpendicular to both of the above mentioned directions is labeled π_2. σ, π_1, π_2 form a right handed coordinate system.

In the case of absorption, when incident light is polarized along

a direction $\hat{\mu}$, the interaction of this light with the various defect configurations r_i^B, where B is σ, π_1, π_2 results in an absorption coefficient given by (52)

$$a_{\hat{\mu}} = \bar{\sigma}\Sigma n_i |\hat{\mu}\cdot\hat{r}_i^{\sigma}|^2 + \bar{\pi}_1 \Sigma n_i |\hat{\mu}\cdot\hat{r}_i^{\pi_1}|^2 + \bar{\pi}_2 \Sigma n_i |\hat{\mu}\cdot\hat{r}_i^{\pi_2}|^2 \qquad (24)$$

Here $\bar{\sigma}$, $\bar{\pi}_1$, $\bar{\pi}_2$ are factors unique to the dipole axes and contain several constants, n_i is the number of centers whose major axis lies along one of the orientations shown in Fig. 3. The results of this type of calculation are shown in Table IV for light propagating along <100> and <110> directions.

The optical anisotropy is defined as

$$A_{100} = a_{100} - a_{010} = -A_{010}$$

$$A_{110} = a_{110} - a_{1\bar{1}0} = -A_{1\bar{1}0}$$

and so the results at the bottom of Table IV follow immediately. For the case in which we have a random orientation of centers ($\mu_i = \bar{n}$) the absorption is isotropic and $A_{\mu} \equiv 0$.

In cubic crystals containing anisotropic defects such as F_2, F_3 or $[X_2^-]$ (V_K) centers, it is possible to produce a preferred orientation of the centers causing the absorption by bleaching with polarized light and thus give a macroscopic optical anisotropy. Two experiments are sufficient to determine whether the optical dipoles are oriented parallel to <100>, <110> or <111> directions. If anisotropies are produced in the spectra taken with [110] and [1$\bar{1}$0] light after orientation with [110] light, the dipoles may be oriented along <110> or <111>

TABLE IV

ABSORPTION COEFFICIENT FOR LINEARLY POLARIZED LIGHT AS A FUNCTION OF CENTER ORIENTATION

Type of Center	<100>	<110>	<111>
$\alpha_{100}(\varepsilon)$	$\sigma(\varepsilon)[n_1]$ $+\frac{1}{2}\pi(\varepsilon)[n_2 + n_3]$	$\frac{1}{2}\sigma(\varepsilon)[n_1 + n_2 + n_5 + n_6]$ $+\frac{1}{2}\pi_1(\varepsilon)[n_1 + n_2 + n_5 + n_6]$ $+ \pi_2(\varepsilon)[n_3 + n_4]$	$\frac{1}{3}\sigma(\varepsilon)[n_1 + n_2 + n_3 + n_4]$ $+\frac{1}{3}\pi_1(\varepsilon)[n_1 + n_2 + n_3 + n_4]$ $+\frac{1}{3}\pi_2(\varepsilon)[n_1 + n_2 + n_3 + n_4]$
$\alpha_{010}(\varepsilon)$	$\sigma(\varepsilon)[n_2]$ $+\frac{1}{2}\pi(\varepsilon)[n_1 + n_3]$	$\frac{1}{2}\sigma(\varepsilon)[n_1 + n_2 + n_3 + n_4]$ $+\frac{1}{2}\pi_1(\varepsilon)[n_1 + n_2 + n_3 + n_4]$ $+\pi_2(\varepsilon)[n_5 + n_6]$	$\alpha_{100}(\varepsilon)$
$\alpha_{110}(\varepsilon)$	$\frac{1}{2}\sigma(\varepsilon)[n_1 + n_2]$ $+\frac{1}{4}\pi(\varepsilon)[n_1 + n_2 + 2n_3]$	$\sigma(\varepsilon)[n_1 + \frac{1}{4}(n_3 + n_4 + n_5 + n_6)]$ $+ \pi_1(\varepsilon)[n_2 + \frac{1}{4}(n_3 + n_4 + n_5 + n_6]$ $+\frac{1}{2}\pi_2(\varepsilon)[n_3 + n_4 + n_5 + n_6]$	$\frac{1}{6}\sigma(\varepsilon)[n_1 + n_2 + 3n_3 + 3n_4]$ $+ \frac{1}{6}\pi_1(\varepsilon)[n_1 + n_2 + 3n_3 + 3n_4]$ $+ \frac{2}{3}\pi_2(\varepsilon)[n_1 + n_2]$
$\alpha_{1\bar{1}0}(\varepsilon)$	$\alpha_{110}(\varepsilon)$	$\sigma(\varepsilon)[n_2 + \frac{1}{4}(n_3 + n_4 + n_5 + n_6)]$ $+ \pi_1(\varepsilon)[n_1 + \frac{1}{4}(n_3 + n_4 + n_5 + n_6]$ $+ \frac{1}{2}\pi_2(\varepsilon)[n_3 + n_4 + n_5 + n_6]$	$\frac{1}{6}\sigma(\varepsilon)[3n_1 + 3n_2 + n_3 + n_4]$ $+\frac{1}{6}\pi_1(\varepsilon)[3n_1 + 3n_2 + n_3 + n_4]$ $+\frac{2}{3}\pi_2(\varepsilon)[n_3 + n_4]$
$A_{100} \equiv -A_{010}$	$[\sigma(\varepsilon) - \frac{1}{2}\pi(\varepsilon)][n_1 - n_2]$	$[\frac{1}{2}\sigma(\varepsilon) + \frac{1}{2}\pi_1(\varepsilon) - \pi_2(\varepsilon)][n_5 + n_6 - n_3 - n_4]$	
$A_{100} \equiv A_{1\bar{1}0}$	0	$[\sigma(\varepsilon) - \pi_1(\varepsilon)][n_1 - n_2]$	$[\frac{1}{3}\sigma(\varepsilon) + \frac{1}{3}\pi_1(\varepsilon) - \frac{2}{3}\pi_2(\varepsilon)][n_3 + n_4 - n_1 - n_2]$

directions but not along <100> directions.

If anisotropies are produced in the spectra taken with [100] and [010] light after orientation with [010] light, then the dipoles may be oriented along <100> or <110> directions but not along <111> directions.

The intensity of polarized emission can be calculated by the following equation (52)

$$I_{ji} = p \sum_i n_i |\hat{r}_i^{B_1} \cdot \hat{U}_j|^2 \, |\hat{r}_i^{B_2} \cdot \hat{U}_\ell|^2 \qquad (25)$$

where p is a constant, ℓ and j are the polarization of the excitation and emission respectively and U_j and U_ℓ are the polarization of the light.

When polarized emission and absorption data are available, an intercomparison of the two sets of data allows a determination of the defect population of the orientations shown in Fig. 3.

Crystal Field Theory

The term ligand field theory has been employed to cover all aspects of the manner in which an ion or atom is influenced by its nearest neighbors. In the most general model, the electrons of a central ion are subject to a potential not necessarily of simple electrostatic origin from the ligand atoms. Crystal field is contained as a special case in which the ligands are treated as structureless, orbital-less point charges which set up an electrostatic field.

The properties of the set of five d orbitals are very essential to the crystal field theory of transition metal ions. In this section, it will be shown how the crystal field model leads to a differentiation

of the five degenerate d orbitals into two subshells when they are placed in an octahedral environment.

Assume an atom, surrounded by six negative point charges located at the vertices of a regular octahedron. The distance from the origin, occupied by the hydrogen atom to each negative charge is a.

The potential which arises from the octahedron of charges is given by

$$V(x,y,z) = \sum_{i=1}^{6} V(i,x,y,z) = \sum_{i=1}^{6} eZ_i/r_{ij} \qquad (26)$$

with r_{ij} denoting the distance from the ith charge to the point (x,y,z). An expansion of the inverse of the distance r_{ij} is available in terms of spherical harmonics centered upon the origin of the coordinated system.

$$\frac{1}{r_{ij}} = \sum_{n=o}^{\infty} \sum_{m=-n}^{n} \frac{4\pi}{2n+1} \frac{r_<^n}{r_>^{n+1}} Y_{n_j}^{m} Y_{n_i}^{m*} \qquad (27)$$

Here the distance $r_<$ is the lesser of the distances from the origin to the point i. Since on this crystal field model it is the potential within the octahedron which is of interest, the distance $r_>$ can be written a α and $r_<$ as r. Consequently, eqn. (26) can be put in the form

$$V(x,y,z) = \sum_{i=1}^{6} eZ \left(\sum_{n=o}^{\infty} \sum_{m=-n}^{n} \frac{4\pi}{2n+1} \frac{r^n}{\alpha^{n+1}} Y_n^m Y_{n_i}^{m*} \right) \qquad (28)$$

Since the six charges are located on the coordinate axes, the angles θ_i and ϕ_i which specify them are all O, $\pm \pi/2$ or π and the functions $Y_{n_i}^{m*}$ reduce to simple numbers.

The contribution from the terms with n = odd in V(x,y,z) are not

necessary because θ_n^m is an odd function ($Y_\ell^{m_\ell} = \theta_\ell^{m_\ell} \phi_{m_\ell}$) and:

$$\int_o^\pi \theta_\ell^{m_\ell} \theta_n^m \theta_\ell^{m_\ell *} = 0 \text{ being an integral of odd functions .} \qquad (29)$$

This means that the odd spherical harmonics in V_{oct} do not interact with the d or other orbitals.

Considering the summation term by term

$$n = o,\ m = o \quad \sum_{i=1}^{6} eZ \frac{4\pi}{a} Y_o^o Y_{o_i}^{o*} = \frac{6Ze}{a} \qquad (30)$$

$$n = 2,\ m = o \quad Y_{2_i}^{o*} = (5/8)^{\frac{1}{2}} (2\pi)^{-\frac{1}{2}} (3\cos^2\theta_i - 1)$$

For the points at $(\pm a,o,o)$ and $(o, \pm a,o)$ $\theta_i = \frac{\pi}{2}$, $(3\cos^2\theta_i - 1)^2 = -1$

For the point at (o,o,a) $\theta_i = O$, $(3\cos^2\theta_i - 1) = 2$

For the point at $(o,o,-a)$ $\theta_i = \pi$, $(3\cos^2\theta_i - 1) = 2$

The summation over the six points yields zero.

$$n = 2,\ m = \pm 1,\ Y_{2_i}^{\pm 1 *} = Y_{2_i}^{\mp 1} = (15/4)^{\frac{1}{2}} (2\pi)^{-\frac{1}{2}} \cos\theta_i \sin\theta_i e^{\mp i\phi_i}.$$

For each point $\cos\theta_i \sin\theta_i = O$, so the contribution is zero.

$n = 2,\ m = \pm 2,\ Y_{2_i}^{\mp 2 *} = Y_{2_i}^{\pm 2} = (5/16)^{\frac{1}{2}} (2\pi)^{-\frac{1}{2}} \sin^2\theta_i e^{\pm 2i\phi_i}$. The total contribution is zero.

$n = 4,\ m = o \quad Y_{4_i}^{o*} = Y_{4_i}^{o} = (9/128)^{\frac{1}{2}} (2\pi)^{-\frac{1}{2}} p_4^o(\cos\theta_i)$. The total con-

tribution comes out to be

$$(4\pi/9)(2\pi)^{-\frac{1}{2}}\ (Zer^4/a^5)(9/128)^{\frac{1}{2}}\ (2 \times 8 + 4 \times 3)\ Y_4^o$$

The contributions from n=4, m = ±1, ±2, ±3 are found to be zero. For n = 4, m = ±4

$$Y_{4_i}^{\pm 4*} = Y_{4_i}^{\mp 4} = (315/256)^{\frac{1}{2}}(2\pi)^{-\frac{1}{2}} \sin^4\theta_i\ e^{\mp 4i\phi_i}$$

and the contribution is

$$(4\pi/9)(2n)^{-\frac{1}{2}}(Zer^4/a^5)(315/256)^{\frac{1}{2}}\ 4Y_4^{\pm 4}$$

The total contribution to V(x,y,z) from n = 4 is

$$(49/18)^{\frac{1}{2}}(2n)^{\frac{1}{2}}(Zer^4/a^5)\ \left[Y_4^o + (5/14)^{\frac{1}{2}}(Y_4^4 + Y_4^{-4})\right] \qquad (31)$$

There is no need of expansion to higher terms in the spherical harmonics since

$$\int_o^{\pi}\int_o^{2\pi} Y_n^{m*}\ Y_{n'}^{m}\ Y_n^m\ \sin\theta\ d\theta\ d\phi = o \text{ if } n' > 2n$$

The potential required is then

$$V(x,y,z) = \text{Eqn. (30)} + \text{Eqn. (31)}$$

It is necessary to evaluate the matrix elements

$$\langle R_{n,\ell}\ Y_\ell^{m_\ell} | V_{oct} | R_{n',\ell'}\ Y_{\ell'}^{m_{\ell'}} \rangle \qquad (32)$$

The portion of the potential which arises from Eqn. (30) is independent

of the wave functions chosen and consequently it corresponds to an identical change in the energy of all the free d orbitals. This term is not considered further since only changes taking place in the relative energies of the different d orbitals are of interest.

In evaluating the matrix elements, r may be integrated out immediately via

$$\langle R_{n,2} | r^4 | R_{n,2} \rangle = \langle r^4 \rangle \tag{33}$$

The calculation of the matrix elements is straight forward and the nonvanishing elements are

$$\langle R_{n,2}\ Y_2^0 | V_{oct} | R_{n,2}\ Y_2^0 \rangle = Ze/a^5 \langle r_{n2}^4 \rangle \tag{34}$$

$$\langle R_{n,2}\ Y_2^{\pm 1} | V_{oct} | R_{n,2}\ Y_2^{\pm 1} \rangle = -\ 2/3\ Ze/a^5 \langle r_{n2}^4 \rangle \tag{35}$$

$$\langle R_{n,2}\ Y_2^{\pm 2} | V_{oct} | R_{n,2}\ Y_2^{\pm 2} \rangle = 1/6\ Ze/a^5 \langle r_{n2}^4 \rangle \tag{36}$$

$$\langle R_{n,2}\ Y_2^{\pm 2} | V_{oct} | R_{n,2}\ Y_2^{\mp 2} \rangle = 5/6\ Ze/a^5 \langle r_{n2}^4 \rangle \tag{37}$$

Defining $D = 35Ze^2/4a^5$, $q = 2/105 \langle r_{n2}^4 \rangle$, one can find the energies of the perturbed system by solving the secular determinant

	$\lvert R_{n,2}\, Y_2^2\rangle$	$\lvert R_{n,2}\, Y_2^1\rangle$	$\lvert R_{n,2}\, Y_2^o\rangle$	$\lvert R_{n,2}\, Y_2^{-1}\rangle$	$\lvert R_{n,2}\, Y_2^{-2}\rangle$
$\langle R_{n,2} Y_2^2 \rvert$	Dq-E	0	0	0	5 Dq
$\langle R_{n,2} Y_2^1 \rvert$	0	-4 Dq-E	0	0	0
$\langle R_{n,2} Y_2^o \rvert$	0	0	6 Dq-E	0	0
$\langle R_{n,2} Y_2^{-1} \rvert$	0	0	0	-4 Dq-E	0
$\langle R_{n,2} Y_2^{-2} \rvert$	5 Dq	0	0	0	Dq-E

This determinant can be reduced to the determinant

$$\begin{vmatrix} Dq-E & 5\ Dq \\ 5\ Dq & Dq-E \end{vmatrix} = 0$$

and to E = -4 Dq, E = 6 Dq. Solving the determinant we find the energies E = -4 Dq and E = 6 Dq. From this determinant the following secular equations can be obtained:

$$(Dq-E)C_2 + 5\ Dq\ C_{-2} = 0$$

$$5\ Dq\ C_2 + (Dq-E)\ C_{-2} = 0$$

On substituting

$$E = -4Dq$$

we have

$$-C_{-2} = C_2$$

So the wave function corresponding to the energy E = -4Dq is:

$$|\psi\rangle = C_2[|R_{n,2}\ Y_2^2\rangle - |R_{n,2}\ Y_2^{-2}\rangle] \tag{38}$$

The normalization condition require that $C_2 = C_{-2} = \frac{1}{\sqrt{2}}$ which gives for $\psi = d_{xy}$. Similarly for E = 6Dq, the corresponding wave function is $\psi = d_{x^2-y^2}$, so collecting all the eigenvalues we find that

for $E = -4Dq$ — d_{xy}, d_{yz}, d_{xz} (39)

for $E = 6\ Dq$ — d_{z^2}, $d_{x^2-y^2}$ (40)

The d orbitals of an atom are split into doubly degenerate and triply degenerate levels in an octahedral crystal field.

Dq is defined so that the separation between the two sets of split orbitals is 10 Dq.

Group Theoretical Considerations

By using the set of five d wave functions as a basis for a representation of the point group of a particular environment it is possible to determine the manner in which the set of d orbitals is split by the environment.

The characters of the reducible representation can be obtained from

(75)

$$X(\alpha) = \frac{\sin(\ell + \frac{1}{2})\alpha}{\sin \alpha/2} \tag{41}$$

The calculation of the characters is simple and the representation obtained Γd is reducible to

$$\Gamma d = E_g + T_{2g} \tag{42}$$

i.e., the five-fold degenerate d wavefunctions in a free ion are split into a triply degenerate set t_{2g} and a doubly degenerate ℓ_g.

Weak and Strong Field Discussion

The general problem in the examination of the effect of a crystal field on a polyelectron configuration is to set up the secular determinant whose Hamiltonian is

$$H = -\frac{\hbar^2}{2m}\Sigma\nabla_i^2 - \sum_i \frac{Ze^2}{r_i} + \frac{1}{2}\sum_{i\neq j}\frac{e^2}{r_{ij}} + \Sigma\zeta_i(\bar{r})\bar{\ell}\cdot\bar{S} + U \tag{43}$$

where the summation is over all the optical electrons. The first term is the sum of the kinetic energies of the electrons, the second term is the potential energy of the electrons, the third term represents the coulombic repulsion between the electrons, the fourth term the spin-orbit coupling and the last term is the crystal field.

As a consequence of the spin of an electron there is a magnetic moment associated with it. The electron is in motion around the nucleus with velocity $\bar{v}$ and consequently there is a magnetic field associated with this motion. The interaction between this field and the magnetic

dipole of the spinning electron is expressed in a final form which gives the spin-orbit energy as

$$\varepsilon = \zeta \bar{S} \cdot \bar{\ell} \ . \tag{44}$$

This result is correct for a one electron atom, and for many electron atoms the spin-orbit interaction is usually approximated as a sum

$$\sum_i \zeta \bar{S}_i \cdot \bar{\ell}_i \tag{45}$$

The observable effect of the spin-orbit interaction is simply to couple orbital and spin angular momenta, so that neither is a good quantum number. Instead, the resultant of these, called J, the total angular momentum has to be used.

The approach to this problem starts with the introduction of the approximation that the crystal field is a perturbation small compared to the electronic repulsion effects within the configuration but large compared to spin-orbit coupling, i.e.

$$\zeta(\bar{r}) \bar{\ell} \cdot \bar{S} \ \langle U \rangle \ \frac{e^2}{r_{ij}} \tag{46}$$

This is the weak field approximation. The crystal field sorts out the various wave functions of a free ion term without altering them.

The qualitative features of the crystal field splittings due to an octahedral field are most simply obtained by group theory. By applying (41) to the states composed by (d^n) electrons:

$$S \rightarrow A_1$$

$$P \rightarrow T_1$$

$$D \rightarrow E + T_2$$

$$F \rightarrow A_2 + T_1 + T_2$$

$$G \rightarrow A_1 + E + T_1 + T_2$$

$$H \rightarrow E + 2T_1 + T_2$$

The splitting of a free ion term is completely analogous to the splitting of a one electron orbital.

The strong crystal field is introduced by the assumption that the interelectronic repulsions act as perturbations to the crystal field, i.e.,

$$U(r) > \frac{e^2}{r_{ij}} \tag{47}$$

For the case of d electrons, a strong field configuration is obtained by assigning each d electron to either a t_{2g} or an e_g orbital in an octahedral environment. Thus, if there are n electrons assigned to t_{2g} orbitals and m to e_g orbitals, the strong field configuration is

$$t_{2g}^n \; e_g^m$$

A d^4 configuration contains e^4, e^3t_2, $e^2t_2^2$, et_2^3, t_2^4.

Just as a free ion configuration is split into terms by intraelectronic repulsions, so by treating intraelectronic repulsions as perturbations on strong field configurations, these are also split in terms.

During a transition from the weak to the strong field limit a continuous change takes place with increasing Dq. Correlation diagrams show the behavior of the energy levels of an ion as a function of the strength of the interaction with an environment of a certain symmetry.

CHAPTER V

COLOR CENTER ABSORPTION AND EMISSION IN $RbMgF_3$

Experimental Data

V_K Centers

The absorption spectrum following a brief (< 60 sec) 1.5 MeV electron irradiation at 77K is shown in Fig. 10. The band occurring at 330 nm (3.76 eV) is present only at low temperatures and saturates after a very short irradiation time (< 60 sec).

Its behavior is almost identical with the behavior of the V_K absorption band in $KMgF_3$, the only difference being a small shift in the peak position.

However, the structure of $RbMgF_3$ is a hexagonal one and this causes some differences to appear in this material. From polarized absorption data for crystals cut with the $c_{//}$ and $c_{\perp}$ (c meaning the crystal axis which happens to be also the optic axis), one notices that when the electric vector $\vec{E}$ of the incoming light is oriented along the c axis $\vec{E}||C$, no absorption is evident at 330 nm. But when the electric vector is perpendicular to the c axis, $\vec{E}\perp C$, the absorption band is evident.

In addition, when the light is propagating along the c axis--which means that $\vec{E}$ is always perpendicular to it--no dichroism of the absorption band is observed. The band can be made dichroic in the last case by bleaching for one hour with 330 nm polarized light. Information

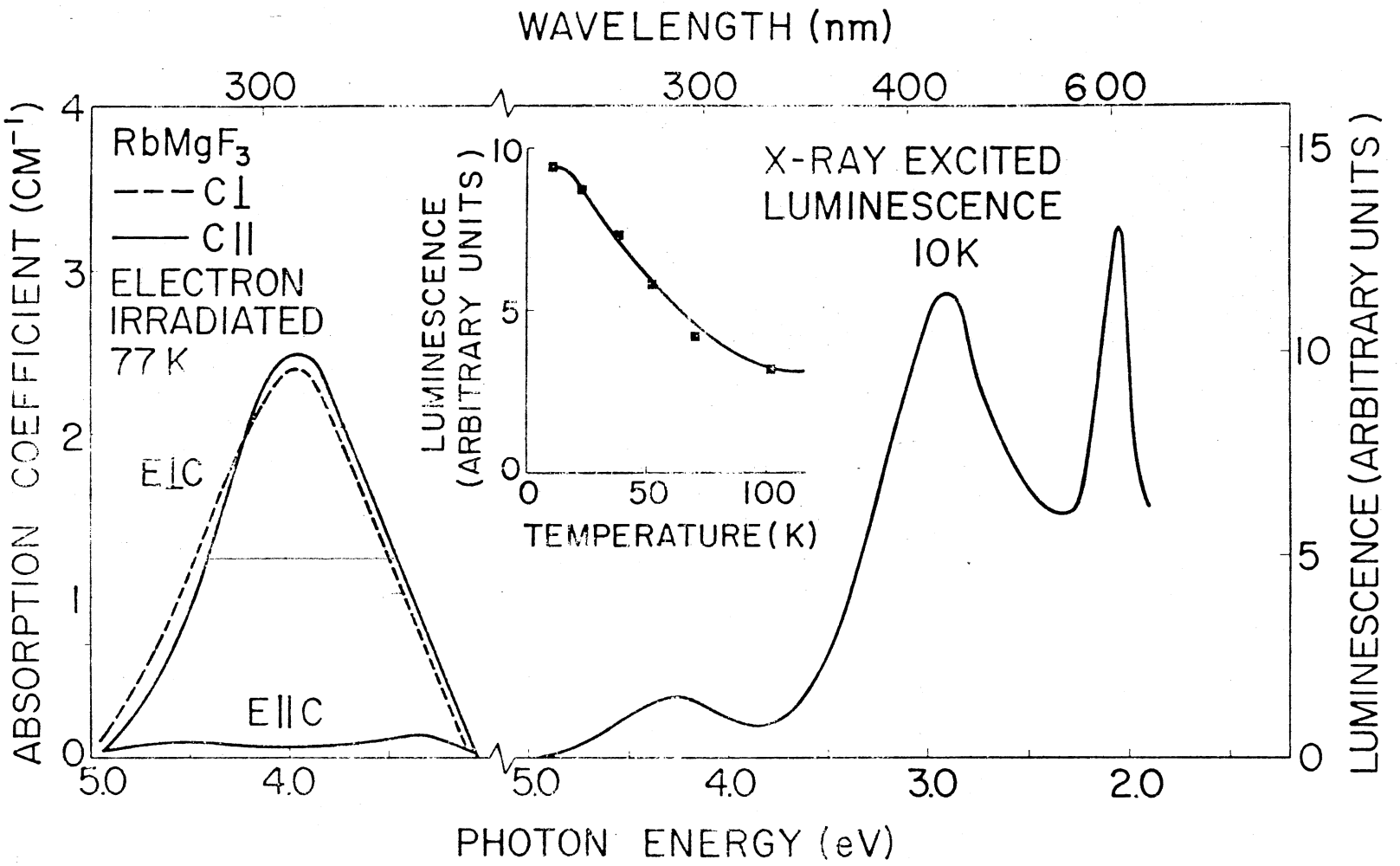

Figure 10. X_2^- (V_K) Absorption at 77K and x-ray Excited Luminescence at 10K. The Absorption Spectrum is Plotted for Different Electric Vector, E, Polarizations and Orientations, $c_{//}$ and $c_{\perp}$, of the Optic Axis. The Inset Shows the Temperature Dependence of the x-ray Excited Luminescence, ($c_{\perp}$ Indicates the c-axis is Perpendicular to the Crystal Face)

about the direction of polarization is contained in Fig. 1.

In Fig. 10 the x-ray excited luminescence of the V_K centers at 10K is also depicted. In general the interaction which produces the above luminescence is due to electrons and holes never completely escaping from the excited ion, so that the emission is produced by a recombination of the associated charges.

Three emission bands are present at 288 nm (4.3 ev), 428 nm (2.9 ev) and 600 nm (2.05 ev). The use of a filter to cut off all emitted light with energy greater than 3.4 ev shows that although there is some second order contribution at 600 nm from the 288 nm emission band, a 600 nm band exists. One would expect the emission to be polarized since the absorption is polarized. However, no polarization of the x-ray excited emission could be detected.

In $KMgF_3$, it was possible to detect the optically excited emission from V_K centers by shining light of such energy that electrons were released from their traps and their subsequent recombination with V_K centers would give off luminescence. In $RbMgF_3$ such emission was not detectable owing to the small concentration of V_K centers and to their very rapid reduction with the bleaching light.

The temperature dependence of the 428 nm emission is also shown in Fig. 10. The emission intensity quenches at approximately 80K. The further behavior is not shown in the figure but above 100K the intensity increases again.

A comparison of all the characteristics of the luminescence of the V_K centers in $KMgF_3$ together with the thermal annealing verify the fact that the bands in $RbMgF_3$ are indeed due to V_K centers.

Figure 11 portrays the isochronal annealing of the 330 nm absorp-

tion. The curves are drawn from data taken on $C_{\perp}$ samples which were bleached with light polarized along the directions indicated in the figure. One sees that these are two annealing stages for the V_K center at ~100K and 140K, which suggests that probably there are two types--at least--of V_K centers annealing out.

F Centers

When $RbMgF_3$ is irradiated at temperatures below 400K an absorption band is formed in addition to the 330 nm band just ascribed to V_K centers. This band is due to F center absorption, a conclusion derived by comparison with the position as well as other characteristics that will be mentioned in the following paragraphs of the F band in $KMgF_3$ and MgF_2. Due to the complexity of the structure ESR measurements were not carried out so far.

In Figure 12 the absorption of the F band is illustrated for crystals with $c_{\perp}$ and $c_{//}$ and with the electric vector $\vec{E}$ propagating along and perpendicular to the c axis. The crystals were irradiated at R.T. When inpolarized light is used to measure the absorption in a $c_{//}$ sample, an apparent reduction in the absorption coefficient of the band compared to that in a $c_{\perp}$ specimen results because of the polarization. A correction factor of 1.35 is sufficient to bring unpolarized measurements on $c_{//}$ and $c_{\perp}$ crystals into agreement. In the following discussion a derivation of this factor will be performed. One important fact is that in contrast with $KMgF_3$ room temperature irradiation of $RbMgF_3$ does not create any other optically detectable bands besides the F.

Figure 13 shows F center growth curves at different temperatures for samples with $c_{\perp}$ and $c_{//}$. It is interesting to see that the growth

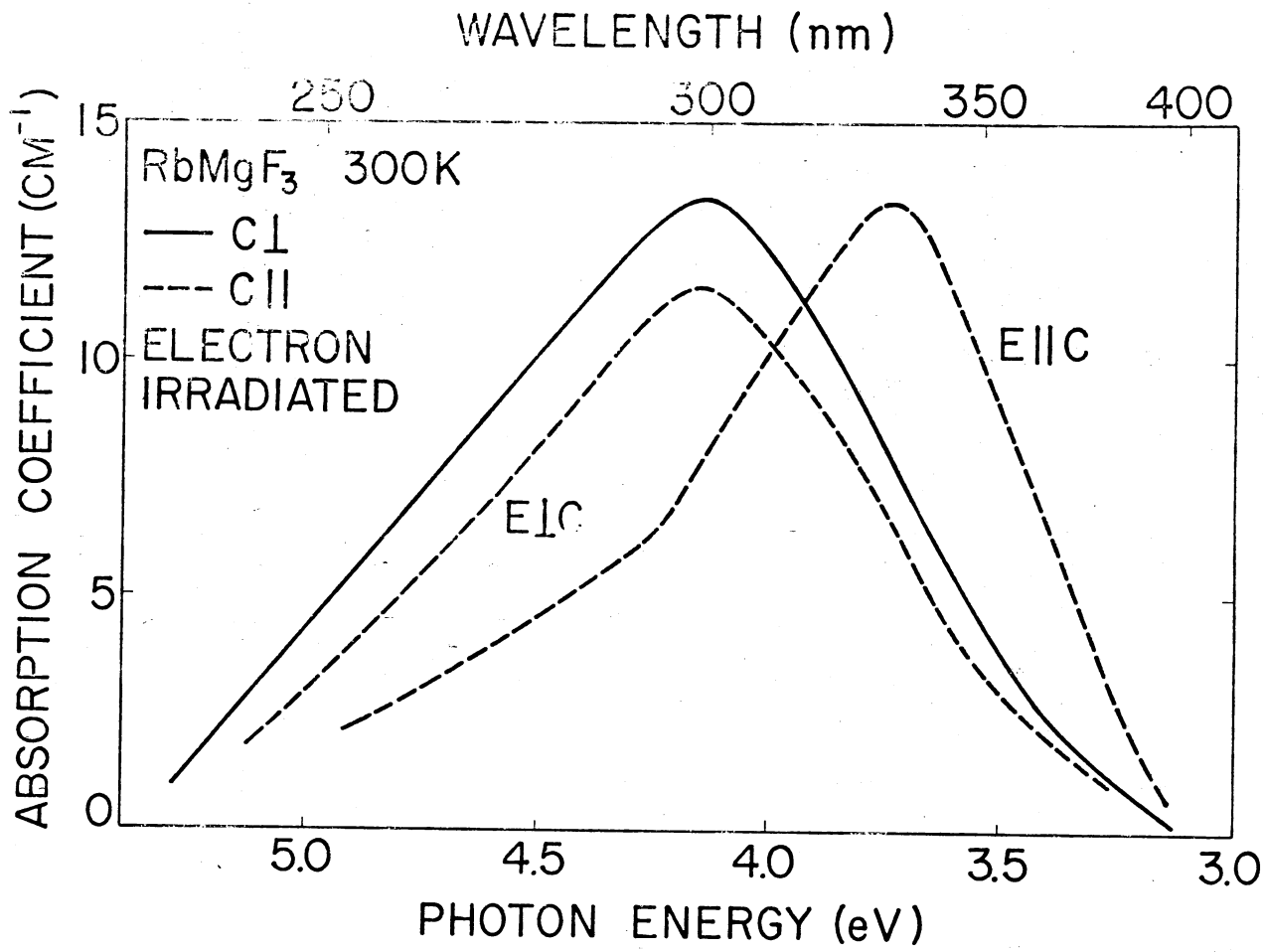

Figure 12. F Center Absorption Spectra for Different E Polariaztions and Orientations, $c_{//}$ and $c_{\perp}$, of the c Axis

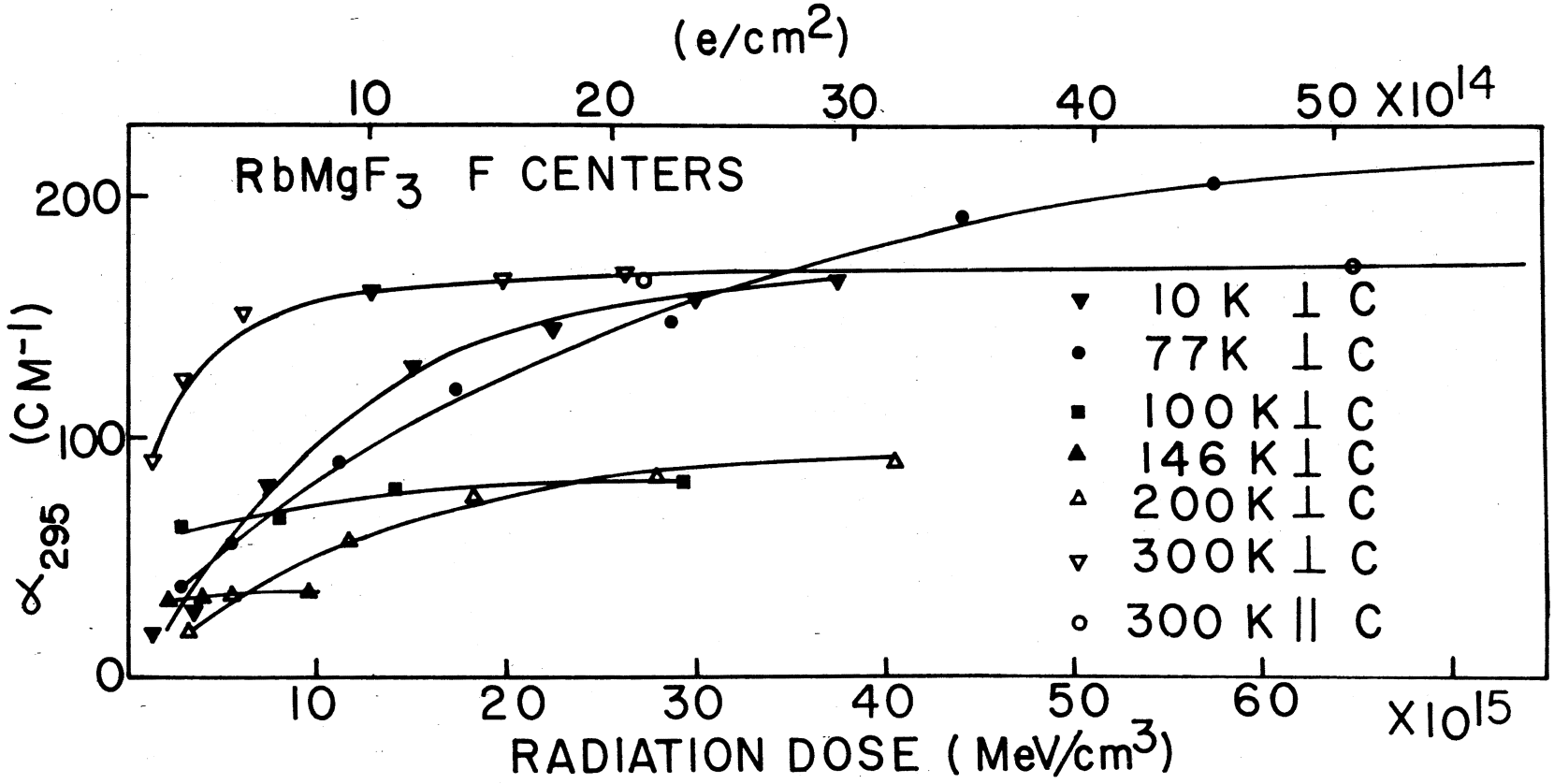

Figure 13. F Center Absorption, α, as a Function of Absorbed Energy for Crystals Electron Irradiated at Different Temperatures

curves go through a minimum between 140K and 200K. The growth curves for crystals with $c_{//}$ and for crystals with $c_{\perp}$ irradiated at the same temperatures are identical providing that the $c_{//}$ growth curve is multiplied by the 1.35 factor.

The results of an isochronal anneal of a sample electron irradiated at 300K and of sample very lightly irradiated (10^{15} Mev/cm^3) at 77K are shown in Fig. 14. The lightly irradiated sample had a very small concentration of F centers and the sudden drop at ~150K is probably due to recombination with V_K centers.

For the room temperature irradiated samples, there is a main annealing stage of the F centers accompanied by the growth of a band at ~550K and of a second band at ~670K whose growth follows the annealing of the at 550K grown in band.

A knowledge of the variation of the width at half maximum is a necessary step for the determination of parameters needed for the construction of a configuration coordinate diagram. So Fig. 15 portrays a plot of $\coth^{-1}[W^2(T)/W^2(10)]$ versus 1/T with W(300) = .92 ev and W(10) = .72 ev. The expression $W(T)^2 = W(^2 10) \coth h\nu_g/2KT$ gives a value for $\nu_g = 283$ cm^{-1} derived from the slope of the line. Also, from the relationship $W(10)^2 = S(h\nu)8 \ln 2$ a value of S = 78 is obtained for the Huang-Rhys factor (64). No emission band associated with the F absorption has been detected.

F_2 Centers

As mentioned before, the thermal annealing of the F band causes a new band to grow in at 550K. Actually, three new bands growing at 387 nm (3.2 ev), 285 nm (4.3 ev) and 230 nm (5.4 ev). From these only the

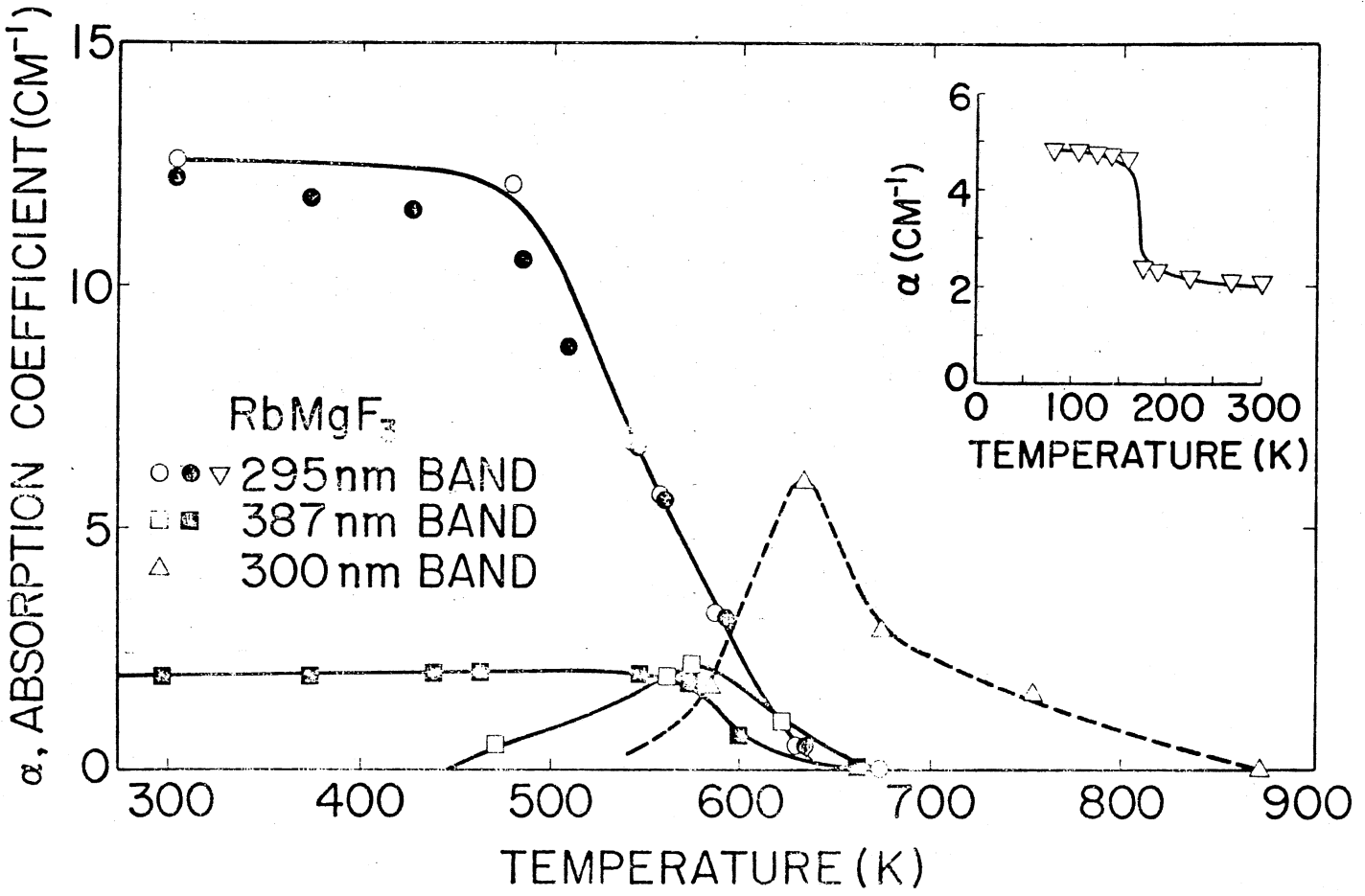

Figure 14. Thermal Annealing Curves for F, F_2 and F_3 Centers. The Inset Shows the Annealing Behavior of the F Center at Low Temperatures for a Light Dose (10^{15} MeV/cm^3) of Irradiation. The Full Squares Represent Data on a Sample Irradiated at 550K

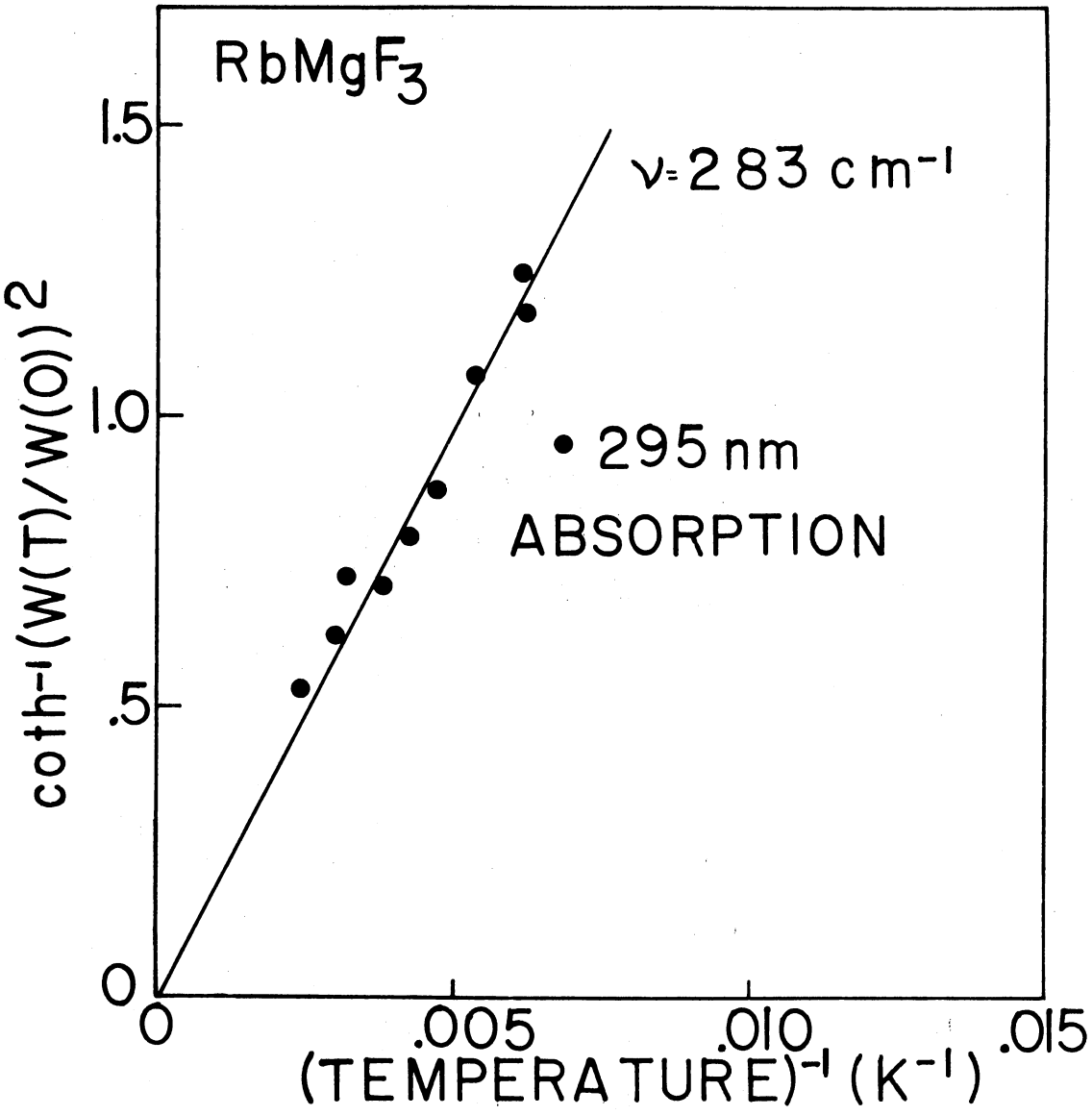

Figure 15. The Temperature Dependence of the Width at Half-Maximum, W, for F Absorption

387 nm band is shown in Fig. 13. Besides the thermal annealing of the F centers, other methods to form these bands are:

(a) Irradiation with 1.5 MeV electrons at 550K.

(b) Bleaching with 300 nm light at 400K of a crystal with previously introduced F centers.

The thermal annealing of this absorption band introduced by bleaching with F light at 400K is shown in Fig. 14.

The absorption at R.T. of a specimen irradiated at 300K and annealed at 575K for 30 minutes is shown in Fig. 16. This absorption is tentatively assigned to F_2 center absorption.

Polarized bleaching of these bands did not induce any kind of dichroism optically detectable. However, all the bands are polarized with the 387 nm band absorbing light with the electric vector $\vec{E} \perp C$ and the band at 230 nm absorbing light with the electric vector $\vec{E} \parallel C$. The band at 285 nm appears to be at most partially polarized with $\vec{E} \perp C$. The two other bands present at 300 nm and 320 nm are due to F centers.

Exciting with 387 nm light produces an emission band at 430 nm. This emission is associated with the M absorption and is shown in Fig. 17 at 10K. No polarization was observed. Actually, emission and absorption are portrayed at this temperature, showing a mirror symmetry about the zero phonon lines which are at the same energy for both.

The excitation spectrum of the 430 nm luminescence is shown in Fig. 18. The spectrum matches the absorption but the 230 band was not detectable because the xenon lamp has a very low intensity at this region.

The temperature variation of the width at half-maximum of the 387 nm absorption and 430 nm emission bands are shown in Fig. 19, where

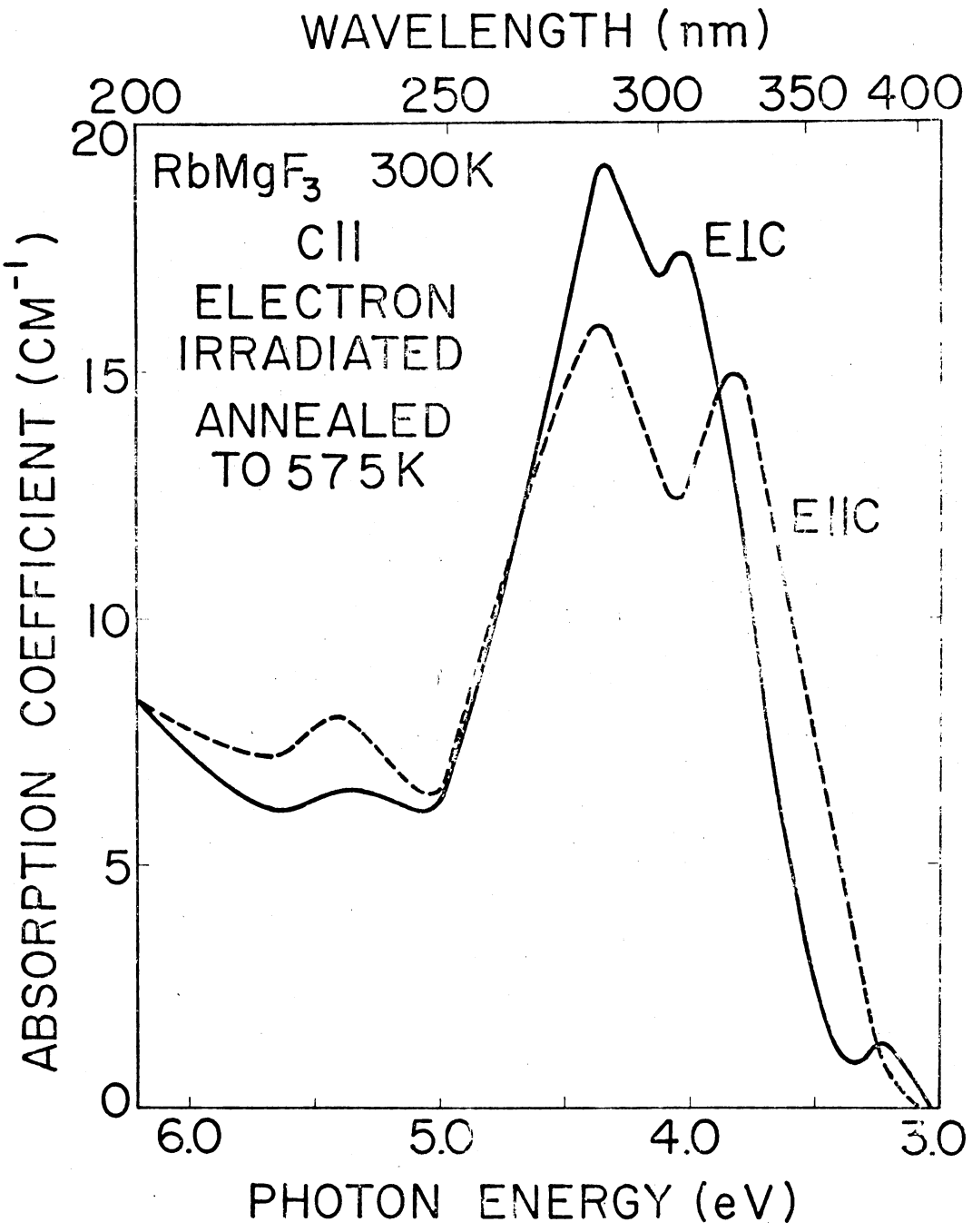

Figure 16. F_2 Center Absorption for Different E Polarizations of a Crystal Irradiated at 300K and Annealed at 575K for 30 Min. The Peaks at 300 nm and 320 nm are Due to F Centers

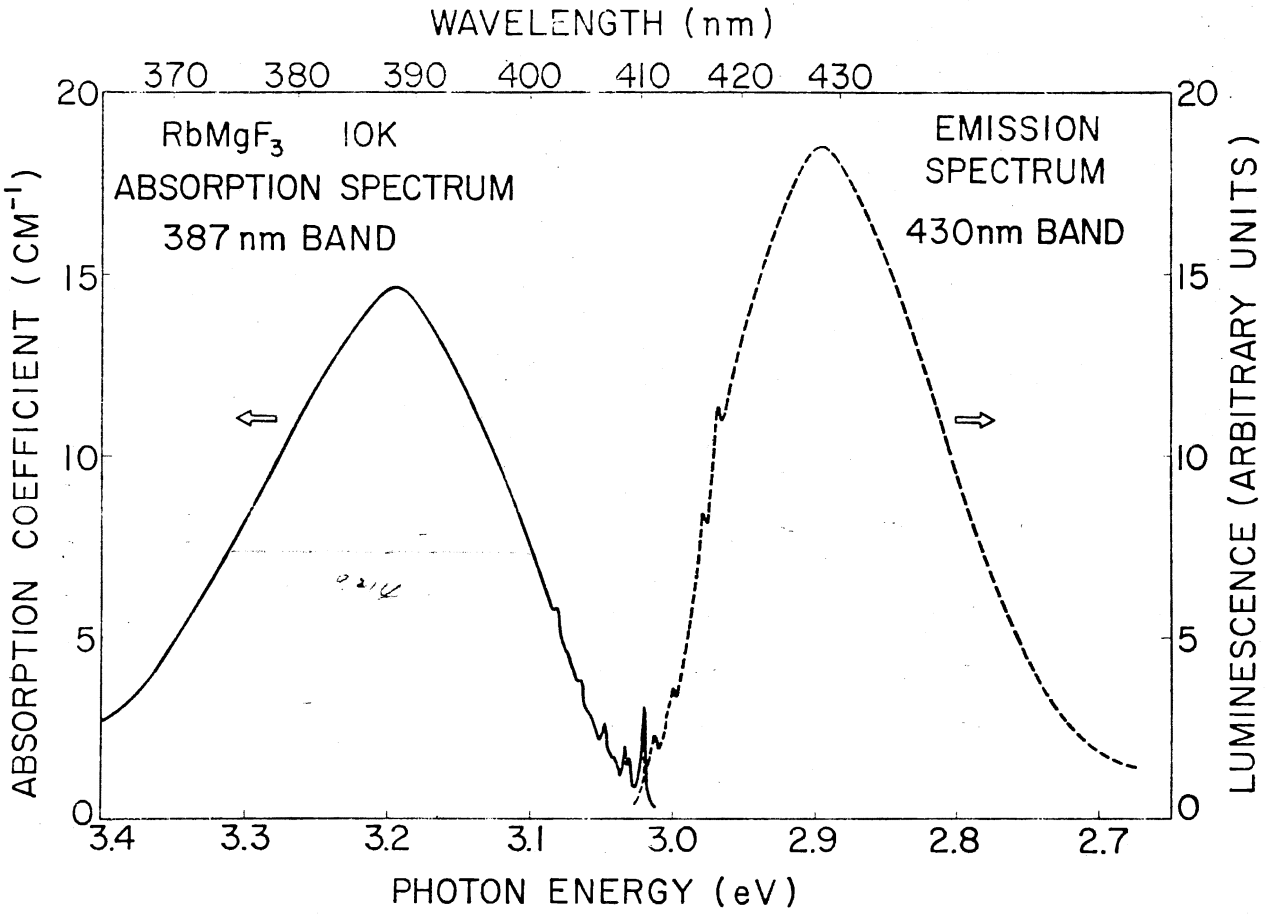

Figure 17. F_2 Center Absorption and Emission Bands in $RbMgF_3$ at 10K

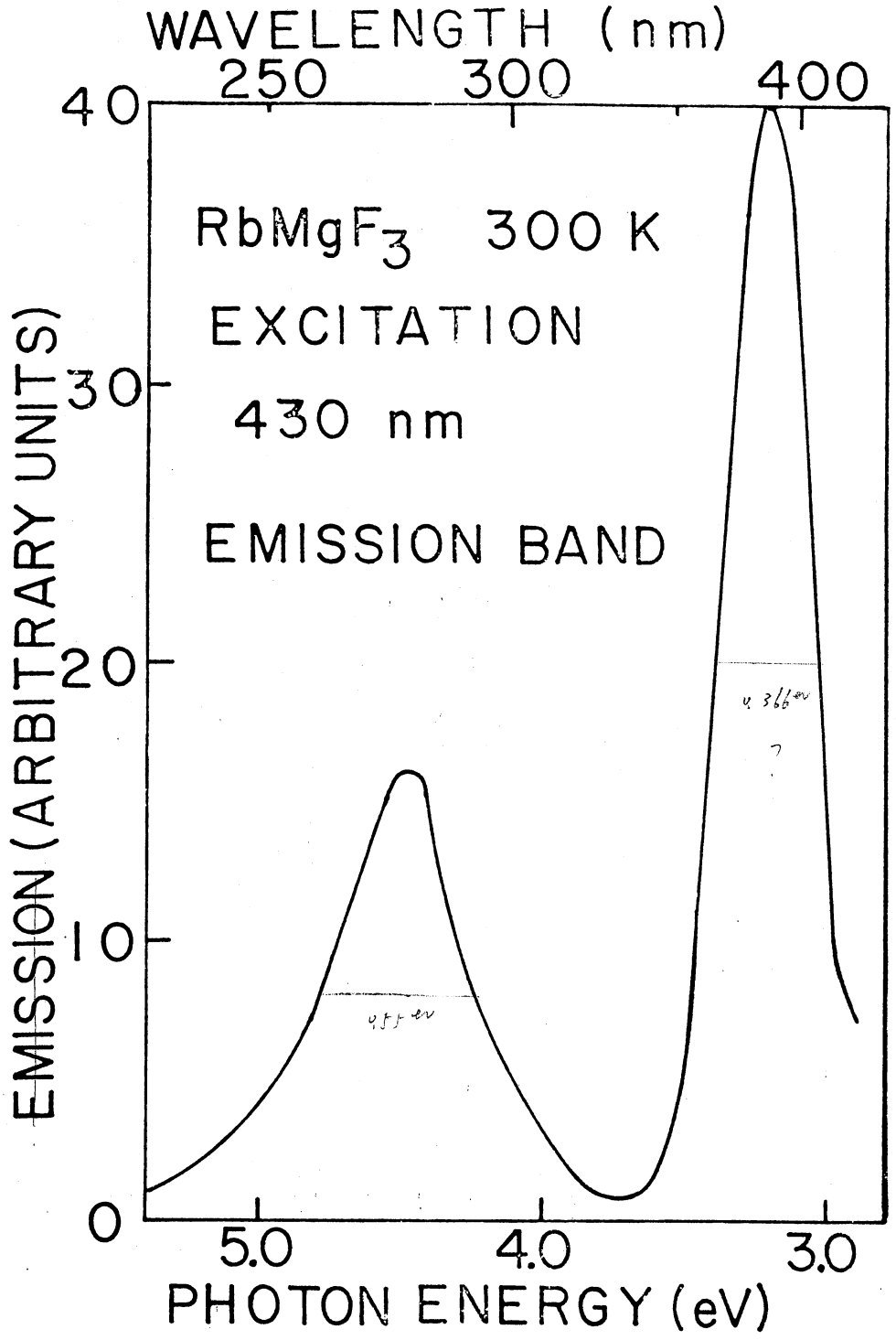

Figure 18. F_2 Center Excitation Spectrum at 300K

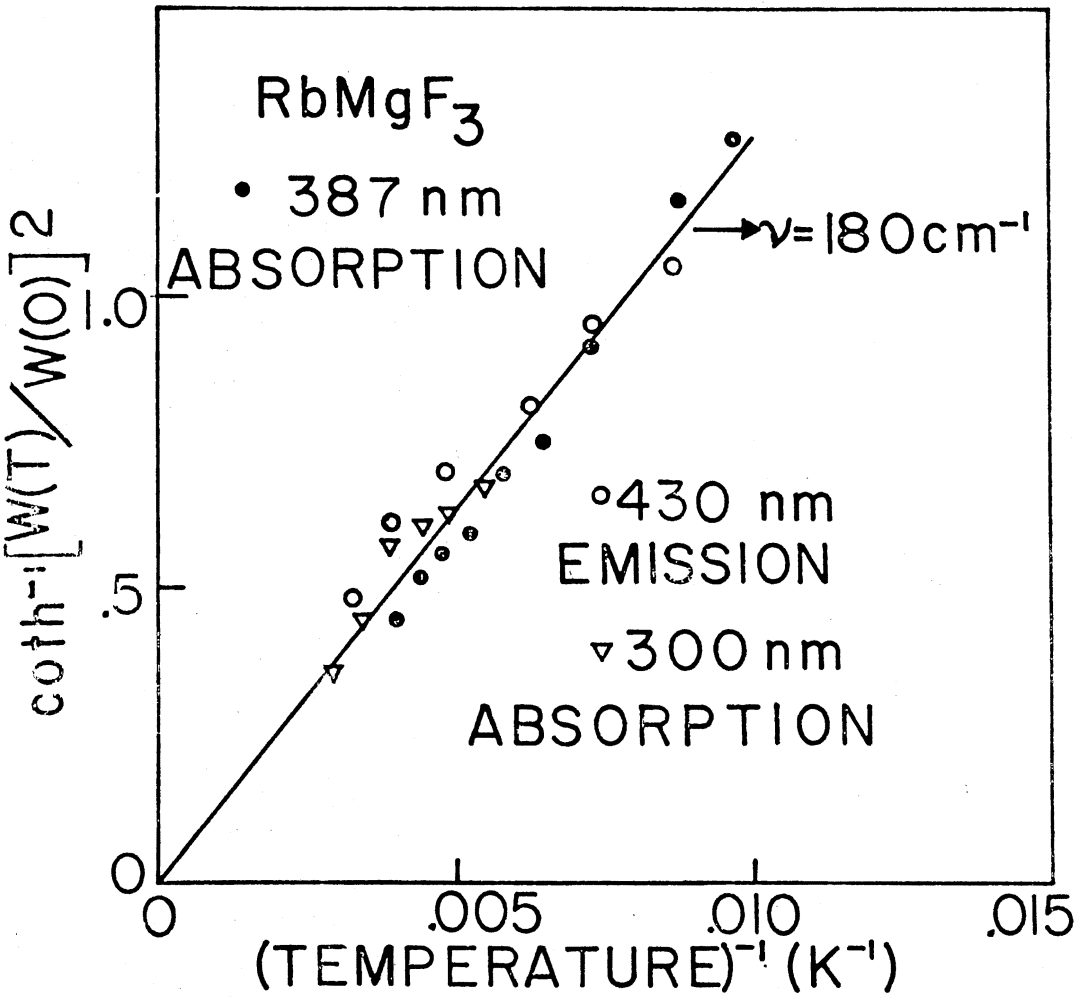

Figure 19. The Temperature Dependence of the Width at Half-Maximum, W, for F_2 Absorption and Emission and F_3 Absorption

$\coth^{-1} W_{\frac{1}{2}}(T)/W(10)$ is plotted against 1/T. The values for $W_{\frac{1}{2}}(10)$ emission and $W_{\frac{1}{2}}(10)$ abs. are 0.173 ev and 0.200 ev respectively. From the slope of the line a value of $v_g = v_e = 180\ cm^{-1}$ was obtained and from half-width data the Huang-Rhys factors for absorption and emission were calculated to be $S_{abs} = 14$; $S_{em} = 10$. Area measurements--total area under the whole band including the phonon lines divided by the area under the zero phonon line yields $S_{abs} = 10$ and $S_{em} = 7$. Finally a simple linear coupling model for the electron-phonon interaction gives a value of $S = (E_{abs}-E_{em})/2hv = 7.0$.

F_3 Centers

In Fig. 14 where the thermal annealing of the F centers is portrayed, an optical absorption at 300 nm (4.13 ev) grows in at about 625K as the F and F_2 centers anneal out. Figure 20 portrays the absorption of this band together with one luminescence band, the excitation spectra and the polarization properties of the absorption band. The fact that the growth of this band follows the thermal annealing of the F and F_2 bands suggests that this band might be the R band.

Polarized bleaching did not introduce any dichroism. However, the band shows a complete dichroism for different orientations of the c axis.

In the inset of Fig. 20 this dichroism is shown. When the electric vector $\vec{E}$ propagates parallel to the c axis no absorption is evident. When though $\vec{E}$ is perpendicular to the c axis the absorption band is present. For light propagating along the c axis--which means that the electric vector $\vec{E}$ is always perpendicular to it--no dichroism was observed. The polarization properties of the absorption band of the

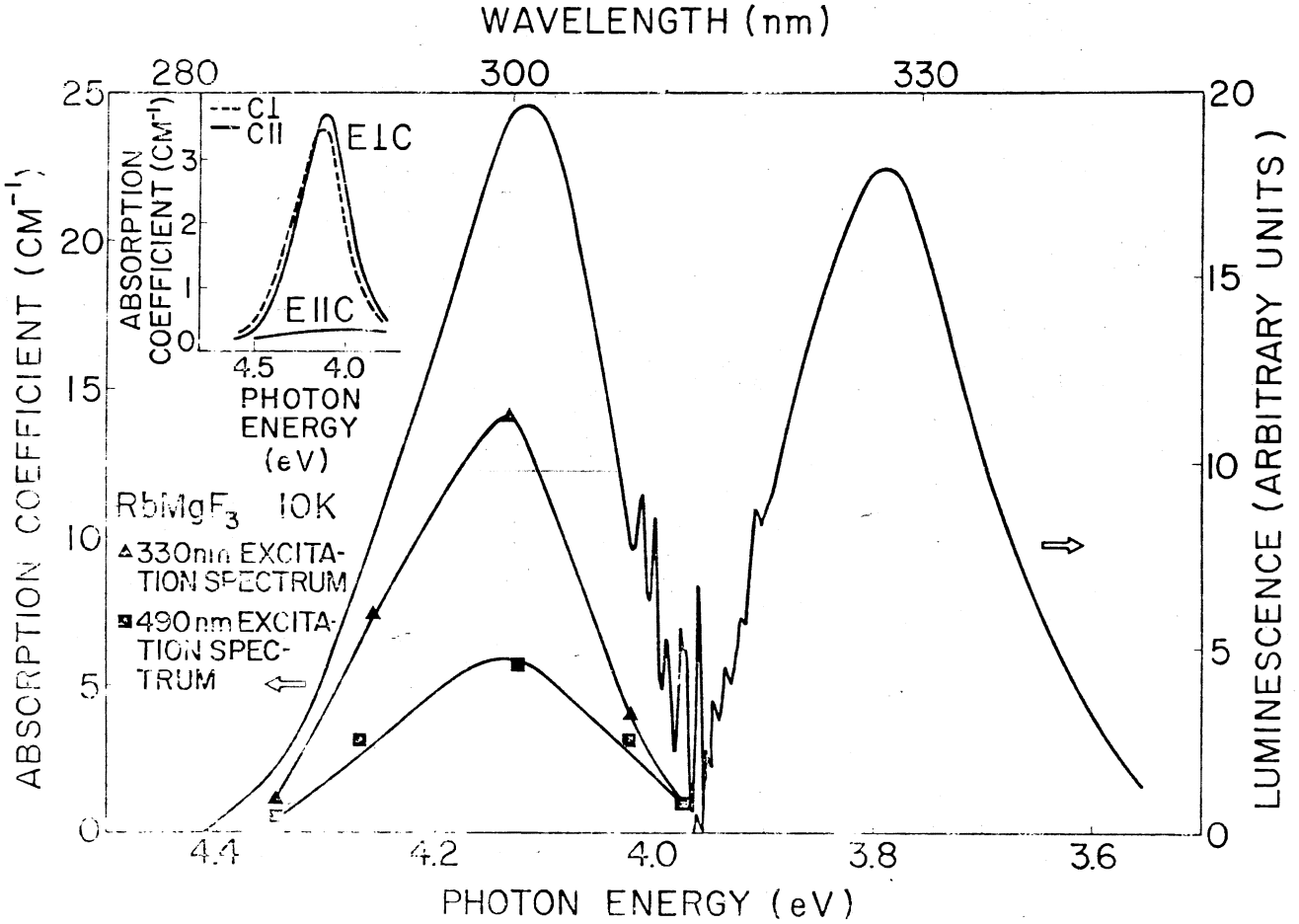

Figure 20. F_3 Center Absorption and Emission Bands at 10K. Also Shown are the Excitation Spectra for the 330 nm and 490 nm Bands. The Inset Shows the Absorption Spectrum of the F_3 Center in Another Sample for Different Polarizations E and Orientations $c_\perp$ and $c_{||}$ of the C Axis

F_3 centers are very similar with the equivalent V_K center properties.

Two luminescence bands are observed when the crystal is excited with 300 nm after the F_3 center absorption is introduced. The band at 330 nm is observed at low temperatures. This band is shown in Fig. 20 together with the absorption band at 10K. The zero phonon line occurs at the same energy for both bands. Table V shows the energy spacing between the sharp lines in emission and absorption for both F_2 and F_3 centers.

At higher temperatures another luminescence band grows in at 490 nm (2.53 ev) at the expense of the 330 nm band. The excitation spectrum for both luminescence bands matches precisely with the absorption spectrum as is shown in Fig. 20.

Figure 21 shows the luminescence bands due to the 300 nm excitation at 300K. Both bands are polarized with the electric vector $\vec{E}$ perpendicular to the c axis. The inset in Fig. 21 shows the temperature dependence of their intensity. Their lifetime, measured at R.T. was found to be 11 ns.

A temperature dependence of the width at half-maximum of the 300 nm absorption and the 330 nm luminescence were measured. A plot of the expression $\coth^{-1} W(T)^2/W(10)^2$ against 1/T is shown in Fig. 15 together with the data for the absorption and luminescence of the M band, and the value for vg obtained is again $v_g = 180\ cm^{-1}$.

However, the temperature change of the half-width of the 330 nm luminescence is very small not being detectable up to 250K, so a plot of it was not possible.

Another point of experimental importance is that when only the 300 nm absorption band is present in a crystal and the crystal is then

TABLE V

SPACING OF SHARP ABSORPTION AND EMISSION LINES IN $RbMgF_3$

387 nm Absorption		430 nm Emission	
Peak (eV)	Difference (cm^{-1})	Peak (eV)	Difference (cm^{-1})
3.020		3.019	
3.031	88	3.010	72
3.034	112	2.996	184
3.040	160	2.984	280
3.046	208	2.971	384
3.058	304	2.958	408
300 nm Absorption		330 nm Emission	
3.966		3.971	
3.974	64	3.960	88
3.976	104	3.948	192
3.988	200	3.936	288
4.000	296	3.922	400
4.010	376	3.911	488
		3.900	576

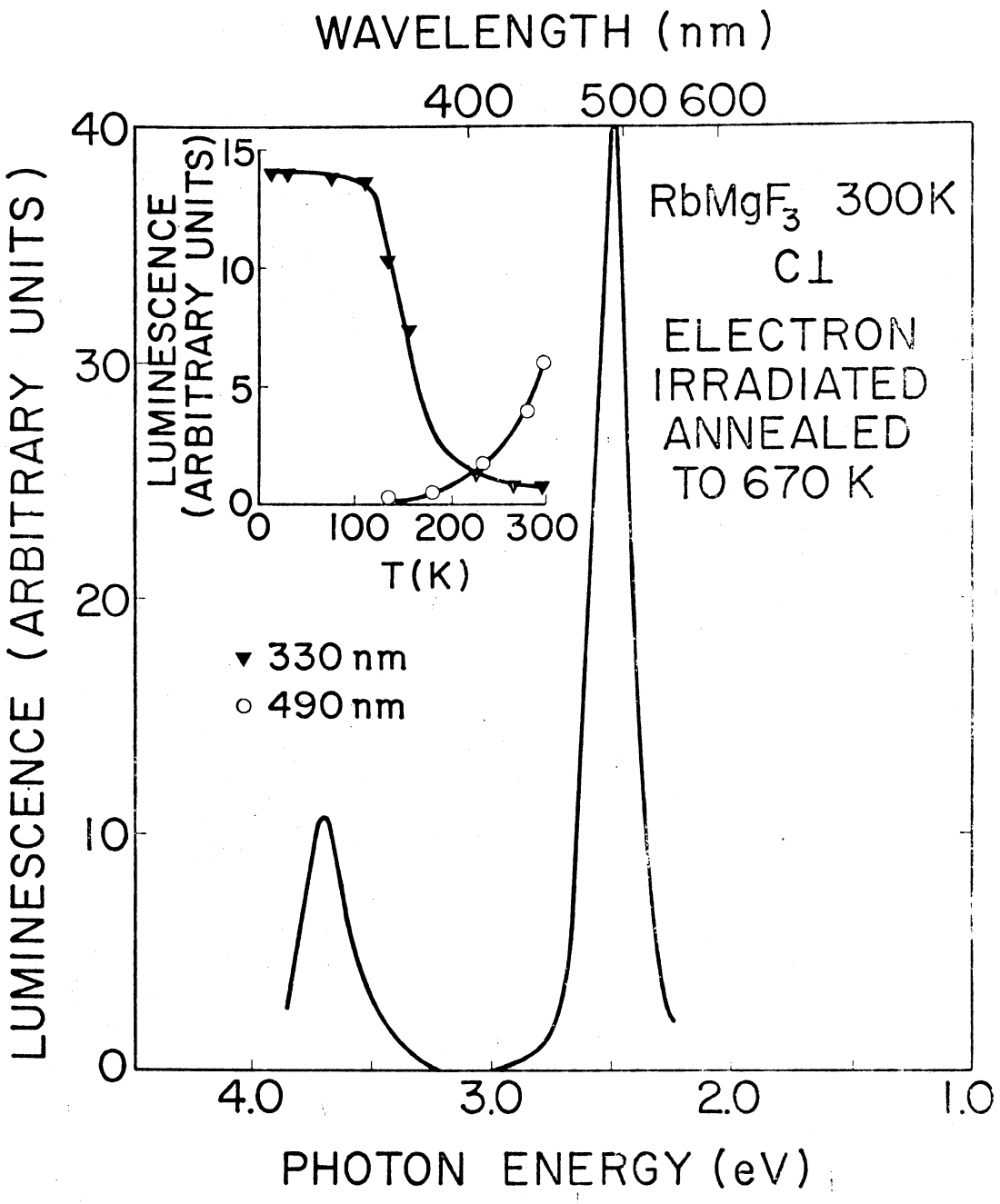

Figure 21. F_3 Center Emission at 300K. The Inset Shows the Temperature Dependence of the Luminescence

irradiated briefly with 1.5 MeV electrons or gamma rays, the bands attributed to F and F_2 centers grow back to almost their initial size as the 300 nm band decreases.

This is further evidence that we are dealing with F, F_2 and F_3 centers since similar events occur in the well studied alkali halides.

Table VI gives the chemical analysis of one of the crystals done with mass spectroscopy.

Discussion of Color Center Results

General

Due to the lower symmetry of $RbMgF_3$ lattice, one expects to find sites in the lattice where a configuration of ions has a different energy than at another site. To illustrate this point, Fig. 1 which gives three basal planes of $RbMgF_3$ perpendicular to the c axis, shows that three positions exist for the triads of fluorine ions with no Mg^{2+} above or below the configuration. This configuration is an ideal low energy configuration for the formation of V_K, F, F_2 and F_3 centers. Indeed, all the experimental data show a strong evidence that the assumption is basically correct.

V_K Centers

Any molecular fluorine ion formed by the fluorines of the low energy triads would give rise to a V_K center. The fact that the absorption of the V_K center is dichroic without any previous bleaching suggests that the observed 330 nm absorption is due to a dipole lying on a basal plane. The dipole is a σ or π dipole. The behaviour of the V_K

TABLE VI

IMPURITY ANALYSIS $RbMgF_3$ (ppm)

Ag	~1	Cu	10	Pb	<25
Al	1075	Fe	100	Pt	<50
Au	<5	Ga	<3	Sb	<100
B	75	Fe	<5	Si	60
Ba	2400	Hg	<100	Sn	<10
Be	<20	K	1700	Sr	~50
Bi	<4	Li	120	Ta	<100
Ca	1040	Mn	<10	Ti	~150
Cd	<30	Mo	<5	V	<40
Co	<75	Na	540	W	<50
Cr	<6	Nb	<10	Zn	<50
Cs	<30	Ni	<10	Zr	<50

center as a function of temperature is shown in Fig. 11. It becomes mobile at about 90K and recombines with electrons at impurities or it is trapped near impurity ions to form V_{K_A} centers. The second stage of the thermal annealing, occurring at 135K is probably due to V_{K_A} centers recombining with electrons at electron traps. The V_{K_A} center differs very slightly from the self-trapped center, its thermal stability being its chief distinguishing characteristic. Similar results were obtained for $KMgF_3$ (16) and alkali halides (65).

Two facets of the emission due to recombination of the electron with the self-trapped hole appear important. The most direct experimental correlation for the morphology of the V_K centers is the observation of linearly polarized luminescence upon the recombination of electrons with an oriented array of V_K centers. However, the x-ray luminescence measured at 10K as shown in Fig. 10 was not polarized. This indicates that two possible explanations exist. Either that the emission is π polarized, an observation confirmed before in different systems, or that the centers formed by the x-ray irradiation are created at random and rapidly relax even at 15K to a basal plane configuration. The 600 nm emission band is most likely due to Mn^{2+}. It was observed before (44) that Mn^{2+} emits 590 nm light in $KMgF_3$.

The second aspect of importance in the x-ray excited emission is that although this emission is thermally quenched above 80K, as shown in the inset of Fig. 10, the emission intensity from these centers apparently increases above 100K. Similar effects are observed in $KMgF_3$. Actually, thermoluminescence measurements of $KMgF_3$ show a 390 nm peak at 150K which could be due to V_K centers. This temperature is considerably above the temperature at which the normal V_K emission is thermally

quenched. The given interpretation involves again V_{K_A} centers and says that the quenching of luminescence from impurity trapped V_K centers is markedly different from self-trapped centers and these V_{K_A} centers emit light until they anneal out. The decreasing of luminescence efficiency at higher temperatures is explained as being due to thermal excitation of the excited states to the conduction band or directly to the ground state. Blaire, Pooley and Smith (66) proposed a model for the excited state of the V_K+e^- configuration based on a M_2X_2 rather than on a X_2^{2-} molecule, i.e., they took into account the presence of the next neighbor cations. This model is in accord with the suggestion explaining the increase of V_K luminescence above 100K.

F Centers

According to the model for the position of the defects formed upon irradiation, any fluorine of the low energy fluorine triad would give rise to an F center. This implies that the F center in this material should have a C_{2v} symmetry with three non-degenerate 2p-type excited states. From the absorption taken with the $\vec{E}||C$ and $\vec{E}\perp C$ it appears that the basal plane $2p_x$ and $2p_y$ levels are accidentally degenerate with the $2p_z$ level lower, the peak positions of the absorptions corresponding to these levels, being at 295 nm and 325 nm respectively. In order to verify that this was indeed the energetically favorable position for the F formation even at 10K, crystals of $RbMgF_3$ were irradiated at ~10K for a period of time necessary for the F center creation, and even at this temperature the similarity of the F absorption spectrum with the R.T. temperature irradiated samples confirms that the F center lie on the low energy configuration.

The correction factor of 1.35, used to bring unpolarized measurements on $C\perp$ and $C\parallel$ crystals into agreement, was obtained as follows: The intensity of light is given by the formula

$$I = I_o e^{-\alpha t}$$

where α is the absorption coefficient and t is the thickness of the crystal.

Three measurements were taken. In the first, light was propagating along the C axis with the electric vector $\vec{E}$ always perpendicular to C, and

$$I_1 = I_o e^{-\alpha_\perp t_1} = I_o e^{-\alpha_\parallel t_1}$$

In the second and third measurements, light was propagating perpendicular to the C axis with $\vec{E}\perp C$ and $\vec{E}\parallel C$, respectively. The intensity of unpolarized light propagating perpendicular to the C axis would be

$$I_2 = \frac{I_o}{2} e^{-\alpha_\perp t_2} + \frac{I_o}{2} e^{-\alpha_\parallel t_2} = \frac{I_o}{2} e^{-\alpha_2 t_2}$$

The logarithm of the ratio I_1/I_2 gives a value for α_1/α_2 of 1.35. This is an experimental result obtained from the experimental values for the absorption coefficients of the F center in $C\parallel$ and $C\perp$ faces of one crystal.

The production of F centers in this material seems to be dominated by a photochemical damage, since F centers can be readily produced with a production energy far less than one would expect for elastic collision processes. A simple calculation from Fig. 14 which gives F growth

curves at different temperatures, gives a production rate at R.T. of ~1000 F centers for electron hit. The production efficiency for stable F centers appears to go through a minimum around 175K. At this temperature--or at least at the vicinity of this temperature--some type of back reaction occurs and the efficiency apparently decreases. Probably the suppression of the colorability is due to an inhibition of the primary process of F center production which arises because impurities act as electron traps stopping or slowing down the V_K+e recombination which is a mechanism for F center production. The interstitials formed during irradiation are evidently mobile enough at higher temperatures that they aggregate to form immobile interstitial clusters.

In the case of thermal annealing, as the F concentration decreases with temperature, F_2 centers are formed and at higher temperatures F_3 centers are formed. The F centers become mobile at about 470K and calculations based on a very simple model can give a rough estimate for the activation of the F center. If x is the distance that the F center moves in one direction and a is the lattice constant, the

$$\frac{x}{a} = \sqrt{\nu t} \tag{48}$$

where t is the time during which the sample is kept at a particular temperature and $\nu = \nu_0 e^{-E_j/KT}$ is the attack frequency of the defect in the potential well it sits in with E_j its activation energy. Substituting for $x = 10^{-6}$ cm--the distance between two F centers along one particular direction when the concentration is 10^{18} F/cm^3, a saturation value at R.T.--t = 600 sec, a $= 3 \times 10^{-8}$ cm then the activation energy is $E_j = 1.55$ eV.

If one assumes that the interstitials produced during irradiation cluster into large aggregates and the vacancies, because they are immobile at room temperature, have a statistical distribution in the lattice, then it is possible to calculate the relative oscillator strengths of F, F_2 and F_3 centers. Consider first the F and F_2 centers. For the temperature range of 425K → 565K in Fig. 14 if one assumes that all the F centers at a rate of $\Delta N_F = 2\Delta N_{F_2}$ then using Smakula's equation (3)

$$N_i f_i = .87 \times 10^{17} C_i W_i \alpha_i \tag{49}$$

we can directly determine the corresponding decrease in absorption coefficient at the peak position of the F band, $-\Delta\alpha_F$

$$\Delta n_F = \frac{0.87 \times 10^{17} C_F W_F \Delta\alpha_F}{f_F} \tag{50}$$

and since the corresponding change in Δn_i is determined from a measure of $\Delta\alpha_i$, it follows that

$$\left|\frac{\Delta n_F}{\Delta n_{F_2}}\right| = \frac{W_F}{W_{F_2}} \frac{f_{F_2}}{f_F} \left|\frac{\Delta\alpha_F}{\Delta\alpha_{F_2}}\right| \tag{51}$$

and by using the assumption

$$\frac{\Delta N_F}{\Delta N_{F_2}} = 2 \tag{52}$$

we get

$$f_{F_2} = 2 \frac{W_{F_2}}{W_F} \left| \frac{\Delta\alpha_{F_2}}{\Delta\alpha_F} \right| f_F \tag{53}$$

One of the F_2 center transitions occur at 387 nm and has a half-width of W(300) = .29 eV at R.T. while the F center absorption at 295 nm has a halfwidth at R.T. of W(T) = .95 eV. Substituting in Eqn. (53), f_{F_2} is given by

$$f_{F_2} = .28\ f_F \tag{54}$$

For the F_3 center, assuming that $\frac{\Delta N_F}{\Delta N_{F_3}} = 1$ we get that

$$f_{F_3} = \frac{W_{F_3}}{W_F} \left| \frac{\Delta\alpha_{F_3}}{\Delta\alpha_F} \right| f_F \tag{55}$$

The 300 nm transition of the F_3 center has a W(300) = .33 eV and substituting in Eqn. (55), f_{F_3} is given by:

$$f_{F_3} = .31\ f_F \tag{56}$$

If the case of $\Delta N_{F_2} = \Delta N_{F_3}$ is considered, fair agreement is obtained with the previous case of $\Delta N_F = \Delta N_{F_3}$. This agreement in f values whether we consider F or F_2 centers in calculating f_{F_3} is pleasing. Obviously the calculation is only valid if no F centers are lost to sources other than vacancy aggregation. As a check to determine if vacancies are conserved during the annealing process, we gave a brief reirradiation to a crystal which was heat treated to 650K and found that the aggregate centers were destroyed and eventually only the initial F

band absorption, at the same intensity as prior to heat treatment is observed, which verifies the conservation of vacancies. When samples are heated above 850K there is a definite loss of F_3 centers. Most of these centers disappear and a brief irradiation does does not return the crystal to the original F center density. This suggests that the immobile interstitial clusters begin to disintegrate around 700K and a vacancy interstitial recombination occurs. The data so far indicate that the F center is mobile around 500K and the empty negative ion vacancy moves around 360K.

A review of F_2 center oscillator strengths is given by Compton and Rabin (3). The oscillator strength of the F_2 center in KCl as measured by H. Ohkura (66), T. Tomiki (67) and C. Delbecq (68) is 0.23, with the oscillator strength of the F center taken as 0.53. For the same f_F value the above calculation gives

$$f_{F_2}(387) = .15 \tag{57}$$

The oscillator strength for the other transition of the F_2 center can also be calculated. From Fig. 16, one sees that these transitions occur at 285 nm and 230 nm. The oscillator strength of the 285 nm transition is found to be

$$f_{F_2}(285) = .6\, f_F \tag{58}$$

By taking $f_F = .53$, the value for the oscillator strength is

$$f_{F_2}(285) = .32$$

a value very close to the ones calculated by the above mentioned re-

searchers.

F_2 Centers

Following the thermal annealing of the F center absorption, the F_2 center absorption bands come into the picture with transitions occurring at 387 nm, 285 nm and possibly at 230 nm. In Fig. 16 the band shown growing in is the 387 nm band. A quadratic relation at equilibrium between F and M centers was long established in other systems (3), so a similar relation in this system would be a strong evidence for the identity of the F_2 band. Unfortunately, the fact that the F_2 absorption band saturates very fast with thermal annealing did not allow such an expression to be established. Any two of the F centers of the low energy fluorine triads would bive rise to an F_2 center. So it would be expected for the F_2 center to lie on a hexagonal plane. The polarization of the F_2 absorption bands, the 387 and 285 nm bands absorbing light with the electric vector $\vec{E} \perp C$ and the 230 nm band absorbing light with the $\vec{E} \parallel C$, suggest that the σ dipole and one of the π dipoles lie on the hexagonal plane and the other π dipole is parallel to the c axis. Polarized bleaching measurements in the 387 nm band did not induce any dichroism. This was not surprising if the symmetry of the long dipole is taken into account.

Figure 18 shows together with the absorption at 10K, the 430 nm emission band resulting from excitation with 387 nm light--F_2 center absorption. There was no polarization of the luminescence observed, which suggests a mixing of the excited states. Actually, since the F_2 model is analogous to the H_2 molecule, we expect this center to have the same excited states as the H_2 molecule. Table VII gives the elec-

TABLE VII

ELECTRONIC ENERGIES OF THE SINGLET AND TRIPLET STATES OF THE M CENTER (ev)

State	Single	Triplet
A_{1g}	-11.70	
A_{1u}		-11.52
B_{1u}	- 8.60	- 6.38
B_{1g}	- 6.70	- 6.31
B_{2u}	- 6.10	- 7.19
B_{2g}	- 7.13	- 6.60
B_{3u}	- 6.76	- 7.84
B_{3g}	- 6.28	- 5.75

tronic energies of the singlet and triplet states of the M center in LiF as worked out by Wood and Meyer, (69) showing the complexity of the problem.

The intensity of 430 nm emission changes rapidly with temperature so that the area under the emission band is decreased at temperatures above 120K. This could indicate a thermal quenching of the emission, but this is not very likely. More likely this decrease is a transfer from the singlet excited state to the lower triplet state via thermal vibrations (69).

The F_2 centers according to the low energy configuration they possess in the basal plane, will be relatively loosely coupled to the lattice. This is evidenced by the small Stokes shift between absorption and emission and the presence of zero phonon lines. Furthermore, the absorption and emission bands for these centers show a mirror symmetry about the zero phonon lines. This is a behaviour expected from a linearly coupled electron-phonon system. Besides, by plotting $\cot^{-1} \frac{W(T)}{W(10)}$ versus 1/T for the absorption and the luminescence we obtain the same value for the dominant interacting phonon mode v_e and the dominant interacting phonon mode in the ground state $v_e = v_g = 180\ cm^{-1}$, which further suggests that the linearly coupled model approximation is valid. Of course there are many sophisticated methods of evaluating electron-phonon interaction for color centers (70). However, in some instances the simple configuration coordinate approximation (4,6) can lead to a valuable insight and a system in which $v_g = v_e$ should be ideal for this treatment. In this treatment the total energy of the system is plotted on the ordinate and the abscissa specifies the configuration coordinate x. The ground and excited levels are represented by para-

bolic curves with force constants K_g and K_e. The minima of the lowest two states are separated by an energy E_o which is related to the zero phonon energy E_{oo} by the expression

$$E_o = E_{oo} - \frac{1}{2} h\nu_e + \frac{1}{2} h\nu_g \tag{60}$$

It is assumed that the primary mode of lattice vibration influencing the defect, is a "breathing" mode and that the transitions between the levels are vertical. From the data available on the F_2 center we find:

$$E_{abs.} = E_o + \frac{1}{2} K_e X_o^2 - \frac{1}{2} h\nu_g = 3.20 \text{ eV} \tag{61}$$

$$E_{em.} = E_o - \frac{1}{2} K_g X_o^2 + \frac{1}{2} h\nu_e = 2.89 \text{ eV} \tag{62}$$

$$E_o = E_{oo} - \frac{1}{2} h\nu_e + \frac{1}{2} h\nu_g = 3.02 \text{ eV} \tag{63}$$

$$v_e = v_g = 180 \text{ cm}^{-1} \text{ or } h\nu = 0.022 \text{ eV} \tag{64}$$

$$W_{abs}(10) = (4\ln 2 h\nu_g/K_g)^{\frac{1}{2}} K_e X_o = 0.200 \text{ eV} \tag{65}$$

$$W_{em}(10) = (4\ln 2 h\nu_e/K_e)^{\frac{1}{2}} K_g X_o = 0.173 \text{ eV} \tag{66}$$

In order to obtain additional information, it is necessary to assume a mass for the oscillator. The usual method is to consider the mass of the oscillator in the ground state to be the reduced mass of the nearest neighbours. So, if we assume a mass for the ground state of 4×10^{-22} g then we find $X_o = 0.11\text{Å}$, $K_g = 29 \text{ eV/Å}^2$ and $K_e = 32 \text{ eV/Å}^2$. The consistency of this approach can now be checked by comparing the

S values derived from the expression

$$Sh\nu + \frac{1}{2} h\nu = \frac{1}{2} KX_o^2 \qquad (67)$$

From this expression we find $S_{abs} = 7.4$ and $S_{em} = 6.7$. This is essentially in agreement with the value measured from the expression $W^2(10) = S(h\nu)^2 91n2$ and the value obtained from the ratio of the total area under the band divided by the area under the zero phonon line, which is equal to e^S, and suggests that in some cases the simple configurational coordinate approach can be helpful. The discrepancy in S values obtained from half-width and area measurements probably arises fron non-linear coupling to phonons.

The configuration coordinate diagram constructed from the parameters found in the previous calculations is shown in Fig. 22.

F_3 Centers

As the thermal annealing of the F centers continues, the F_2 centers anneal out and the F_3 centers absorption band grows in with an absorption peak at 300 nm. The triad of the F centers in the low energy configuration scheme would be an ideal position for the formation of F_3 centers. Indeed, polarized absorption measurements present strong supporting evidence for this assumption. The inset of Fig. 20 shows the dichroism of the F_3 band. As it was mentioned before, when $\vec{E} \,||\, C$, no absorption optically detectable is observed. This suggests that the F_3 center lies on a hexagonal plane and the 300 nm absorption band is due to absorption by the σ dipole.

Excitation in the 300 nm region results in two luminescence bands.

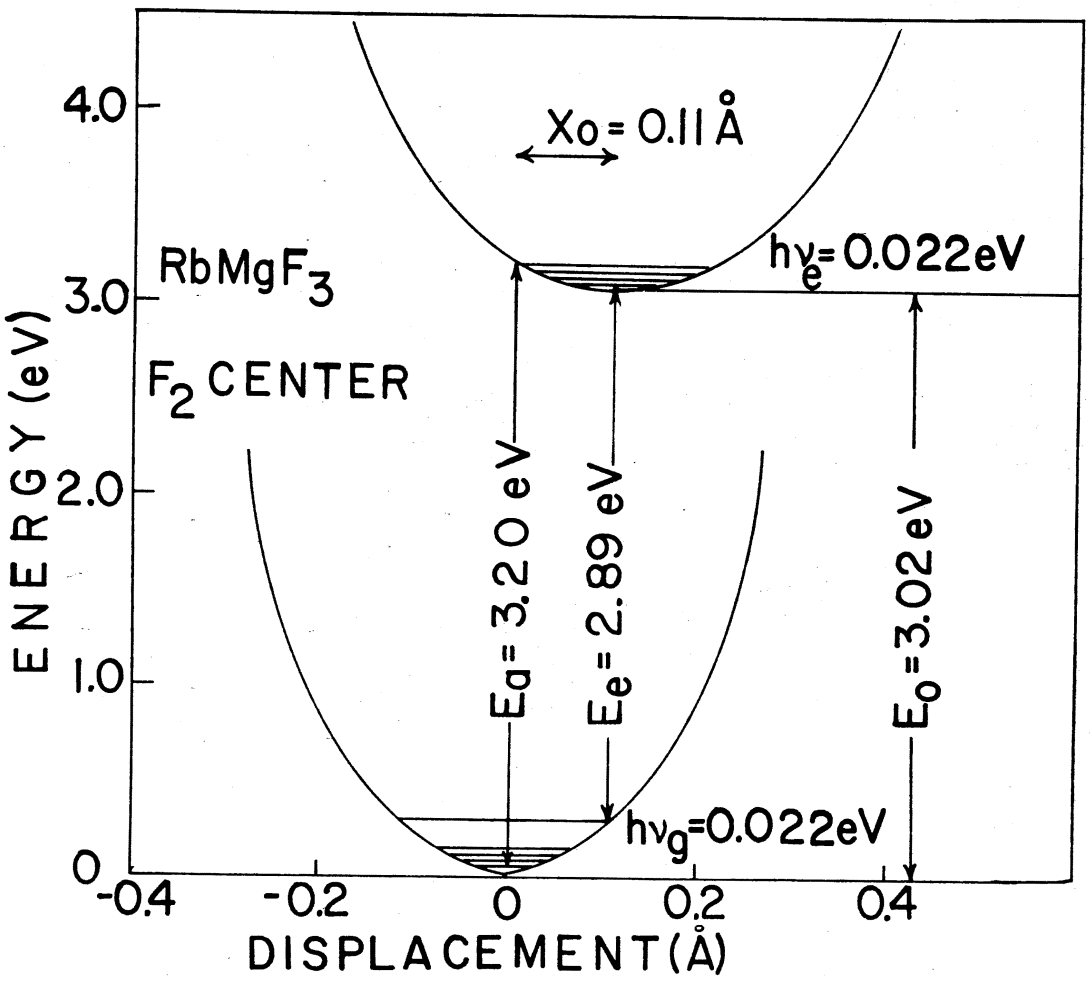

Figure 22. Configuration Coordinate Diagram for F_2 Centers in $RbMgF_3$

The 330 nm band is observed at low temperatures, but then as the temperature increases another band grows in at 490 nm at the expense of the 330 nm band. The inset in Fig. 21 is indicative of this behaviour. The F_3 center model proposed by Van Doorn, has a C_{3v} symmetry and the states of that center will belong to representations E, A_1 or A_2 of that point group. The F_3 center has been studied in detail by Silsbee (71). From stress experiments and the H_3 molecule work of Hirschfelder (72) he was able to establish the energy level sequence in KCl. In the F_3 center in $RbMgF_3$ it was found that both emission bands are polarized with $E \perp C$. This suggests transitions from the $^2A_1$ and $^2A_2$ levels to ^2E ground state, which is an assignment in accord with Silsbee's investigation. The half-width of the 330 nm emission band remains essentially constant from 10K to at least 200K. This means that the excited electronic state in a configuration coordinate diagram would be relatively flat. The thermal growth of the 490 nm emission band indicates that the level responsible for this band is only slightly higher in its relaxed state than the level giving rise to the 330 nm emission, so that as the temperatures rises a "thermal feeding" of the higher band is taking place. Moreover, the fast lifetime of the 490 nm emission suggests it is an allowed transition.

Table V gives the spacing of sharp absorption and emission lines in $RbMgF_3$ for F_2 and F_3 centers. The spacing indicates that a number of low lying lattice modes interact with these defects. Since little or no infrared or raman data much less neutron scattering data are available on $RbMgF_3$ it is not possible at this time to make an analysis of the electron-phonon interaction in these crystals. However, it is interesting to see that the splittings are similar for absorption and for

emission for these two types of centers. This suggests that the ground and excited states of these defects interact with the same phonon modes.

CHAPTER VI

PERTURBED Mn^{2+} ABSORPTION AND EMISSION IN $RbMgF_3$:Mn

Experimental Results

$RbMgF_3$ crystals doped with 1 atomic percent manganese were used for these measurements. When irradiated with 1.5 Mev electrons at 300K, only one optical absorption band is growing in at 295 nm (4.2 eV) with width at half-maximum of .95 eV, which is increasing with radiation dose. This band, observed before in nominally pure $RbMgF_3$ crystals, is the F band. Figure 23 illustrates the growth of the F band as a function of temperature for both pure and manganese doped crystal. From the figure, it is obvious that the number of observable F centers at a given irradiation dose is reduced in the doped material. Furthermore, the growth curves for the doped $RbMgF_3$ irradiated at 77K and 10K are identical, something that was not true for the pure material. Figure 24 illustrates the thermal annealing behaviour for pure (24a) and doped (24b) $RbMgF_3$. In Figure 24a the thermal annealing of the F band is accompanied by the growth of F_2 absorption band and at even higher temperatures of the F_3 band. However the thermal annealing of the F band in $RbMgF_3$:Mn is followed by the growth of a series of absorption bands at 600 nm, 425 nm, 343 nm, 328 nm, 297 nm, and 273 nm. In Figure 24b the growth of the 425 nm band is plotted although the others also grow

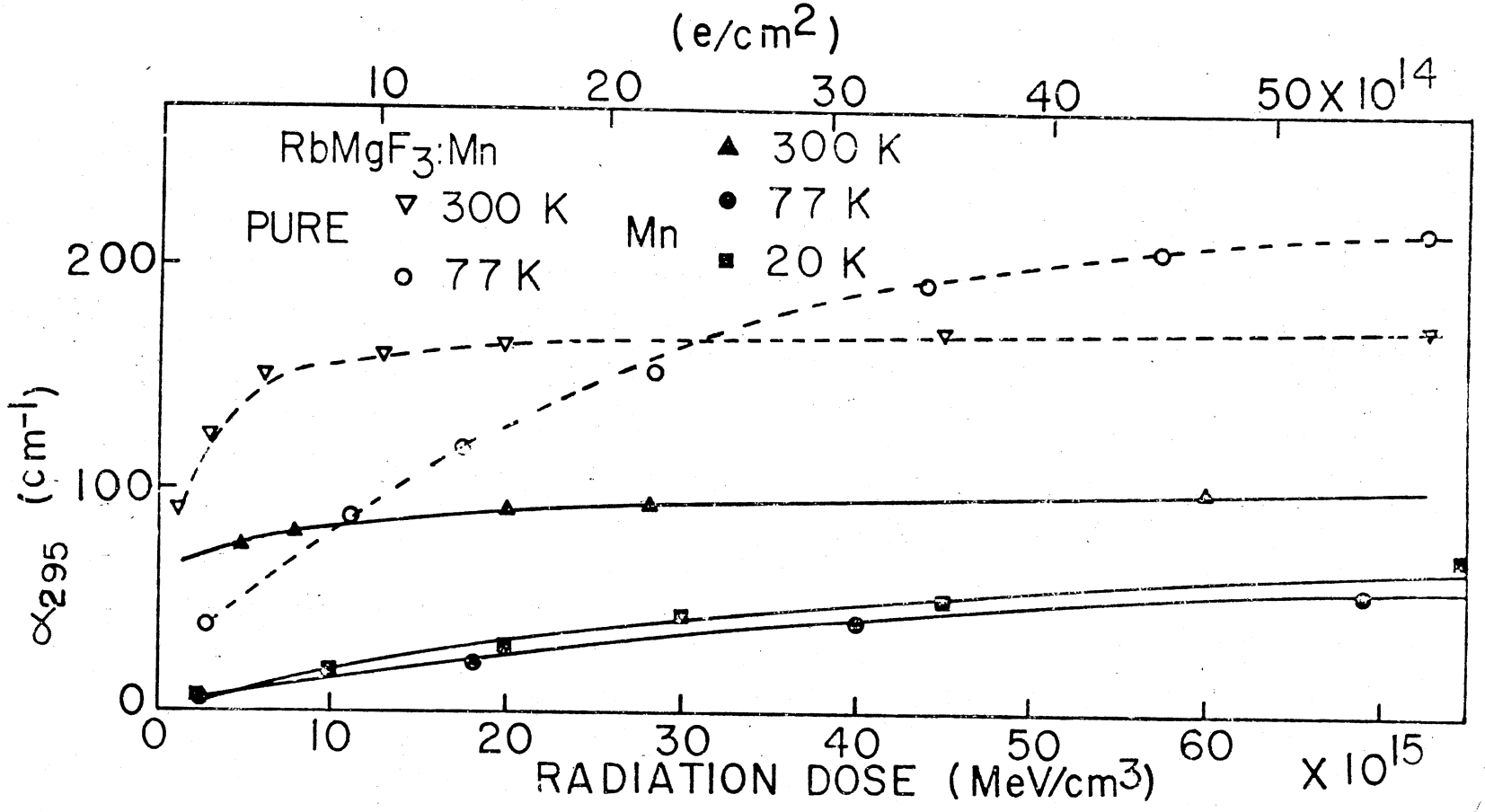

Figure 23. F Center Absorption, α_{295}, as a Function of Absorbed Energy for Pure (Open Symbols) and Mn-doped (Full Symbols) Crystals Electron Irradiated at 77K and 300K

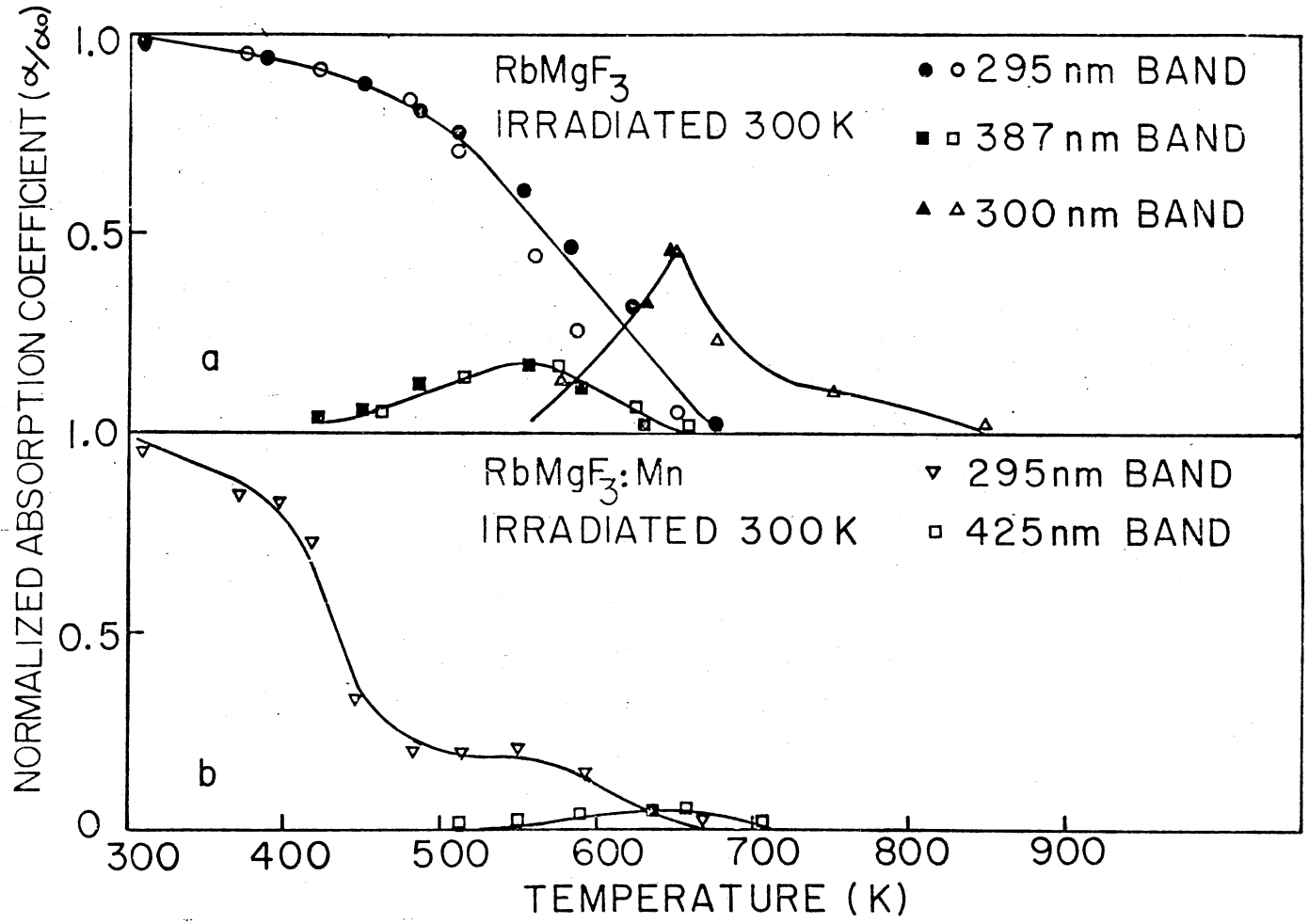

Figure 24. (a) Normalized Thermal Annealing Data for Nominally Pure $RbMgF_3$ Samples Electron Irradiated to Different Doses. (b) Normalized Thermal Annealing Data for $RbMgF_3$:Mn Specimens

in simultaneously, since the formation of the one defect complex is responsible for all of them. F_2 and F_3 bands are also observed to grow in the impurity doped samples at about the same temperature as for the undoped material, but these bands are much smaller due to the competition from the presence of Mn^{2+}. Figure 25 shows the series of absorption bands present in the heat treated doped samples at 15K. All these bands can be eliminated by optical bleaching with light of wavelength shorter than 350 nm. At 77K and 300K, a 425 nm optical bleach does not decrease the intensity of this series of bands, but two hours bleaching with 300 nm light causes it to disappear completely leaving only the small F_3 band visible at 300 nm. Another interesting observation was that it was possible to bleach out the small F_2 band with 430 nm light at 300K, something that had not happened in $KMgF_3$ (14). Heat treatment to high temperatures should return the bleached series of bands to their original intensity, since it would release the electrons from their traps. Indeed, by heating the crystal up to 500K returns the series of bands to about 60% of its original intensity, but treatment at higher temperatures evidently destroys the complex. In Figure 24b it should be noted that the F band anneals more rapidly for the impure specimen than for the pure ones. In an effort to determine whether this annealing is due to a mere valence change--i.e., electrons leaving the F centers and getting trapped at some impurity or interstitial so that the vacancies are preserved--or to an interstitial-vacancy recombination, a sample was irradiated at 300K and then heat-treated for 10 minutes at 500K with a resultant loss of F centers. The sample was then given a very short (60 seconds) re-irradiation with 1.5 MeV electrons and no recovery of the F band was observed. This suggests that

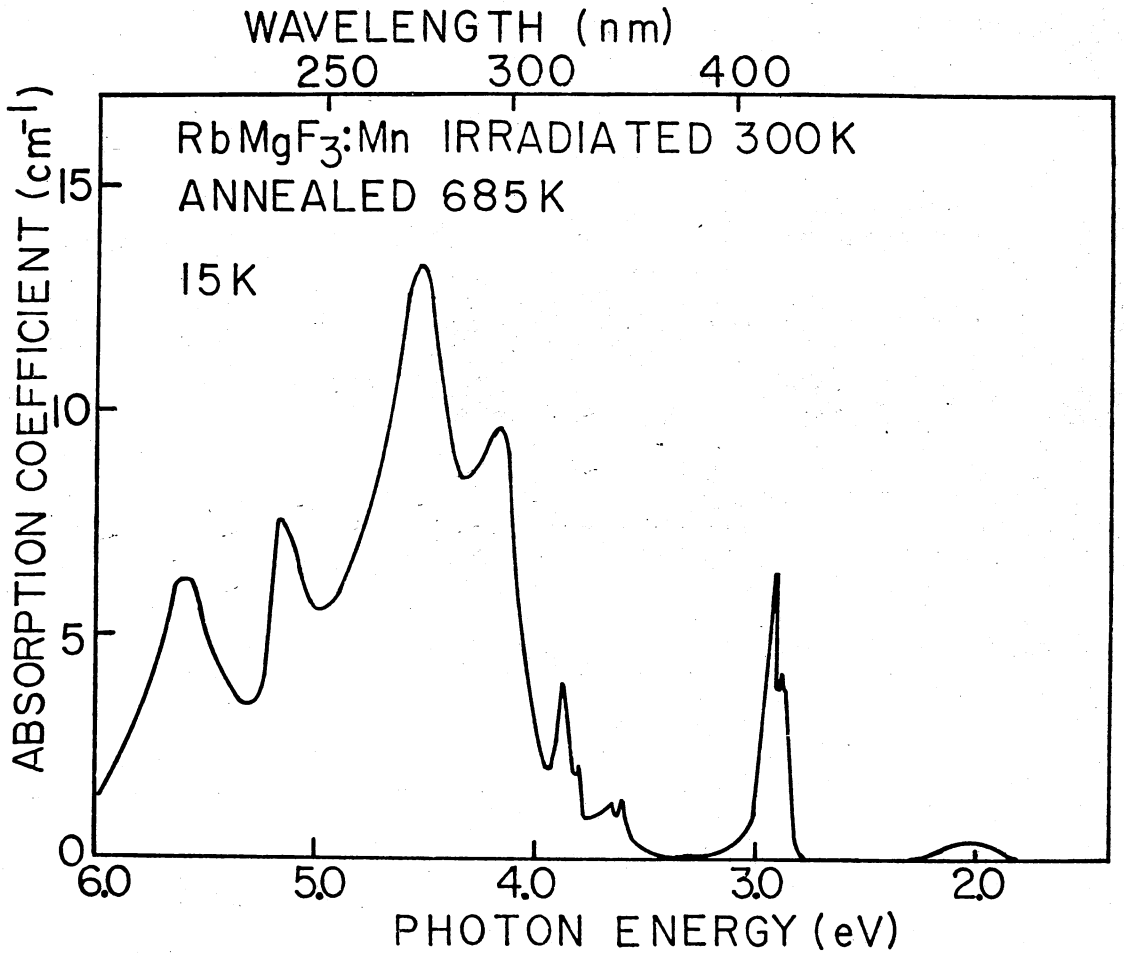

Figure 25. Optical Absorption at 15K for a $RbMgF_3$:Mn Sample Electron Irradiated at 300K and Annealed 10 Minutes at 685K. In Order to Show all the Bands a Specimen Cut With the c Axis 45° to the Crystal Face was Used

some type of interstitial-vacancy motion occurs and the apparent loss of F centers is not due to simple valence changes.

After a doped sample is irradiated at 300K so that only the F band exists, excitation with F-light produces an optical emission band at 590 nm (2.1 ev). The higher the F concentration the more intense the luminescence. This band has a very long lifetime--in fact we were obliged, in order to see the luminescence to use only the preamplifier without the chopper and the lock-in amplifier. This has been observed before (16). It is most likely due to luminescence coming from unperturbed Mn^{2+}. After the doped sample is heated to about 650K and the absorption series of lines is observed, concurrently, optical emission bands are observed at 720 nm (1.72 ev) and 830 nm (1.47 ev). Figure 26 illustrates the luminescence bands at 15K. The 720 nm band is the most easily observed and is similar to an emission band that appears in manganese doped MgF_2 and $KMgF_3$ (42,44). An emission band at about 560 nm (2.2 ev) is also present but it is difficult to describe, because of the low intensity of this band, its behaviour with heat treatment. The excitation spectra of the 830 nm and 720 nm luminescence bands are depicted in Figures 27 and 28, together with the temperature dependence of the intensities of the excitation bands. It is interesting to observe that the excitation spectrum of the 720 nm luminescence corresponds to the absorption spectrum observed after irradiation at 300K and heat treatment to 650K, while the 830 nm excitation displays a somewhat different spectrum. Table VIII gives an impurity analysis of the crystals of $RbMgF_3$:Mn used for this investigation.

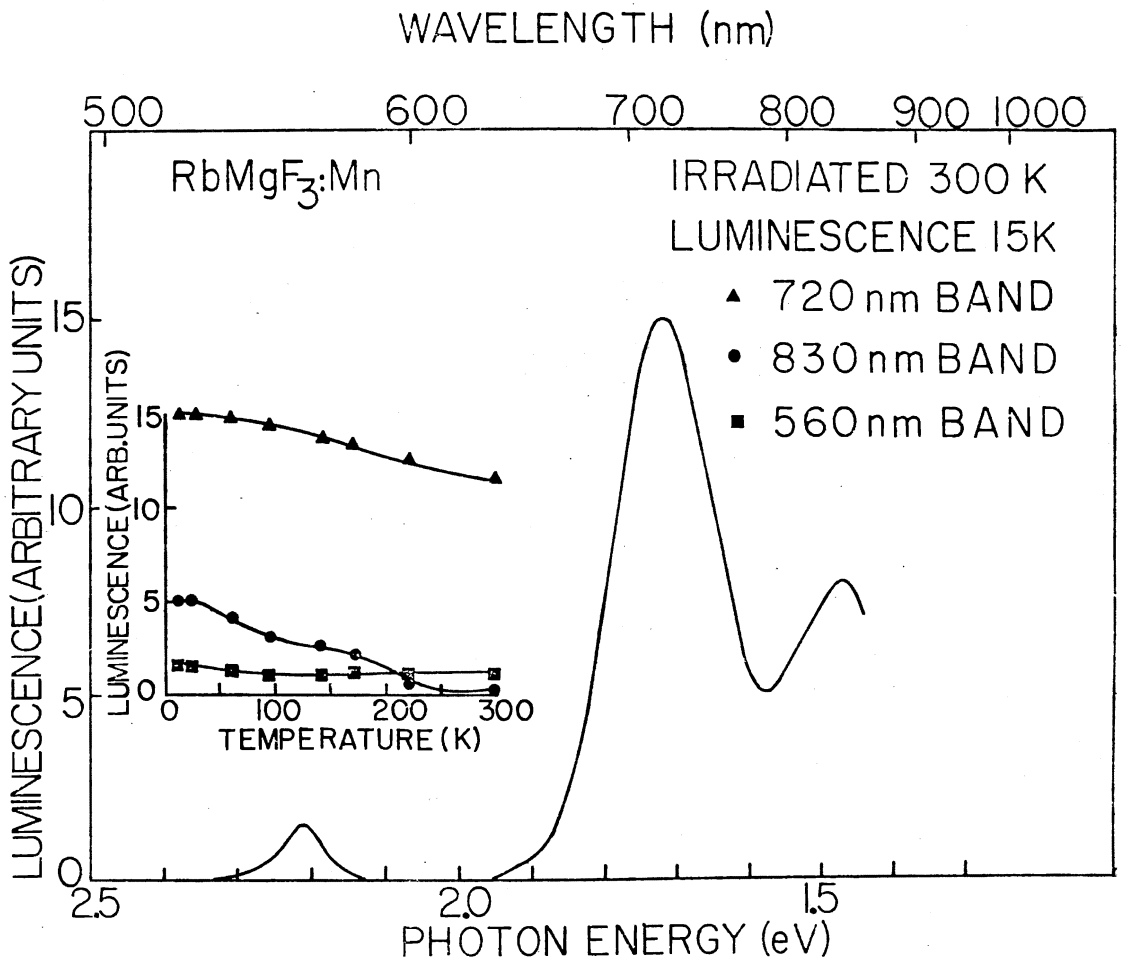

Figure 26. The Emission Spectrum at 15K From a Crystal Irradiated at 300K Annealed to 685K and Excited With 425 nm Light. The Inset Illustrates the Temperature Dependence of the Intensity of the Three Bands

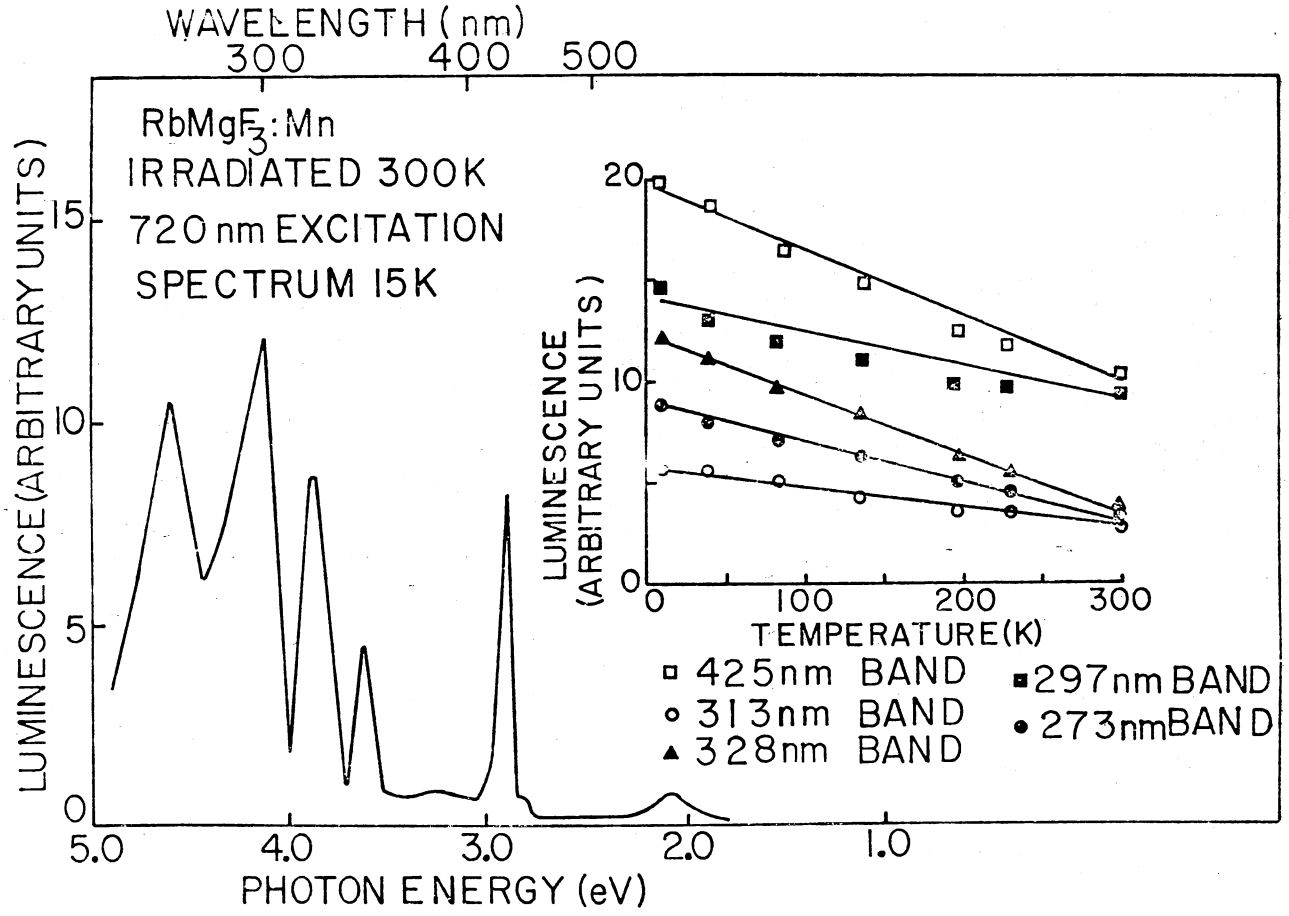

Figure 27. Excitation Spectrum at 15K for the 720 nm Emission Band in the Crystal Used for the Data in Fig. 26. The Inset Shows the Temperature Dependence of the Bands

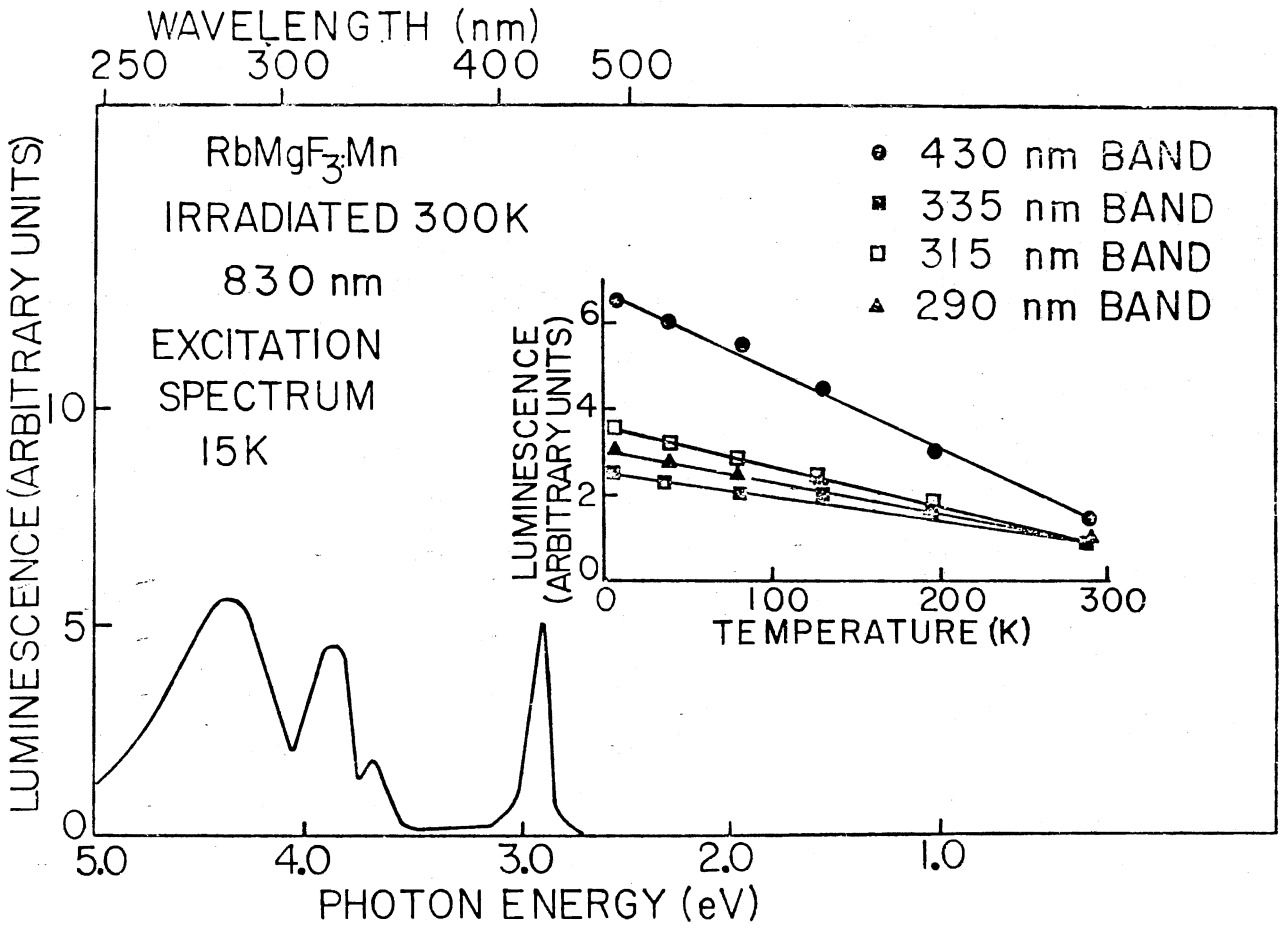

Figure 28. Excitation Spectrum at 15K for the 830 nm Emission in the Crystal Used for the Data in Fig. 26. The Inset Shows the Temperature Dependence of the Excitation Peaks

TABLE VIII

IMPURITY ANALYSIS OF Mn DOPED $RbMgF_3$

Ag	1	Mn	1500
Al	30	Mo	<1
Au	<5	Na	100
B	4	Nb	<10
Ba	<2	Ni	<2
Be	<.5	Pb	<10
Bi	<2	Pd	0
Ca	<1	Pt	<10
Cd	<5	Rb	M
Co	<5	Sb	<10
Cr	<2	Si	3
Cs	<50	Sn	<2
Cu	2	Sr	<100
Fe	≤1	Ta	<10
Ga	<2	Te	<20
Ge	<2	Ti	<1
Hg	<5	V	20
K	1000	W	<10
Li	40	Zn	<100
Mg	M	Zr	<2

Discussion

In Figure 23 which shows the F growth as a function of dose, it is obvious that the apparent F center production in Mn doped crystals is suppressed in comparison to that in pure specimens.

The suppression occurs at low temperatures--i.e., 77K and 10K--while the 300K growth curves for the pure sample show a rather wide variation in their behaviour depending on the impurity concentration in the crystal. It is not obvious, however, whether the apparent decrease at low temperatures is the result of a suppression of the production mechanism, enhanced interstitial-vacancy recombination or valence changes which leave some negative ion vacancies without electrons. Meanwhile, the annealing curve in Fig. 24b for F centers in impure crystals does show a recombination annealing stage at a temperature below that at which F centers are generally mobile--seen in Fig. 24a. The experimental evidence given before suggests that it is very unlikely that valence changes occur in the annealing of F centers. The destruction of F centers in impure crystals is probably due to the release of impurity trapped interstitials or to F centers moving to nearby interstitials. The activation energy for the F center calculated previously for the pure $RbMgF_3$ is 1.50 eV. The interstitial is mobile at much lower temperatures--in alkali halides it is reported that it is mobile at 40K (73) and there is evidence that in $RbMgF_3$ the interstitial is mobile at least in 30K. This would make the suggestion that the interstitial is the mobile unit much more convenient.

In general, optical transitions from substitutional Mn^{2+} impurities in $RbMgF_3$ are strongly forbidden by both spin and parity selection

rules. The crystal field states have even parity because of the inversion symmetry of the Mn^{2+} ion sites and the spin has to be changed by $\Delta S = \pm 1$ in a single ion excitation since the Mn^{2+} ion has a sextet ground state and quartet excited states. When though 3d impurity ions are nearest neighbors with radiation induced defects the forbiddeness is lifted and large oscillator strength changes occur. Recently, it has been shown that in $KMgF_3$ doped with Mn^{2+} and Co^{2+} (42) transitions are enhanced by the presence of defects through exchange interaction that increase the oscillator strength. Actually, the work of Young et al. (43) in conjunction with some earlier research indicated that in irradiated $KMgF_3$:Mn one set of perturbed Mn^{2+} transitions is due to F center-Mn^{2+} pairs. The optical spectra of these perturbed transitions are very similar to the unperturbed transitions studied by McClure, Ferguson and others (21-23). The fact that the vacancy is not mobile at 300K makes the formation of F-Mn^{2+} complexes in $RbMgF_3$ doped with Mn^{2+} after irradiation dependent on a statistical basis. Such a relation between Mn-F complexes can be derived in the following way.

A given volume of the crystal at a given instant of e^- irradiation contains N_F F centers and N_{Mn} manganese. During a subsequent incremental interval of e^- irradiating the amount of F centers increases by dN_F and the number of Mn sitting next to F centers by dN_{FMn}. Considering the total number of fluorines surrounding a given Mn^{2+} ion so that any F center created at one of these sites results in a Mn-F formation and taking N_o as the total number of halogen sites in the unit volume of the crystal, we have

$$dN_{Mn-F} = 6 \frac{N_{Mn} dN_F}{N_o} \tag{68}$$

which gives

$$N_{Mn-F} = 6 \frac{N_{Mn} N_F}{N_o} \tag{69}$$

Since the samples contain nominally-1 at % Mn^{2+}-actually from the analysis it is shown that they contain much less, i.e., 0.15%--we find that

$$N_{F-Mn} = 2 \times 10^{-2} N_F .$$

From Figure 23 N_F is determined to be $N_F = 10^{18}/cm^3$. Assuming that the oscillator strength of the F center is unity then $N_{F-Mn} = 10^{16}/cm^3$, a maximum value for the concentration which is very difficult to observe in absorption even for an F oscillator strength of unit. At higher temperatures though, the vacancy becomes mobile and aggregation can occur, in which case the N_{F-Mn} concentration should increase. The series of bands which appears upon heat treatment of Mn-doped crystals are remarkably similar in both absorption and emission to that in $KMgF_3$:Mn (42) Table IX gives the observed Mn^{2+} transitions in $RbMnF_3$ and their oscillator strengths. Also shown are the transition energy values for the data in $RbMgF_3$:Mn depicted in Figure 25. The $4T_2$ level shows a splitting probably due to spin-orbit coupling while the ^4E level splitting might be due to either spin orbit coupling or Jahn-Teller effect. Figure 29 illustrates the polarization dependence of the various transitions. The measurements were made for a $C_{//}$ sample and the polarizers used were rotated in steps of 15^o. The 90^o reading corresponds to the case with the electric vector $\vec{E}$ perpendicular to the optic or C axis. The nature of these polarizations mostly agrees with what is predicted for Mn transitions. The polarization of the 600 nm band

TABLE IX

OBSERVED AND CALCULATED ENERGIES FOR Mn^{2+} TERMS FOR $RbMnF_3$[7] AND $RbMgF_3$:Mn

Level	Calculated Energy (With Spin-Orbit) cm^{-1}	Observed Energy 77K cm^{-1}	f	Irradiated $RbMgF_3$:Mn (1%) 15K cm^{-1}	f	Predicted Polarization
$^4A_2(^4F)$	40117	41158		36693		z
$^4T_1(^4D)$	32887	39700				
	32848	38000				
	32781	32798	1.5×10^{-7}	33629		x,y
	32780	32446				
$^4E(^4D)$	29657	30478				
	29588		1.5×10^{-7}	31209	$.002f_F$[b]	z
	29561	30140				
$^4T_2(^4D)$	27891	28385		30645		
	27802	28258	1.1×10^{-7}	29435		x,y
	27601	28129		29113		
	27590	27917				

TABLE IX (Continued)

Level	Calculated Energy (With Spin-Orbit) cm^{-1}	Observed Energy 77K cm^{-1}	f	Irradiated $RbMgF_3$:Mn (1%) 15K cm^{-1}	f	Predicted Polarization
$^4A(^4G)$	23977[a]	25759 25543	9.2×10^{-7}	23669	$.05f_F$[b]	z
$^4E(^4G)$	23990 23989 23982	25336 23195	9.2×10^{-7}	23580 23250	$.05f_F$[b] $.05f_F$[b]	z
$^4T_2(^4G)$	21968 21965 21880 21840	23106	1.6×10^{-7}			
$^4T_1(^4G)$	18236 18197 18142 18126	19150	2.0×10^{-7}	16451	$\sim 10^{-3} f_F$[b]	x,y
$^6A(^6S)$						

[a] In $KMgF_3$:Mn Ferguson, et al. observe the ^4E transition lowest.

[b] f_F the F center oscillator strength is most likely between 0.5 and 1.

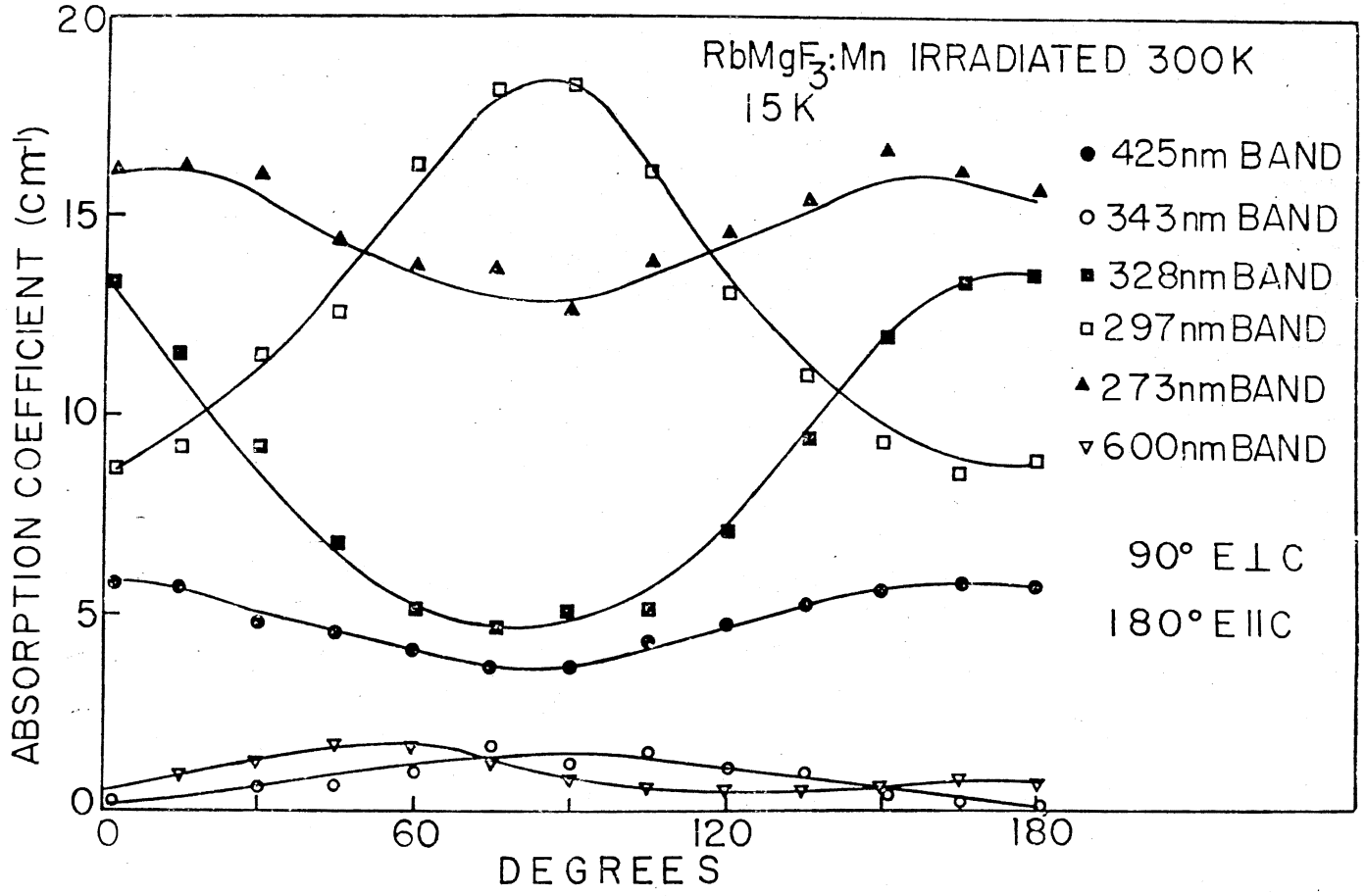

Figure 29. Polarization Dependence at 15K of the Absorption Bands in a $C_{//}$ $RbMgF_3$:Mn Crystal Electron Irradiated at 300K and Heat Treated to 685K. The 90° Point is When $E \perp C$ and 0° and 180° Have $E \parallel C$

shows a "retardation" in comparison with the others but because it is rather broad and not very pronounced, this could be due to experimental error.

As it was mentioned before, optical bleaching with F light at 300K and 77K destroys all these transitions, an observation which is in agreement with what has been previously observed in $KMgF_3$:Mn. This suggests that these transitions are due to Mn^{2+} and that the oscillator strength enhancement is due to exchange. Because the bleaching releases electrons from the F centers into other traps and since the vacancy is not mobile the site symmetry remains the same for the Mn^{2+}-vacancy as for the F-Mn^{2+}. Therefore there is enough justification in indicating that exchange plays a major role in the enhancement of optical transitions. It is very interesting to note that as the F centers migrate to the Mn^{2+} ions the F absorption disappears as the perturbed Mn^{2+} transitions grow in. On the other hand, albeit the disappearance of the F absorption, bleaching in the F region destroys the perturbed Mn^{2+} transitions. In order to obtain an order of magnitude concept of the oscillator strength enhancement of Mn^{2+} caused by the presence of next neighbor F centers, an analysis similar to the one used for the oscillator strength of F_2 and F_3 centers in the pure material can be carried out. Thus, from Fig. 24b, we equate the number of F center-Mn^{2+} complexes formed in the annealing stage 550K-650K with the number of F centers lost, i.e., we assume that F centers are not lost to any other trap. This requirement is translated as

$$\frac{\Delta N_F}{\Delta N_{Mn-F}} = 1$$

From Smakula's formula $\Delta N_F = \dfrac{.87 \times 10^{17} \; C \; W_F \; \Delta\alpha_F}{f_F}$

$$\Delta N_{Mn-F} = \frac{.87 \times 10^{17} \; C \; W_F \; \Delta\alpha_F}{f_{Mn-F}}$$

From these two relations we obtain

$$\frac{\Delta N_F}{\Delta N_{Mn-F}} = \frac{W_F}{W_{Mn-F}} \; \frac{f_F}{f_{Mn-F}} \; \frac{\Delta\alpha_F}{\Delta\alpha_{Mn-F}}$$

The half widths and the corresponding oscillator strengths for the bands at 425 nm, 320 nm and 575 nm are

$$W_{425} = .14 \text{ ev}, \quad f_{425} = .05 \; f \tag{73}$$

$$W_{320} = .15 \text{ ev}, \quad f_{328} = .002 \; f \tag{74}$$

$$W_{575} = .17 \text{ ev}, \quad f_{600} = 10^{-3} \; f \tag{75}$$

A comparison of these oscillator strengths, assuming $f_F = 1$, with those for $RbMnF_3$ shown in Table IX indicates that the presence of F centers enhances the transition probability by about 10^4-10^5.

In the experimental part of the discussion it was reported that after irradiation at R.T. so that only F centers are introduced, excitation with F light at R.T. causes a 590 nm luminescence to appear. A tentative explanation of the mechanism is the following

$$M_n^{3+} + e \rightarrow [Mn^{2+}]^* \rightarrow Mn^{2+} + h\nu \tag{76}$$

i.e., e^- irradiation creates also Mn^{3+} ions and as electrons are released from the F centers by bleaching with F light, Mn^{3+} trap an electron, go to an excited Mn^{2+} state and they reach the ground state by emitting the characteristic Mn^{2+} unperturbed luminescence observed before (16). This luminescence depends on the number of F centers present and also on the temperature not being observable at 10K.

The 720 nm luminescence is the dominant emission introduced after the heat treatment. It comes from the $^4T_1$ level and does not depend strongly on temperature as it is shown in Fig. 26. Its excitation spectrum reproduces the absorption spectrum of R.T. irradiated and heat treated $RbMgF_3$:Mn.

The 830 nm emission band disappears at R.T. and its excitation although similar to the 720 nm excitation, does not show the 600 nm peak. A suggestion is that this band could be due to a second type of perturbed Mn^{2+} complex whose origin is not clear yet.

CHAPTER VII

SUMMARY AND PROBLEMS FOR FURTHER STUDY

The identification of the absorption bands due to F, F_2, F_3 and V_K centers was tentaively made in $RbMgF_3$ by the use of optical techniques. The F center has absorption bands at 295 and 325 nm, the F_2 center has absorption bands at 387, 285 and 230 nm and emission at 430 nm and the F_3 center shows a 300 nm absorption and 330 and 490 nm emission. The identification of all these bands was made on the basis of their annealing characteristics and their polarization properties. The V_K center absorption occurs at 330 nm and its emission is at 428 nm. This identification was made on the basis of its saturation with electron irradiation, its annealing behaviour and its polarization. An analysis of the temperature dependence of the F, F_2 and F_3 centers gave the following values. $S_{Fabs.} = 78$, $\nu_{Fg} = 283\ cm^{-1}$, $S_{F_2abs.} = 10$ and $S_{F_2em.} = 7$ with

$\nu_{F_2g} = \nu_{F_2e} = 180\ cm^{-1}$ and $\nu_{F_3g} = 180\ cm^{-1}$.

The process of radiation damage in $RbMgF_3$ was found to be very similar to that in $KMgF_3$. The dominant damage mechanism is photochemical as it is indicated by the F center production per electron hit. The temperature dependence of the coloration process shows that the efficiency for defect production goes thru a minimum of around 175K probably due to some "back reaction."

A very important result was that the negative ion vacancy is not mobile until the temperature reaches 550K. This enabled us to determine the oscillator strength for the F_2 and F_3 centers by assuming a .53 value for the oscillator strength of the F centers.

In the Mn doped $RbMgF_3$, the absorption bands due to Mn substitutional ions perturbed by F centers trapped next to them introduced by electron irradiation and thermal annealing, have been assigned to various energy levels by means of comparison with equivalent bands in $KMgF_3$ and their polarization properties. The luminescence coming from the Mn-F center complex has been studied and it was found to consist of three bands at 560, 720 and 830 nm.

The property of the negative ion vacancy not being mobile at R.T. made it possible for the first time to calculate the oscillator strength enhancement due to electron exchange between the F center and the Mn^{2+}. This increase was found to be 10^4-10^5 for the various transitions. It was also found that both the radiation production and the annealing of the radiation damage is different in the pure and doped specimens. It appears that in the Mn doped material many of the interstitials do not form large clusters but are trapped in a more statistical distribution in the lattice.

Several suggested future projects are listed below:

1. A study of the low temperature irradiated $RbMgF_3$:Mn. It has been observed that $RbMgF_3$:Mn electron irradiated at 77K introduces a number of luminescence and absorption bands which have similar characteristics with the bands introduced after electron irradiation at 300K and subsequent thermal annealing. Identification of the Mn^{2+}-defect complex giving rise to these bands would give a new depth in the under-

standing of exchange interaction.

2. A study of the H center mobility in $RbMgF_3$ pure and doped. The interstitial being mobile at far lower temperatures than the negative ion vacancy is most likely responsible for some or all of the Mn^{2+} perturbed bands introduced at low temperature irradiation. An understanding of its behaviour and the possibility of its forming di-interstitial bands at the Mn^{2+} sites would shed a lot of light in a rather obscure field.

3. A study of $RbMg_xF_3:Mn_{1-x}$ covering the whole range from pure $RbMgF_3$ to pure $RbMnF_3$. Since $RbMgF_3$ is hexagonal and $RbMnF_3$ is cubic, the polarization properties of the different bands in $RbMgF_3$ would decrease and eventually disappear at a certain point. Valuable information about phase transitions could be obtained.

4. A study of the 830 luminescence band in 300K electron irradiated $RbMgF_3$. Its excitation spectrum does not exactly reproduce the absorption spectrum due to the $F\text{-}Mn^{2+}$ complex as does the 720 nm luminescence, i.e., a 600 nm peak is missing. The presence of a new Mn^{2+}-defect complex or the presence of another impurity is very possible.

5. Radiation effects on 4f impurity ions should be studied to see whether or not the oscillator strength can be enhanced by nearby radiation defects.

REFERENCES

1. Seitz, F., Rev. Mod. Phys. 18, 384 (1946).

2. Schulman, J. H. and W. D. Compton, Color Centers in Solids (Pergamon, New York, 1971).

3. Compton, W. D. and Rabin, Solid State Physics 16, 121 (1964) edited by F. Seitz and D. Turnbull (Academic Press, New York).

4. Fowler, W. B., Physics of Color Centers (Academic Press, New York 1968).

5. Crawford, J. H. and L. M. Slifkin, Point Defects in Solids (Plenum, New York, 1972).

6. Markham, J. J., Solid State Physics, Suppl. 8 (Academic Press, New York, 1966).

7. Vehse, W. E., W. A. Sibley, F. J. Keller and Y. Chen, Phys. Rev. 167, 828 (1968).

8. Hersh, H. N. and Bronstein, Am. J. Phys. 25, 306 (1957).

9. Sonder, E., W. A. Sibley, In Point Defects in Solids, edited by J. H. Crawford and L. M. Slifkin (Plenum, New York, 1972).

10. Hall, T. P. P. and A. Leggeat, Solid State Commun. 7, 1657 (1969).

11. Riley, C. R. and W. A. Sibley, Phys. Rev. B1, 2789 (1970).

12. Riley, C. R., Ph.D. Thesis (University of Tennessee, 1970).

13. Riley, C. R., S. I. Yun, and W. A. Sibley, Phys. Rev. B5, 3285 (1972).

14. Yun, S. I., Ph.D. Thesis, (Oklahoma State University, 1973).

15. Lewis, J. T., J. L. Kolopus, E. Sonder and M. M. Abraham, Phys. Rev. B7, 810 (1973).

16. Alcalá, R., N. Koumvakalis, W. A. Sibley, Phys. St. Solidi (a)30, 449 (1975).

17. Ludekens, W. L. W., and A. J. E. Welch, Acta Cryst. 5, 841 (1952).

18. Shafer, M. W., and T. R. McGuire, J. Phys. Chem. Solids 30, 1989 (1969).

19. Burbank, R. D., and H. T. Evans, Jr., Acta Cryst. 1, 330 (1948).

20. Ferguson, J., H. J. Guggenheim and Y. Tanabe, J. Phys. Soc. Japan 21, 692 (1966).

21. McClure, D. S., Solid State Physics 9, 399 (1959) edited by F. Seitz and D. Turnbull (Academic, New York).

22. Hush, N. S. and R. J. M. Hobbs, Progress in Inorganic Chemistry 10, 259 (1968), edited by F. A. Cotton (Interscience, New York).

23. Ferguson, J., Progress in Inorganic Chemistry 12, 159 (1970), edited by S. J. Lippard (Interscience, New York).

24. Tanabe, Y. and S. Sugano, J. Phys. Soc. Japan 9, 753 (1954).

25. Ballhausen, C. J., Introduction to Ligand Field Theory (McGraw-Hill, New York, 1962).

26. Ferguson, J., H. J. Guggenheim, and Y. Tanabe, J. Appl. Phys. 36, 1046 (1965).

27. Bethe, H. A., Ann. Physik, 3, 133 (1929).

28. Van Vleck, J. H., The Theory of Electric and Magnetic Susceptibilities, Oxford, 1932.

29. Van Vleck, J. H., J. Chem. Phys., 3, 803 (1935).

30. Van Vleck, J. H., J. Chem. Phys., 3, 807 (1935).

31. Van Vleck, J. H., Phys. Rev. 41, 208 (1932).

32. Van Vleck, J. H., and W. G. Penney, Phil. Mag., 17, 961 (1934).

33. Van Vleck, J. H., J. Chem. Phys. 7, 61, 72 (1939).

34. Van Vleck, J. Phys. Chem., 41, 67 (1937).

35. Penney, W. G., and Schlapp, R., Phys. Rev., 41, 194 (1932).

36. Schlapp, R., and W. G. Penney, Phys. Rev. 42, 666 (1932).

37. Van Vleck, J. H., J. Chem. Phys. 8, 787 (1940).

38. Finkelstein, R., and J. H. Van Vleck, J. Chem. Phys. 8, 790 (1940).

39. Hartmann, H., and H. L. Schaefer, Z. Phys. 197, 115 (1951).

40. Ilse, F. E., and H. Hartmann, Z. Phys. 197, 239 (1951).

41. Mehra, A., and P. Venkatewarlu, J. Chem. Phys. 47, 2334 (1967).

42. Lee, K. H. and W. A. Sibley, Phys. Rev. B12, 3392 (1975).

43. Young, M. A., E. E. Kohnke and L. E. Halliburton, Bull. Amer. Phys. Soc. 20, 328 (1975) and submitted to J. Phys. C.

44. Yun, S. I., K. H. Lee, W. A. Sibley and W. E. Vehse, Phys. Rev. B10, 1665 (1974).

45. Vehse, W. E. and W. A. Sibley, Phys. Rev. B6, 2443 (1972).

46. Sibley, W. A., S. I. Yun, W. E. Vehse, J. Phys. C6, 1105 (1973).

47. Bridgman, P. W., Proc. Am. Acad. Arts Sci. 60, 303 (1925).

48. Stockbarger, D. C., Rev. Sci. Instr. 7, 133 (1936).

49. Stockbarger, D. C., Discussion Faraday Soc. 5, 294, 299 (1949).

50. Ritz, V. H., and C. H. Cheek, Radiation Research 25, 537-551 (1965).

51. Feofilov, P. P., The Physical Basis of Polarized Emission (Consultant, New York, 1961).

52. Fowler, W. B., Physics of Color Centers (Academic Press, New York, 1968).

53. Castner, T. G., and W. Känzig, J. Phys. Chem. Solids 3, 178 (1957).

54. Delbecg, C. J., A. K. Ghosh and P. H. Yuster, Phys. Rev. 151, 599 (1966).

55. Murray, R. B., and F. J. Keller, Phys. Rev. 153, 993 (1967).

56. Delbecg, C. J., B. Smaller, and P. H. Yuster, Phys. Rev. 111, 1235 (1958).

57. Murray, R. B., and F. J. Keller, Phys. Rev. 137, A942 (1964).

58. Wood, R. F., Phys. Rev. 151, 629 (1966).

59. Kabler, M. N., and D. A. Patterson 19, 652 (1967).

60. Kabler, M. N., Phys. Rev. 136, A1296 (1964).

61. Pooley, D., and W. A. Runciman, J. Phys. C3, 1815 (1970).

62. Huang, K., and A. Rhys., Proc. Roy. Soc. (London) A204, 406 (1950).

63. Corbett, J. W., Electron Radiation Damage in Semiconductors and Metals (Academic Press, New York, 1966).

64. Fitchen, B. D., In Physics of Colour Centers ed. W. B. Fowler (Academic Press, N.Y., 1968), p. 293.

65. Ikeya, M. and J. H. Crawford, Phys. Letters A45, 213 (1973).

66. Ohkura, H., J. Phys. Soc., Japan 12, 1313 (1957).

67. Tomiki, T., J. Phys. Soc., Japan 15, 488 (1960).

68. Delbecg, C., Z. Physik 171, 560 (1963).

69. Wood, R. F., and A. Meyer, Sol. State Commun. 2, 225 (1964) and R. F. Wood, Phys. Rev. 151, 629 (1966).

70. Möstoller, M., B. N. Ganguly and R. F. Wood, Phys. Rev. B4, 2015 (1971).

71. Silsbee, H. R., Phys. Rev. 138, A180 (1965).

72. Hirschfelder, G. J., J. Chem. Phys. 6, 795 (1938).

73. Sonder, E., Phys. Rev. 5, 3259 (1972).

74. Cotton, F. A., Chemical Applications of Group Theory (Wiley, New York, 1971).

75. Treadaway, M. J., Ph.D. Thesis (Oklahoma State University, 1974).

VITA

Nicholas Koumvakalis

Candidate for the Degree of

Doctor of Philosophy

Thesis: OPTICAL STUDIES AND RADIATION INDUCED DEFECTS IN PURE AND Mn DOPED $RbMgF_3$

Major Field: Physics

Biographical:

Personal Data: Born in Salonika, Greece, November 1, 1946.

Education: Attended elementary schools in Salonika, Greece, and was graduated from Experimental University High School in 1964. The following October, after entrance examinations, entered the Physics Department of the Aristotelian University of Salonika and in November, 1969, received the Diploma in Physics. On April 13, 1970 joined the Royal Greek Navy where the author served until June 22, 1972. Accepted a Fulbright Scholarship and entered the Graduate School of Oklahoma State University and received the Doctor of Philosophy degree with a major in Physics in July, 1976.